Critical dynamics: a field-theoretical approach

2006 J. Phys. A: Math. Gen. 39 R207

(http://iopscience.iop.org/0305-4470/39/24/R01)

INSTITUTE OF PHYSICS PUBLISHING JOURNAL OF PHYSICS A: MATHEMATICAL AND GENERAL

J. Phys. A: Math. Gen. **39** (2006) R207–R313 doi:10.1088/0305-4470/39/24/R01

TOPICAL REVIEW

Critical dynamics: a field-theoretical approach

R Folk[1] **and G Moser**[2]

[1] Institute for Theoretical Physics, University of Linz, Austria
[2] Institute for Physics and Biophysics, University of Salzburg, Austria

E-mail: reinhard.folk@jku.at

Received 21 February 2006, in final form 13 April 2006
Published 31 May 2006
Online at stacks.iop.org/JPhysA/39/R207

Abstract

We review the progress made in dynamic bulk critical behaviour in equilibrium in the last 25 years since the review of Halperin and Hohenberg. We unify the presentation of the theoretical background by restricting ourselves to the field-theoretic renormalization group method. The main results obtained in the different universality classes are presented. This contains the critical dynamics near the gas–liquid transition in pure fluids (model H), the plait point and consolute point in mixtures (model H′), the superfluid transition in ^{4}He (model F) and ^{4}He–^{3}He mixtures (model F′), the Curie point (model J) and Neel point (model G) in Heisenberg magnets and the superconducting transition. In comparison with experimental results, it became clear that in most cases one has to consider apart from the universal asymptotic critical behaviour also the non-universal effective behaviour. Either because it turned out to be inevitable due to a small dynamical transient exponent inhibiting the system to reach the asymptotics (e.g., at the superfluid transition) or because one is interested in the region further away from the phase transition like in pure fluids and mixtures at their gas–liquid or demixing transition. The calculation of the critical dynamics is adequate in most cases only in two-loop order. We review these results and present the solution to unreasonable features found for some models. Thus, we consider model C where relaxational and diffusive dynamics are coupled and the scaling properties and the limit to a purely relaxational model (model A) have not been understood. In general for models where the order parameter couples to other conserved densities time scale ratios between the kinetic coefficients of the order parameter and the conserved densities play an important role. Their fixed-point values and the approach to the fixed point are changed considerably in two-loop order compared to their values in one-loop order. These considerations are relevant for the explanation of the dynamical critical shape functions of systems such as superfluid helium (model F) and the isotropic antiferromagnet (model G). As far as possible, the comparison of results obtained by the renormalization group theory with numerical simulations has been made.

PACS numbers: 05.10.Cc, 64.60.Ht

Contents

1. Introduction

Although the renormalization group theory explained dynamical critical phenomena in principle when the classical review by Hohenberg and Halperin was written in 1977 [1], a lot of problems remained open. Some of them emerged by looking closer at the phenomena in the following years. Especially, the field-theoretic method in dynamics [2–5] turned out to be fruitful and a strong method in calculating critical properties of measurable quantities. It is the aim of this review to present the field-theoretic method and to give an overview of some developments made in the years after 1977. However, this requires restrictions of the topics treated and we mainly discuss the results for the classical set of models within the universality classes defined in [1].

Critical behaviour near a second-order phase transition is usually connected with singularities in static quantities—like the specific heat—or dynamic quantities—like the thermal conductivity—which are described by power laws with universal exponents and universal amplitude ratios. In the renormalization group theory, this special behaviour is connected to the approach of a so-called fixed point stating that the system considered remains invariant under length scale transformations and the correlation length diverges. At the fixed-point asymptotic universal critical behaviour emerges. Being further away from the critical point, one might describe the specific behaviour by linearizing about the fixed point leading to universal transient exponents which describe the corrections to the power laws disappearing when the critical point is approached. This picture has worked well for many critical systems in statics but also in dynamics.

The consequence of that picture was the division of the models into different universality classes characterized by the fixed point of the static and dynamic functionals. These functionals define the asymptotic universal properties which are, e.g., values of exponents and amplitude

ratios, shape functions of dynamical correlations and crossover functions. They may describe the asymptotic critical behaviour in different regions of scaling variables. An example might be the crossover from the hydrodynamic region where $k\xi < 1$ (with k being the wave vector modulus and ξ the correlation length) to the critical region where $k\xi > 1$. It might also describe the crossover between the critical behaviour of two fixed points where one of them is unstable. The stability of a fixed point and the corrections to scaling were obtained by linearization about the fixed point.

There were several reasons to go beyond that picture and to consider the whole flow to the stable fixed point starting from some point further away in a region where non-universal behaviour is expected. This flow might extend into the region where fluctuation effects are small and the dependence of the physical quantities is analytical in the various parameters such as temperature distance from the critical point T_c, the wave vector k or the frequency ω. Such an extended description of the critical behaviour is accomplished by the so-called non-asymptotic renormalization group theory.

One reason to consider the theory beyond its asymptotic formulation might be that at least one transient exponent is so small and the approach to the fixed point so slow that the experimental region is far outside that asymptotic region where the critical behaviour can be described by the fixed-point properties. The most prominent example of that kind is the critical dynamics of the superfluid transition at T_λ in ^{4}He. The comparison of the thermal conductivity agreed with predicted divergence by RG calculations. However, deviations from the expected critical exponent could be found [6]. Subsequent highly precise measurements were performed over a wide range of temperatures and pressures [7, 8] which quantified the deviations from the results calculated within an asymptotic RG theory. The universal amplitude of the second sound damping below T_λ was also far from the expected universal value. In addition, the light scattering deviated considerably from scaling theory (see figure 7 in [1]). It was recognized later that the dynamic model describing the asymptotics of the superfluid transition in dimension $d = 3$ (the OP has $n = 2$ components) lies in the d–n-plane near the stability boundary where two dynamical fixed points change their stability [9]. Near this boundary, a small dynamical transient exponent exists with the consequence that the experimental region around the transition temperature T_λ is outside the asymptotic region although one can approach the transition temperature T_λ closer than in any other system. Thus only in a non-asymptotic field-theoretic RG theory [10, 11] the temperature and pressure dependences of the second sound damping amplitude ratio R_2 below T_λ and of the thermal conductivity amplitude ratio R_λ above T_λ as well as the light scattering [12] can be described.

Another reason is that often the experimentally accessible region is further away from the transition and therefore outside the asymptotic regime. Non-universal behaviour might be observed in this region in different manners:

- Power laws are applicable to the measured quantity but with effective exponents deviating from the universal exponents.
- Enhancements of finite quantities at the phase transition induced by fluctuations (enhancement) are observed leading to deviations from the regular behaviour.

Therefore, it is of interest to develop a theory which includes beside the asymptotic properties also the crossover to the regular behaviour far away from the transition, where fluctuations are negligible (background region). One might also use the known regular dependence of the background values of physical quantities (e.g., the transport coefficients) on physical parameters (such as pressure or concentration) to predict the non-asymptotic non-universal (effective) critical behaviour.

In order to give an example let us consider mixtures of two fluids. Binary liquid mixtures belong to the universality class of pure fluids at the liquid vapour critical point although the order parameter (OP) may be different (two extreme cases are the plait point and the consolute point in a mixture where the entropy density or the concentration is the OP respectively). The dynamical universality class for a pure fluid is defined by the equations of motion for a conserved OP (the entropy density) and the transverse momentum current describing the shear mode. These two equations are coupled by reversible terms (mode coupling terms). The thermal conductivity and the shear viscosity diverge with an asymptotic power law at the critical point. In binary liquid mixtures, the dynamics is described by two conserved densities corresponding to the heat mode and the mass diffusion mode. Both equations coupled to the shear mode-by-mode coupling terms but are also coupled among themselves by a diffusive term (the thermal diffusion ratio). Due to this diffusive coupling, the measurable thermal conductivity (at vanishing mass current) is finite at these second-order phase transitions but in some cases a considerable enhancement might be visible (see, for example, the case of an equimolar methane–ethane mixture [13] or ^{3}He–^{4}He mixtures [14]). This behaviour can quantitatively be described by the non-asymptotic field-theoretic renormalization group theory (RG) [15, 16]. Moreover, in changing the concentration of the mixture to the limit of one of the pure constituents one recovers a divergent thermal conductivity. In the mixture, the asymptotic critical behaviour of the mass diffusion is the same as the asymptotic critical behaviour of thermal diffusion in the pure fluid while the critical behaviour of the shear viscosity is the same in mixtures as in pure fluids. Thus, both systems belong to the same dynamic universality class but in order to understand the complete dynamical behaviour it might be necessary to extend the model within a dynamic universality class.

In mixtures of ^{3}He–^{4}He near the superfluid transition, one also has an enhanced but finite thermal conductivity (at vanishing mass current). With RG theory, one can calculate this concentration-dependent enhancement and the crossover to the divergence in the limit of zero concentration of ^{3}He in ^{4}He [17].

It is an interesting coincidence that in the case of ^{4}He where one can approach the phase transition closer than in any other system with a second-order phase transition the slow dynamic transient does not allow to reach the asymptotic regions (see the remarks in [18] in the section on the dynamics of the superfluid transition). But independent of the presence of a small transient as at the superfluid transition such a non-asymptotic theory has been asked for other systems too [19]. At the gas–liquid phase transition, the approach of the asymptotic regime is inhibited on earth by gravitation, which couples to the OP. In solid-state systems, other disturbances (e.g., defects) inhibit reaching such small relative temperature distances as in ^{4}He. Thus also for these systems it is worthwhile to apply the non-asymptotic theory in order to cover the crossover to the background behaviour.

After the time of the review by Hohenberg and Halperin theory and experiment as well as computer simulations have reached a level such that accurate quantitative comparison of experiment and/or simulations with theory is possible. Surprisingly enough some open problems within dynamical critical theory have been solved only recently although they have been known since 1970s.

- The scaling behaviour of a simple relaxational model coupled statically to a conserved density (model C) [20, 21] was not understood. There seemed to exist regions in the plane of spatial dimension d and number of components n of the OP where the concept of dynamic scaling could not be applied. Later for the special case of $n = 2$, a result different from [21] for the field-theoretic function was published [22], which however did not lead to model A when the conserved density is much faster than the OP. This has

been resolved only recently after (i) a correct field-theoretic two-loop calculation [23] and (ii) by observing that an ε-expansion is restricted to $n < 2$.

- Sasvari, Schwabl and Szepfalusy set up a model, where an n-component OP couples via reversible terms to $n(n-1)/2$ conserved densities (SSS model) [24]. This model reduces to the planar ferromagnet for $n = 2$ (model E) and to the isotropic antiferromagnet for $n = 3$ (model G). The dynamic scaling properties in the d–n-plane turned out to be not well defined [25]. An unexpected region in the d–n-plane has been found—using the ε-expansion—where two dynamic fixed points are stable. Avoiding the ε-expansion of logarithmic terms in the fixed-point equation, the overlap of the stability regions of the two dynamic fixed points disappears.
- The critical dynamics in Heisenberg magnets was also not so well understood. The dynamical critical exponents could be exactly expressed for the ferromagnet as well as for the antiferromagnet. Besides the dynamical critical exponent other important quantities like the dynamic structure factor at T_c were calculated by RG but the results for the ferromagnet were in conflict. In [26] the shape function for the isotropic ferromagnet had its peak at zero frequency whereas in [27] it had a peak at a finite frequency. Later, in [28], this conflict was resolved in favour of the dynamic shape function with its peak at zero frequency [26]. These calculations were then extended to temperatures above T_c in [29] and successfully applied in neutron scattering experiments.
- For antiferromagnets, the structure factor at T_N remained in disagreement with measurements. RG calculations in lowest loop order [30, 31] did not reproduce the quasielastic component found in $RbMnF_2$ [32] and later confirmed in [33].

Dynamical critical effects show up also in other dynamical quantities than those described by the model equations of the universality class. An example is the critical behaviour of the sound mode. The sound mode couples to the original equations defining the universality class. The critical non-asymptotic behaviour of the frequency dependence of the sound velocity or the sound attenuation can then be calculated using non-universal dynamical parameters already known (see the calculations in pure fluids [34], mixtures [16] or at the superfluid transition [35]). However, the criticality of the sound mode will be mentioned only shortly in this review.

Several other important topics cannot be treated in this review or topics treated here have also been reviewed in other context. We give a short list of some of these: dynamics near multicritical points were reviewed in [36], ageing properties of critical systems in [37], the field theory approach to percolation processes in [38], the critical dynamics of magnets in [41] and the universal critical point amplitude relations in [19]. We do not consider the critical dynamics in disordered systems, in finite systems (see, e.g., [39] and references therein), dipolar systems or dynamics on surfaces (see, e.g., [40] and references therein), dynamics on networks or percolating clusters or reaction–diffusion problems [42]. For an application of field theory and RG theory to turbulence see [43].

Critical dynamics has also been treated in the books of Vasil'ev [44] and an overview on fluid systems have been presented by Anisimov [45] and Onuki [46]. Useful information can also be found in the draft of the textbook of Täuber [47].

The review is organized in the following way: (i) after an overview of the dynamical models (section 2) the field-theoretic formalism is presented including the essentials of the statics and the definition and structure of the dynamical vertex and correlation functions (up to section 6). Then, the renormalization is introduced in section 7 and the corresponding field-theoretic functions are defined. The possible fixed points and the consequences for the dynamical critical exponents are exploited (up to section 8.3). (ii) In the following,

the different models (sections 9–18) and the results obtained are discussed and compared with experiments and computer simulations. (iii) Field-theoretic results are cumulated in appendix A for the dynamic field-theoretic functions (mostly in two-loop order).

2. Definition of models

Near a second-order phase transition the correlation length diverges and the physical system loses its typical length scale. Scale invariance follows and using the renormalization group theory the specific critical behaviour of physical quantities near such a phase transition can be determined [48]. In statics singular behaviour, like the divergence of the specific heat or of the susceptibility, is observed in the form of a power law. The set of all universal quantities for a system, like the exponents of these power laws, the scaling functions written as functions of scaling variables, etc define the static universality classes although the systems might be microscopically quite different. These static universality classes are characterized by quite general properties of the systems such as spatial dimension, number of components of the OP (if it is a scalar, a two-component vector or a three-dimensional vector), its symmetry properties, either isotropic or of cubic symmetry and the range of interaction (for a review see [49]).

These static universality classes subdivide into several dynamic universality classes. In dynamics, one also finds singular behaviour and power laws, e.g., in the kinetic coefficients (KCs) of the specific dynamic equations. The main effect near the phase transition is the critical slowing down, i.e., the increase of the relaxation time in which the system reaches equilibrium. Due to the different behaviour of the relaxation times of the relevant dynamical densities, these universality classes further divide into dynamical subclasses characterized by the critical dynamic exponents appearing in the dynamical models. These dynamical universality classes have been categorized by capital letters in the review of Hohenberg and Halperin. They are distinguished by the structure of the dynamical equations necessary to describe the relevant slow variables in the physical system. These slow variables are (i) the OP itself because of critical slowing down and (ii) other densities which obey a continuity equation. Thus, we have to consider the following items:

- Is the OP conserved or non-conserved?
- Does the OP couple to other conserved densities? What is the tensor character of these secondary densities? For example, scalars, vectors or tensors.
- How does the OP couple to the conserved densities? Statically and/or dynamically, e.g., via irreversible and/or mode coupling terms.

An overview may be found in table 1 where we list the densities involved in the critical dynamics of the different models. More details are given in the accompanying sections where several models are presented.

Symmetry properties determine the possible irreversible couplings as well as the mode couplings of the equations of motion of the different densities. This is important for the asymptotic critical dynamics as well as for the non-asymptotic region further away from T_c and will be discussed in the corresponding sections of the different models.

Besides the arrangement of the dynamical systems in universality classes in table 1 (the unprimed classes), the non-asymptotic properties have become more and more important. In consequence, it is necessary to distinguish between systems within one universality class if non-universal quantities become important (see the primed classes in table 1).

Table 1. Different dynamic models considered with their name, the reference where the model was set up (column reference) and some examples for which the models apply (last column). In columns 2–6 several features of the models are presented. Column 2 indicates if the order parameter (OP) is conserved (c) or non-conserved (nc). Column 3 gives the number of secondary densities (SD) together with their tensor character where the abbreviations s for scalar, v for vector or a component of a vector and t for a tensor of second rank are used. Columns 4–6 give information about the static and dynamic couplings appearing in the models. sc indicates the number of static couplings, ic the number of irreversible couplings (kinetic cross coefficient) and mc the number of reversible mode couplings.

Model	OP	SD	sc	ic	mc	Reference	System
A	nc	0	0	0	0	[50]	Relaxation
B	c	0	0	0	0		Diffusion
C	nc	1s	1	0	0	[20]	Relaxation/diffusion, structural PT
C′	nc	2s	1	1	0	[20]	Relaxation/diffusion, structural PT
D	c	1s	1	0	0	[51]	Global conservation
E	nc	1v	0	0	1	[52]	Planar magnet $h_z = 0$
E′	n	2v	0	1	2	[52]	Planar magnet $h_z = 0$
F	nc	1s	1	0	1	[52]	Planar magnet $h_z \neq 0$
							Superfluid ^{4}He
F′	nc	2s	1	1	2	[53]	Superfluid ^{3}He–^{4}He mixture
G	nc	1v	0	0	1	[20]	Heisenberg antiferromagnet
H	c	1v	0	0	1	[52]	Gas/liquid
H′	c	1v + 1s	1	1	1	[52]	Binary mixture
J	c	0	0	0	1	[54]	Heisenberg ferromagnet
DP	nc	1v	0	0	1	[4]	Heisenberg antiferromagnet
SSS	nc	1t	0	0	1	[24]	Structural PT

3. General dynamic equations

Due to the critical slowing down, the dynamics of a phase transition of second order is determined by slowly (compared to the time scale of microscopic processes) varying dynamic variables $\{a_i\}$, which are related to macroscopic observable quantities. Based on the considerations made by Green [55], where stochastic equations for a set of slow variables have been extracted from microscopic molecular variables by averaging over phase space volumes, Zwanzig [56] developed a projector method, which forms the cornerstone for equations of critical dynamics. In his approach, the slow variables define a subspace in phase space. The projector separates the Liouville equations for the microscopic variables into a part which is 'parallel' to the subspace of the slow variables and a part which is 'perpendicular'. The latter one describes the influence of the fast microscopic variables acting like a noise onto the slow variables. Replacing it by a stochastic force turns the former deterministic Liouville equation into a stochastic equation. The projected equation can be further separated into a part which is reversible in time and a dissipative part. Neglecting memory effects, one finally obtains the following Langevin-type equations for the dynamic variables $\{a_i\}$ with the static functional $\mathcal{H}$ and the noise θ_i

$$\frac{\partial a_i}{\partial t} = v_i(\{a_k\}) - \sum_j L_{ij} \frac{\delta \mathcal{H}(\{a_k\})}{\delta a_j^+} + \theta_i. \tag{1}$$

The first term on the right-hand side in the above equation is the reversible part given by

$$v_i(\{a_k\}) = \sum_j \left[Q_{ij} \frac{\delta \mathcal{H}\{a_k\})}{\delta a_j^+} - \frac{\delta Q_{ij}}{\delta a_j^+} \right]. \tag{2}$$

The functions Q_{ij} are determined by the Poisson brackets

$$Q_{ij} = k_B T \left\{ a_i, a_k^+ \right\}. \tag{3}$$

We want to emphasize that these Poisson brackets are not the usual microscopic brackets derived in mechanics. They represent generalized Poisson brackets of macroscopic observables. Basically, there are two methods to obtain such generalized Poisson brackets. The first one is to transform the commutators in quantum mechanics into classical Poisson brackets by using the correspondence principle. This method works only for macroscopic observables which have a microscopic counterpart (magnetization spin for example). Macroscopic densities like the entropy density for instance do not correspond to a microscopic expression. For such quantities, the second method must be used where symmetry operations valid in a system and their corresponding group generators are used to obtain Poisson brackets. Only Poisson brackets which contain at least one group generator may be different from zero. All other Poisson brackets are zero. Considering as an example a hydrodynamic system with the entropy density, the mass density and the momentum current as macroscopic observables, the momentum current is the generator of the translation operation under which the system has to be invariant. Thus, the Poisson brackets between different momentum current components and a momentum current component and the entropy or mass density are finite, while the Poisson bracket between mass density and entropy density is zero. More details to the definition of generalized Poisson brackets can be found in [57].

The second term in (1) is the dissipative part. The coefficients L_{ij} are related to the KCs. The way how these coefficients are related to the Onsager coefficients is determined by a fundamental property of the corresponding dynamic variables.

(i) *Non-conserved densities*. In this case, the total amount of the macroscopic densities changes with time which means

$$\frac{\mathrm{d}}{\mathrm{d}t} \int \mathrm{d}^d x \, a_i(x,t) < 0. \tag{4}$$

This always happens when a finite amount of the dynamic quantity flows into microscopic degrees of freedom, which are not covered by the macroscopic set of dynamic variables. A continuous loss in the total amount of the considered quantity is the consequence usually denoted as relaxation described by the equation

$$\frac{\partial a_i}{\partial t} = -\sum_j \Lambda_{ij} a_j. \tag{5}$$

The coefficients Λ_{ij} then represent the relaxation coefficients. In order to connect the relaxation coefficient with the coefficients L_{ij} from (1), we have to distinguish between the two cases of either real or complex dynamic variables.

Real-valued dynamic variables. The static functional $\mathcal{H}$ is in the simplest case of Gaussian form. For real dynamic variables this is

$$\mathcal{H} = \frac{1}{2} \sum_k \int \mathrm{d}^d x \, a_k^2 \tag{6}$$

and (5) can be rewritten as

$$\frac{\partial a_i}{\partial t} = -\sum_j \Lambda_{ij} \frac{\delta \mathcal{H}(\{a_k\})}{\delta a_j}. \tag{7}$$

Thus, we simply may identify $L_{ij} = \Lambda_{ij}$ in this case.

Complex-valued dynamic variables. For complex dynamic variables, the Gaussian static functional is

$$\mathcal{H} = \frac{1}{2}\sum_k \int \mathrm{d}^d x\, a_k^+ a_k = \frac{1}{2}\sum_k \int \mathrm{d}^d x \left(a_k'^2 + a_k''^2\right). \tag{8}$$

Usually, a_k and a_k^+ are considered as dynamic variables instead of the real and imaginary parts a_k' and a_k''. Equation (5) can then be rewritten as

$$\frac{\partial a_i}{\partial t} = -\sum_j 2\Lambda_{ij} \frac{\delta \mathcal{H}(\{a_k\})}{\delta a_j^+}. \tag{9}$$

Now, we may identify $L_{ij} = 2\Lambda_{ij}$.

(ii) *Conserved densities.* The total amount of conserved densities does not change in time, thus we have

$$\frac{\mathrm{d}}{\mathrm{d}t}\int \mathrm{d}^d x\, a_i(x,t) = 0. \tag{10}$$

In the case of local conservation, any alteration of a_i in time in an arbitrary volume element causes a current through the surrounding surface into the neighbouring volume elements and Fick's law is valid. This is expressed by the continuity equation

$$\frac{\partial a_i}{\partial t} + \vec{\nabla}\cdot\vec{J}_{a_i} = 0, \tag{11}$$

where $\vec{J}_{a_i}$ is the current corresponding to a_i. Because we are only interested in the long time behaviour over large scales, we may assume that the current is proportional to the gradient of the densities that is

$$\vec{J}_{a_i} = -\sum_j \Lambda_{ij}\vec{\nabla} a_j \tag{12}$$

which is called Fick's law. Inserting into (11) leads to

$$\frac{\partial a_i}{\partial t} = \sum_j \Lambda_{ij}\nabla^2 a_j. \tag{13}$$

The dissipation of conserved quantities is determined by diffusion. In this case, the coefficients in (1) are $L_{ij} = -\Lambda_{ij}\nabla^2$ where Λ_{ij} are now diffusion coefficients. Conserved dynamic variables are always real in the considered models regardless if they represent the OP or any secondary densities. Therefore, it is not necessary to consider complex dynamic variables in this case.

$\mathcal{H}$ is related to the equilibrium phase space density in the subspace of slow variables and determines a free energy. Usually, a static functional which is capable to describe the static critical behaviour of the system is inserted. Details will be given in a subsequent section.

The functions $\theta_i(x,t)$ have their origin in the part of the Liouville equations which is 'perpendicular' to the subspace of the slow variables. As mentioned earlier, they will be replaced by stochastic forces. Because memory effects have been neglected in (1), the stochastic forces $\theta_i(x,t)$ are determined by a Markovian process. The coefficients L_{ij} fulfil Einstein relations

$$\langle \theta_i(x,t)\theta_j(x',t')\rangle = 2L_{ij}\delta(x-x')\delta(t-t'). \tag{14}$$

L_{ij} has to be inserted according to (i) or (ii) in the discussion above. Note that in (14), and in the following discussions also, possible complex variables and their adjoint are covered by the

indices i and j considering them as individual variables. Therefore, we have written general $\langle\theta_i\,\theta_j\rangle$ correlations instead of only $\langle\theta_i\,\theta_i^+\rangle$ correlations which are different from zero in such a case. This implies that L_{ij} has the substructure

$$[L^{(a_i)}] = \begin{pmatrix} 0 & 2\Lambda_i \\ 2\Lambda_i & 0 \end{pmatrix} \tag{15}$$

for each pair of a_i and $a_{i+1} = a_i^+$.

Under non-equilibrium conditions, several requirements valid in equilibrium dynamics (Einstein relations, integrability for the reversible forces and detailed balance) are not fulfilled. Thus, the non-equilibrium dynamics is not limited by the fluctuation dissipation theorem, which makes possible the separation of static and dynamic properties (for further discussion see, e.g., [58]).

4. Dynamic functional

In order to obtain a dynamic functional which is suitable to perform a loop expansion, we follow the approach of Bausch, Janssen and Wagner [3]. The Einstein relations (14) imply a probability density

$$\bar{\mathcal{W}}(\{\theta_k\}) \sim \exp\left(-\frac{1}{4}\int \mathrm{d}t\,\mathrm{d}x \sum_{i,j}\theta_i(x,t)[L^{-1}]_{ij}\theta_j(x,t)\right). \tag{16}$$

A path probability density for the stochastic variables a_i can be achieved by

$$\mathcal{W}(\{a_k\})\,\mathrm{d}(\{a_k\}) = \bar{\mathcal{W}}(\{\theta_k\})\,\mathrm{d}(\{\theta_k\}), \tag{17}$$

which may be defined as

$$\mathcal{W}(\{a_k\}) \sim \exp(-\mathcal{G}(\{a_k\})). \tag{18}$$

The functional $\mathcal{G}$ can be found by inserting the dynamic equations (1) into (16). Introducing

$$V_i(\{a_k\}) \equiv v_i(\{a_k\}) - \sum_j L_{ij}\frac{\delta\mathcal{H}(\{a_k\})}{\delta a_j^+}, \tag{19}$$

the dynamic equations can be shortly written as $\dot{a}_i = V_i(\{a_k\}) + \theta_i$. Inserting into (16) leads to

$$\mathcal{G}(\{a_k\}) = \frac{1}{4}\int \mathrm{d}t\,\mathrm{d}x\left[\sum_{i,j}(\dot{a}_i - V_i(\{a_k\}))[L^{-1}]_{ij}(\dot{a}_j - V_j(\{a_k\})) + 2\sum_i \frac{\delta V_i(\{a_k\})}{\delta a_i}\right]. \tag{20}$$

The last term in (20) arises from the functional Jacobian. The drawback of the above dynamic functional is that the dynamic variables may appear in high powers especially in V^2 making a perturbation expansion very difficult. The higher the powers of the dynamic variables, the higher the loop order necessary to obtain nontrivial results. This can be avoided by introducing auxiliary variables $\{\tilde{a}_k\}$ and performing a Gaussian transformation. The probability density (18) is related via

$$\mathcal{W}(\{a_k\}) = \int \mathrm{d}(\{\mathrm{i}\tilde{a}_k\})\widetilde{\mathcal{W}}(\{a_k\},\{\tilde{a}_k\}) \tag{21}$$

to a probability density

$$\widetilde{\mathcal{W}}(\{a_k\},\{\tilde{a}_k\}) \sim \exp(-\mathcal{J}(\{a_k\},\{\tilde{a}_k\})), \tag{22}$$

which is now determined by a 'linearized' dynamic functional

$$\mathcal{J}(\{a_k\},\{\tilde{a}_k\}) = \int \mathrm{d}t\,\mathrm{d}x\left[-\sum_{i,j}\tilde{a}_i L_{ij}\tilde{a}_j + \sum_i \tilde{a}_i^+(\dot{a}_i - V_i(\{a_k\})) + \frac{1}{2}\sum_i \frac{\delta V_i(\{a_k\})}{\delta a_i}\right]. \tag{23}$$

Now the powers of $\{a_k\}$ have been reduced at the expense of doubling the number of dynamic variables. Nevertheless, $\mathcal{J}$ is a dynamic functional suitable to perform a loop expansion.

5. Static functionals and correlation functions

5.1. Ginzburg–Landau–Wilson functional

All models considered in this review have in common that their static critical behaviour is completely covered by the Ginzburg–Landau–Wilson (GLW) functional (an exception will be the static functional for the superconductor), which is also known as ϕ^4-model in the literature [59–61]. It represents a free energy functional which is expanded in powers of an order parameter (OP) up to fourth order, and its gradient up to quadratic order which is sufficient for the description of the normal critical point in a system. For multicritical behaviour, the expansion has to be extended either in the powers of the OP (sixth order for tricritical behaviour for instance) or in the powers of the gradient terms (fourth order for Lifshitz points). Further we will restrict ourselves to isotropic systems in the following, thus the functional is of the form

$$\mathcal{H}_{\mathrm{GLW}} = \int \mathrm{d}^d x \left\{ \frac{1}{2} \mathring{r} \vec{\varphi}_0^+ \vec{\varphi}_0 + \frac{1}{2} \sum_{i=1}^{d} \nabla_i \vec{\varphi}_0^+ \nabla_i \vec{\varphi}_0 + \frac{\mathring{u}}{4!} \left(\vec{\varphi}_0^+ \vec{\varphi}_0 \right)^2 \right\}. \tag{24}$$

The parameter $\mathring{r} = a\left(T - T_c^{(0)}\right)$ is proportional to the temperature distance to the critical point which is described by the mean field critical temperature $T_c^{(0)}$. The fourth-order coupling $\mathring{u}$ must be positive otherwise a sixth-order term would be necessary leading to tricritical behaviour or a first-order transition. The OP $\vec{\varphi}_0$ has been written as a complex vector ($\vec{\varphi}_0^+$ is its adjoint vector) representing the most general structure. The actual structure of the OP differs in the dynamic models dependent on the physical quantity which represents the OP in this system. It may range from a simple real scalar function $\vec{\varphi}_0 \equiv \phi_0(x)$, as it is at the gas–liquid critical point in liquids and liquid mixtures (model H, H′) and real n-component vectors $\vec{\varphi}_0 \equiv \vec{\phi}_0(x)$ usually appearing in magnetic systems like the ferromagnet (model J, SSS model) or the antiferromagnet (model G), to scalar complex functions $\vec{\varphi}_0 \equiv \psi_0(x) = \psi_0'(x) + \mathrm{i}\psi_0''(x)$ necessary at the superfluid transition in ^{4}He (model E, F) and ^{3}He–^{4}He mixtures (model E′, F′). In the DP model and in the purely dissipative models (model A, B, C), even $n/2$-component complex vectors $\vec{\varphi}_0 \equiv \vec{\psi}_0(x) = \vec{\psi}_0'(x) + \mathrm{i}\vec{\psi}_0''(x)$ may appear.

Correlation functions within statics are defined as

$$\left\langle \varphi_{i_1}(x_1) \cdots \varphi_{i_r}(x_r) \right\rangle = \frac{1}{\mathcal{N}} \int \mathcal{D}(\vec{\varphi}) \varphi_{i_1}(x_1) \ldots, \varphi_{i_r}(x_r)\, \mathrm{e}^{-\mathcal{H}_{\mathrm{GLW}}} \tag{25}$$

with $\mathcal{N} = \int \mathcal{D}(\vec{\varphi}) \exp\{-\mathcal{H}_{\mathrm{GLW}}\}$ as suitable normalization constant and $\int \mathcal{D}(\vec{\varphi})$ the functional integral over all OP components. In the case of a complex OP, of course only correlation functions containing an equal number of φ_i and φ_i^+ are different from zero. From the correlation functions, usually the cumulants are introduced as

$$\left\langle \varphi_{i_1} \varphi_{i_2} \right\rangle_c = \left\langle \varphi_{i_1} \varphi_{i_2} \right\rangle - \left\langle \varphi_{i_1} \right\rangle \left\langle \varphi_{i_2} \right\rangle, \tag{26}$$

$$\left\langle \varphi_{i_1} \varphi_{i_2} \varphi_{i_3} \right\rangle_c = \left\langle \varphi_{i_1} \varphi_{i_2} \varphi_{i_3} \right\rangle - \left\langle \varphi_{i_1} \varphi_{i_2} \right\rangle_c \left\langle \varphi_{i_3} \right\rangle - \left\langle \varphi_{i_1} \varphi_{i_3} \right\rangle_c \left\langle \varphi_{i_2} \right\rangle - \left\langle \varphi_{i_2} \varphi_{i_3} \right\rangle_c \left\langle \varphi_{i_1} \right\rangle - \left\langle \varphi_{i_1} \right\rangle \left\langle \varphi_{i_2} \right\rangle \left\langle \varphi_{i_3} \right\rangle,$$

$$\vdots \tag{27}$$

The cumulant of a correlation is obtained by subtracting all possible lower cumulants. In a loop expansion, these cumulants are obtained by collecting all graphical contributions which are connected at least with one line, therefore they are also called ‘connected Greens functions’

in several topics of physics. Of special interest are the two-point functions in (26) because they are related to thermodynamic derivatives such as specific heats or susceptibilities. The GLW functional belongs to the class of systems with isotropic symmetry, thus the cumulants of all OP components are related to the same function $\langle\varphi_0(x_1)\varphi_0^+(x_2)\rangle_c$ [62] in the disordered phase ($T > T_c$) and we may write

$$\langle\varphi_{i_1}(x_1)\varphi_{i_2}^+(x_2)\rangle_c = \langle\varphi_0(x_1)\varphi_0^+(x_2)\rangle_c\,\delta_{i_1 i_2}. \tag{28}$$

The Fourier-transformed OP cumulant is defined as

$$\langle\varphi_0(k_1)\varphi_0^+(k_2)\rangle_c = \int \mathrm{d}x_1 \int \mathrm{d}x_2 \langle\varphi_0(x_1)\varphi_0^+(x_2)\rangle_c \exp(-(\mathrm{i}k_1x_1 + \mathrm{i}k_2x_2)). \tag{29}$$

Due to the translation invariance of the cumulant $\langle\varphi_0(x_1)\varphi_0^+(x_2)\rangle_c = \langle\varphi_0(x_1 - x_2)\varphi_0^+(0)\rangle_c$ the Fourier-transformed cumulant can be written as

$$\langle\varphi_0(k_1)\varphi_0^+(k_2)\rangle_c = \mathring{C}^{(s)}_{\varphi\varphi^+}(\mathring{r}, \mathring{u}, k_1)\delta(k_1 + k_2), \tag{30}$$

which is achieved by shifting the first integral in (29) and using an appropriate representation of the Dirac delta function $\delta(k)$. The Fourier-transformed two-point OP cumulant is related to static OP vertex functions $\mathring{\Gamma}_{\varphi\varphi^+}$ by

$$\mathring{\Gamma}_{\varphi\varphi^+}(\mathring{r}, \mathring{u}, k) = \frac{1}{\mathring{C}^{(s)}_{\varphi\varphi^+}(\mathring{r}, \mathring{u}, k)}. \tag{31}$$

The vertex function is determined by a subset of all graphical contributions appearing in the cumulant. It only contains 'one-particle irreducible' graphs, which have the property that they do not decompose into two graphs of lower degree if one line is cut. The OP vertex function will be usually calculated explicitly in loop expansion. A comprehensive survey over the Feynman theory of graphs used in the field of critical phenomena, presenting the rules for construction and calculation of graphs, can be found in [59]. In the above relations, we have considered the general complex case. The static functions calculated with an $n/2$-component complex OP are equal to the corresponding functions calculated with an n-component real OP apart from an overall factor. For two-point functions this means $\langle\varphi_0\varphi_0^+\rangle_c = \langle\varphi_0'\varphi_0'\rangle_c + \langle\varphi_0''\varphi_0''\rangle_c = 2\langle\varphi_0'\varphi_0'\rangle_c$ because the GLW functional is real and therefore symmetric in φ_0' and φ_0''. The vertex functions of a complex and a real system are related by

$$\mathring{\Gamma}_{\varphi\varphi^+}(\mathring{r}, \mathring{u}, k) = \tfrac{1}{2}\mathring{\Gamma}_{\phi\phi}(\mathring{r}, \mathring{u}, k). \tag{32}$$

In order to obtain vertex functions which are (i) finite at $d < 4$ also at infinite cut-off and (ii) resummable although non-convergent when considered as power series of $\mathring{u}$, the following steps have to be performed [66].

- *T_c-shift*. Critical fluctuations induce a shift in the critical temperature T_c compared to the critical temperature $T_c^{(0)}$ of the mean field theory. At the critical temperature, the two-point vertex function, which is an inverse OP susceptibility, has to fulfil

  $$\mathring{\Gamma}_{\varphi\varphi^+}(0, \mathring{u}, 0) = 0. \tag{33}$$

  An examination of the loop expanded expression of the vertex function reveals that at $\mathring{r} = 0$ and $k = 0$ strongly singular contributions remain. Their origin lies in a T_c-shift $\mathring{r}_c$ which is not expandable in integer powers of $\mathring{u}$. The T_c-shift is determined by the condition

  $$\mathring{\Gamma}_{\varphi\varphi^+}(\mathring{r}_c, \mathring{u}, 0) = 0, \tag{34}$$

  a function $\mathring{r}_c(\mathring{u})$ can be generated in every order of loop expansion, which is divergent for any $d > 2$. From dimensional arguments, one obtains [63]

  $$\mathring{r}_c = \mathring{u}^{2/\varepsilon} S(\varepsilon). \tag{35}$$

$S(\varepsilon)$ is a dimensionless function with dimensional poles at $\varepsilon = 2/l$ ($l = 2, 3, 4, \ldots$) The vertex function can now be rearranged internally by introducing the parameter $\mathring{r} - \mathring{r}_c$ in all orders of perturbation expansion

$$\mathring{\Gamma}_{\varphi\varphi^+}(\mathring{r}, \mathring{u}, k) = \mathring{\tilde{\Gamma}}_{\varphi\varphi^+}(\mathring{r} - \mathring{r}_c, \mathring{u}, k) \qquad \text{with} \qquad \mathring{r} - \mathring{r}_c \sim T - T_c. \tag{36}$$

In the rearranged function $\mathring{\tilde{\Gamma}}_{\varphi\varphi^+}(\mathring{r} - \mathring{r}_c\mathring{u}, k)$, all singularities originating from the T_c-shift are collected in $\mathring{r}_c(\mathring{u})$.

- *Correlation length* ξ. Within the GLW model the correlation length is defined as

$$\xi^2(\mathring{r} - \mathring{r}_c, \mathring{u}) = \left.\frac{\partial \ln \mathring{\tilde{\Gamma}}_{\varphi\varphi^+}(\mathring{r} - \mathring{r}_c, \mathring{u}, k)}{\partial k^2}\right|_{k=0}, \tag{37}$$

as a function of the GLW parameters. The definition (37) will be inverted obtaining a function $[\mathring{r} - \mathring{r}_c](\xi^{-2}, \mathring{u})$ order by order. Inserting into $\mathring{\tilde{\Gamma}}_{\varphi\varphi^+}(\mathring{r} - \mathring{r}_c, \mathring{u}, k)$ leads to a vertex function $\mathring{\Gamma}^{(s)}_{\varphi\varphi^+}(\xi^{-2}, \mathring{u}, k)$ having an expansion in integer power of $\mathring{u}$ which may be resummable [64].

This approach has been applied in our calculations to all static and dynamic vertex functions necessary for the renormalization or the calculation of physical quantities in the following and will not be mentioned further. The advantage in using the above rearrangements is on the one hand a simplification of the expressions because only the contributions containing critical singularities have to be calculated explicitly, and on the other hand that expressions are obtained which are ready for applying resummation methods.

An accurate comparison in statics of the GLW model using Borel-summed expressions for the physical quantities and the flow with experimental data at the liquid–vapour critical point of ^{3}He has been performed in [67] using different theoretical approaches of [65] and [66].

5.2. *Extended static functionals*

Although the GLW functional together with the introduction of a suitable OP is sufficient to obtain the asymptotic critical behaviour, especially the universal exponents and amplitude ratios, it is sometimes necessary to extend this functional with secondary densities. The reason for this step may be either that one is interested in non-asymptotic behaviour in temperature regions where the so-called 'irrelevant' quantities, which do not influence the critical behaviour in the asymptotic region, are not negligible. Or considering the critical behaviour in dynamics, when the critical behaviour of diffusion or relaxation coefficients is related to correlation functions of other densities than the OP. The static functional consists in such a case of a part which is of GLW form (but with the parameters $\mathring{\tau}$ and $\mathring{\tilde{u}}$) as

$$\mathcal{H}_\varphi = \int \mathrm{d}^d x \left\{ \frac{1}{2}\mathring{\tau}\vec{\varphi}_0^+\vec{\varphi}_0 + \frac{1}{2}\sum_{i=1}^{d} \nabla_i\vec{\varphi}_0^+\nabla_i\vec{\varphi}_0 + \frac{\mathring{\tilde{u}}}{4!}\left(\vec{\varphi}_0^+\vec{\varphi}_0\right)^2 \right\} \tag{38}$$

and a part which contains secondary densities. It depends on the actual system how many secondary densities have to be considered which couple to the OP. But they all have in common that the secondary densities appear only up to quadratic order otherwise they would influence the critical asymptotic behaviour of the system. Systems like ^{4}He at the superfluid transition (model F) or liquid mixtures at the gas–liquid critical point (plait point) and also at the liquid demixing point (consolute point) both described by model H′ need a simple scalar function

$q_0(x)$ as a secondary density which represents the entropy density or the concentration. In these cases, we have to add the functional

$$\mathcal{H}_m^{(1s)} = \int \mathrm{d}^d x \left\{ \frac{1}{2} a_q q_0^2 + \frac{1}{2} \mathring{\gamma}_q q_0 \vec{\varphi}_0^+ \vec{\varphi}_0 - \mathring{h}_q q_0 \right\} \tag{39}$$

to (38) where $\mathring{h}_q$ denotes the conjugate field to q_0 and is chosen in such a way that the expectation value of q_0 is zero. The constant parameter a_q is related to the background value of a thermodynamic derivative like an inverse specific heat or some kind of susceptibility. The parameter $\mathring{\gamma}_q$ is the static coupling between OP and secondary density. Scalar secondary densities representing entropy, mass, energy densities or concentrations are invariant under time-reversal and contribute according to (39) to the static functional. Because a_q is only a trivial parameter, it will be eliminated usually by rescaling the secondary density and the corresponding parameters. Introducing rescaled secondary densities $m_0 = a_q^{1/2} q_0$, one obtains

$$\mathcal{H}_m^{(1s)} = \int \mathrm{d}^d x \left\{ \frac{1}{2} m_0^2 + \frac{1}{2} \mathring{\gamma} m_0 \vec{\varphi}_0^+ \vec{\varphi}_0 - \mathring{h} m_0 \right\} \tag{40}$$

with rescaled parameters $\mathring{\gamma} = a_q^{-1/2} \mathring{\gamma}_q$ and $\mathring{h} = a_q^{-1/2} \mathring{h}_q$. Explicit calculations and especially calculations of universal exponents or amplitude ratios are usually performed with (40). But for comparison with experimental quantities in the non-asymptotic region, one has to keep in mind that the original functional is (39) and a_q is related to an experimental quantity.

In systems where the secondary density is either related to a vector $\vec{m}_0(x)$, for instance the magnetization vector in the antiferromagnet (model G), or represents a component of a magnetization vector, for instance in the planar ferromagnet (model E), couplings to the OP cannot exist. This follows from the time-reversal invariance of the static functional. If the time and all external magnetic fields are reversed, the functional (38) plus (40) has to be invariant. For a magnetization vector, or a component of it, the term with the OP coupling $\mathring{\gamma}$ changes its sign because the magnetization changes sign with reversed magnetic field. Thus, in such systems the secondary density part of the static functional is simply

$$\mathcal{H}_m^{(1v)} = \int \mathrm{d}^d x \frac{1}{2} m_0^2. \tag{41}$$

The same is true for the mass current $j_0(x)$ changing the sign when the time is reversed. Systems like liquids at the critical point (model H) as well as liquid mixtures at the plait point and the consolute point (model H′) need the mass current in order to describe the critical behaviour of the shear viscosity. Thus, one has to add

$$\mathcal{H}_j = \int \mathrm{d}^d x \frac{1}{2} j_0^2 \tag{42}$$

to the static functional. Analogously to (39) and (40), we have already given the rescaled functionals in (41) and (42).

In cases where more than one scalar secondary density is necessary, for instance in ^{3}He–^{4}He mixtures at the superfluid transition (model F′) where the entropy density and the concentration are necessary secondary densities, the situation gets somewhat more complex. The generalization of (39) to several secondary densities is

$$\mathcal{H}_m^{(Ms)} = \int \mathrm{d}^d x \left\{ \frac{1}{2} \boldsymbol{q}_0 \cdot \boldsymbol{A} \cdot \boldsymbol{q}_0 + \frac{1}{2} \mathring{\gamma}_q \cdot \boldsymbol{q}_0 \vec{\varphi}_0^+ \vec{\varphi}_0 - \mathring{\boldsymbol{h}}_q \cdot \boldsymbol{q}_0 \right\}, \tag{43}$$

where $\cdot$ denotes the dot product and the M scalar secondary densities $q_{i0}(x)$ are written as a column vector

$$\boldsymbol{q}_0(x) = \begin{pmatrix} q_{10}(x) \\ \vdots \\ q_{M0}(x) \end{pmatrix}. \tag{44}$$

The matrix

$$\boldsymbol{A} = \begin{pmatrix} a_{11} & \cdots & a_{1M} \\ \vdots & & \vdots \\ a_{M1} & \cdots & a_{MM} \end{pmatrix} \tag{45}$$

of constant coefficients is related to thermodynamic derivatives taken at temperatures outside the critical region, which is usually denoted as background region. The static couplings $\mathring{\boldsymbol{\gamma}}_q$ and the external fields $\mathring{\boldsymbol{h}}_q$ are

$$\mathring{\boldsymbol{\gamma}}_q = \begin{pmatrix} \mathring{\gamma}_{q_1} \\ \vdots \\ \mathring{\gamma}_{q_M} \end{pmatrix}, \qquad \mathring{\boldsymbol{h}}_q = \begin{pmatrix} \mathring{h}_{q_1} \\ \vdots \\ \mathring{h}_{q_M} \end{pmatrix}. \tag{46}$$

The systematic derivation of a functional like (43) and the identification of the parameters with thermodynamic quantities have been outlined in detail for several systems. At the λ-transition in ^{3}He–^{4}He mixtures, a thermodynamic identification of the coefficients of $\boldsymbol{A}$ has been presented in [68] and [69]. Considering the critical behaviour of first sound in ^{4}He at the λ-transition, an extended dynamical model including the mass density as a second secondary density beside the entropy density is necessary. This demands an extended static functional of type (43) with two secondary densities. The identification of the parameters with thermodynamic derivatives has been presented in [35]. And at least a comprehensive derivation of an extended static functional and the connection of its parameters to experimental quantities for the gas/liquid transition and the liquid/liquid transition in binary fluid mixtures has been presented in [70]. In order to avoid a matrix renormalization scheme for the secondary densities, which would be forced by the static functional (43), a transformation representing an 'orthogonalization' in some sense can be introduced. Independent of the number of secondary densities, it is always possible to introduce transformed secondary densities $\boldsymbol{m}_0 = \boldsymbol{M} \cdot \boldsymbol{q}_0$ where $\boldsymbol{M}$ is an orthogonal transformation matrix ($\boldsymbol{M}^{-1} = \boldsymbol{M}^T$). The transformation has the properties that (i) the matrix $\boldsymbol{A}$ will be diagonalized and (ii) only one secondary density remains coupled to the OP and the rest is simply Gaussian. The general structure of such transformations has been presented in [35, 71] for $M = 2$. After a subsequent rescaling of the transformed secondary densities with the eigenvalues of $\boldsymbol{A}$, one ends up with the functional

$$\mathcal{H}_m^{(Ms)} = \int \mathrm{d}^d x \left\{ \frac{1}{2} \boldsymbol{m}_0 \cdot \boldsymbol{m}_0 + \frac{1}{2} \mathring{\gamma} m_{M0} \vec{\varphi}_0^{+} \vec{\varphi}_0 - \mathring{h} m_{M0} \right\}. \tag{47}$$

In the above expression only the last secondary density m_{M0} couples with $\mathring{\gamma}$ to the OP. All other secondary densities are simply Gaussian.

In the case of vector quantities, the extension of (41) to N secondary densities is evident. Thus, in general the extended static functional of a system with M scalar secondary densities, N vector or vector component secondary densities, and the mass current is of the form

$$\mathcal{H} = \mathcal{H}_\varphi + \mathcal{H}_m^{(Ms)} + \mathcal{H}_m^{(Nv)} + \mathcal{H}_j. \tag{48}$$

Accordingly correlation functions are defined as

$$\langle a_1(x_1)\cdots a_r(x_r)\rangle = \frac{1}{\mathcal{N}'}\int \mathcal{D}(\{a_j\})a_1(x_1)\cdots a_r(x_r)\,\mathrm{e}^{-\mathcal{H}} \tag{49}$$

with the normalization constant $\mathcal{N}' = \int \mathcal{D}(\{a_j\})\exp\{-\mathcal{H}\}$. The densities $a_i(x_i)$ are place holders for any OP component or secondary density corresponding to the dynamic variables introduced in the previous sections. Cumulants and two-point vertex functions are analogously introduced as presented in (26)–(31). The different secondary densities do not couple among each other in the extended functional (48). Therefore, correlations between different secondary densities in (49) factorize and the corresponding cumulants and also the vertex functions vanish. The only nonvanishing vertex functions of the Gaussian secondary densities without static OP coupling $\{m_{i0}\}$ and j_0 are the two-point vertex functions $\mathring{\Gamma}_{m_i m_i} = \mathring{\Gamma}_{jj} = 1$ corresponding to (40) and (42). Only vertex functions which emanate from cumulants containing the OP and/or the coupled secondary densities $\{m_{i0}\}$ are nontrivial. The OP and the secondary densities $\{m_{i0}\}$ are not coupled in the Gaussian part, thus all two-point cumulants $\langle\varphi_0\ m_{i0}\rangle_c$ are zero and the OP cumulant $\langle\varphi_0\ \varphi_0\rangle_c$ and the cumulants $\langle m_{i0}\ m_{j0}\rangle_c$ can be treated separately. According to (47) only the two-point vertex functions $\mathring{\Gamma}_{\varphi\varphi^+}(\mathring{\tau},\mathring{\tilde{u}},\mathring{\gamma},k)$ and $\mathring{\Gamma}_{m_M m_M}(\mathring{\tau},\mathring{\tilde{u}},\mathring{\gamma},k)$ have to be calculated.

As previously mentioned, the extended static functional does not add any new static critical behaviour compared with the GLW functional. Thus, the additional parts in (48) coming from the secondary densities may be integrated out. The integration of the Gaussian functions $\exp\{-\mathcal{H}_m^{(Nv)}\}$ and $\exp\{-\mathcal{H}_j\}$ delivers only constant factors, which are cancelled by the normalization constant in which the integration must also be performed, so that the parameters $\mathring{\tau}$ and $\mathring{\tilde{u}}$ in (38) are not affected by the procedure. But the integration of $\exp\{-\mathcal{H}_m^{(Ms)}\}$ (particularly the contribution of m_{M0}) leads to shifted parameters which have to be equal to the parameters in the GLW functional (24). Thus, one obtains the relations

$$\mathring{r} = \mathring{\tau} + \mathring{\gamma}\mathring{h}, \qquad \mathring{u} = \mathring{\tilde{u}} - 3\mathring{\gamma}^2 \tag{50}$$

between the parameters of the GLW and the extended functional. Using the relations in (50), one can immediately see by a simple internal rearrangement that the OP two-point vertex function of the extended static functional and the GLW functional are identical, that is

$$\mathring{\Gamma}^{(ext)}_{\varphi\varphi^+}(\mathring{\tau},\mathring{\tilde{u}},\mathring{\gamma},k) = \mathring{\Gamma}_{\varphi\varphi^+}(\mathring{r},\mathring{u},k). \tag{51}$$

The introduction of the T_c-shift and the correlation length leads to the same function $\mathring{\Gamma}_{\varphi\varphi^+}(\xi^{-2},\mathring{u},k)$ as presented in the previous subsection. Applying the same procedure together with (50) to the secondary density vertex function leads to

$$\mathring{\Gamma}_{m_M m_M}(\mathring{\tau},\mathring{\tilde{u}},\mathring{\gamma},k) = \mathring{\Gamma}^{(s)}_{mm}(\xi^{-2},\mathring{u},\mathring{\gamma},k) = \left[\mathring{C}^{(s)}_{mm}(\xi^{-2},\mathring{u},\mathring{\gamma},k)\right]^{-1}. \tag{52}$$

We dropped the index M in the second expression because only one function exists after the 'orthogonalization' procedure.

The reduction of the extended static functional to the GLW functional also implies that correlation functions of the density m_{M0} calculated with (49) are related to correlations of the OP calculated with (25). For the expectation value and the two-point correlation function, one obtains the relations

$$\langle m_{M0}(x)\rangle = \mathring{h} - \mathring{\gamma}\left\langle\tfrac{1}{2}|\vec{\varphi}_0(x)|^2\right\rangle, \tag{53}$$

$$\langle m_{M0}(x)m_{M0}(0)\rangle_c = 1 + \mathring{\gamma}^2\left\langle\tfrac{1}{2}|\vec{\varphi}_0(x)|^2\,\tfrac{1}{2}|\vec{\varphi}_0(0)|^2\right\rangle_c. \tag{54}$$

The external field $\mathring{h}$ introduced in (40) and (47) is used to eliminate the finite expectation value of m_{M0}. Choosing $\mathring{h} = \mathring{\gamma}\left\langle\frac{1}{2}|\vec{\varphi}_0(x)|^2\right\rangle$, we have $\langle m_{M0}(x)\rangle = 0$ from (53).

6. Dynamic correlation and vertex functions

6.1. Relation between dynamic correlation and vertex functions

Quite analogous to the correlation functions in statics composed with the corresponding static functional, the dynamic correlation functions are defined as

$$\langle \alpha_1(x_1,t_1)\cdots\alpha_r(x_r,t_r)\rangle = \frac{1}{\mathcal{N}_D}\int \mathcal{D}(\{a_j\},\{\tilde{a}_j\})\alpha_1(x_1,t_1)\cdots\alpha_r(x_r,t_r)\,\mathrm{e}^{-\mathcal{J}} \tag{55}$$

with the dynamic functional $\mathcal{J}$ introduced in (23) and the normalization is $\mathcal{N}_D = \int \mathcal{D}(\{a_j\},\{\tilde{a}_j\})\,\mathrm{e}^{-\mathcal{J}}$. The time-dependent densities $\alpha_i(x,t)$ now represent any dynamic variable $a_i(x,t)$ (OP component or secondary density) or auxiliary density $\tilde{a}_i(x,t)$. The dynamic cumulants are introduced in the same way as it has been done with the static correlation functions in (26). The Fourier transform of the dynamic two-point cumulants is usually introduced as

$$\begin{aligned}\langle \alpha_i(k_1,\omega_1)\alpha_j(k_2,\omega_2)\rangle_c = \int \mathrm{d}x_1 \int \mathrm{d}t_1 \int \mathrm{d}x_2 \int \mathrm{d}t_2 \langle \alpha_i(x_1,t_1)\alpha_j(x_2,t_2)\rangle_c \\ \times \exp(-(\mathrm{i}k_1x_1 + \mathrm{i}k_2x_2))\exp(\mathrm{i}\omega_1t_1 + \mathrm{i}\omega_2t_2).\end{aligned} \tag{56}$$

As in section 5, the correlations are invariant under translations in space and now also under translations in time. This means $\langle \alpha_1(x_1,t_1)\alpha_j(x_2,t_2)\rangle_c = \langle \alpha_i(x_1-x_2,t_1-t_2)\alpha_j(0,0)\rangle_c$ from which follows

$$\langle \alpha_i(k_1,\omega_1)\alpha_j(k_2,\omega_2)\rangle_c = \langle \alpha_i(k_1,\omega_1)\alpha_j(-k_1,-\omega_1)\rangle_c \delta(k_1+k_2)\delta(\omega_1+\omega_2). \tag{57}$$

The auxiliary densities introduced in the current approach for the dynamic functional provide a slightly more elaborate connection between cumulants and vertex functions as in statics. The two-point vertex function is the inverse of the two-point cumulant quite analogous to statics indeed, but we now have to incorporate the matrix structure of the functions. Introducing the dynamic correlation matrix $\mathring{\boldsymbol{C}}(k,\omega)$ with components

$$\mathring{C}_{\alpha_i\alpha_j}(k,\omega) = \langle \alpha_i(k,\omega)\alpha_j(-k,-\omega)\rangle_c, \tag{58}$$

a special structure can be observed when the indices i and j are first running over all dynamic variables a and then over all corresponding auxiliary densities $\tilde{a}$. If the densities are ordered in this way, the matrices of the dynamic two-point correlation functions and two-point vertex functions are related by

$$\begin{aligned}\mathring{\boldsymbol{C}}(k,\omega) &= \begin{pmatrix} [\mathring{C}_{a_ia_j}](k,\omega) & [\mathring{C}_{\tilde{a}_ia_j}](k,\omega) \\ [\mathring{C}_{a_i\tilde{a}_j}](k,\omega) & [0] \end{pmatrix} \\ &= \begin{pmatrix} [0] & [\mathring{\Gamma}_{a_i\tilde{a}_j}](-k,-\omega) \\ [\mathring{\Gamma}_{\tilde{a}_ia_j}](-k,-\omega) & [\mathring{\Gamma}_{\tilde{a}_i\tilde{a}_j}](-k,-\omega) \end{pmatrix}^{-1} = \mathring{\boldsymbol{\Gamma}}^{-1}(-k,-\omega).\end{aligned} \tag{59}$$

From the structure in (59) follows that the nondiagonal submatrices fulfil the relation

$$[\mathring{C}_{a_i\tilde{a}_j}](k,\omega) = [\mathring{\Gamma}_{\tilde{a}_ia_j}]^{-1}(-k,-\omega). \tag{60}$$

The perturbation expansion in dynamics is performed quite analogous to statics described in section 5.1. In order to obtain the dynamic vertex functions in (59), which determine the correlation functions related to experimental quantities as will be discussed subsequently, all one-particle irreducible graphical contributions with two external legs have to be collected in a given order.

6.2. General structure of the dynamic vertex functions

From (59) one can see that in the current approach for every pair of densities a_i, a_j three types of dynamic functions, namely $\mathring{\Gamma}_{a_i\tilde{a}_j}$, $\mathring{\Gamma}_{\tilde{a}_i a_j}$ and $\mathring{\Gamma}_{\tilde{a}_i\tilde{a}_j}$, exist. Due to general properties and internal structures only a small subset of all these functions really has to be calculated as shown in the following.

- In the case of real KCs, the correlation matrix $\mathring{\boldsymbol{C}}$ and also the matrix of vertex functions $\mathring{\boldsymbol{\Gamma}}$ are Hermitian, thus the nondiagonal submatrices have the property $\big[\mathring{\Gamma}_{\tilde{a}_i a_j}\big] = \big[\mathring{\Gamma}_{a_i\tilde{a}_j}\big]^+$.
- Recently [72], a closer examination of the two loop expansion has revealed that the dynamic response vertex functions $\mathring{\Gamma}_{a_i\tilde{a}_j}$ have the general structure

$$\mathring{\Gamma}_{a_i\tilde{a}_j}(\xi, k, \omega) = -\mathrm{i}\omega\mathring{\Omega}_{a_i\tilde{a}_j}(\xi, k, \omega) + \sum_l \mathring{\Gamma}^{(s)}_{a_i a_l}(\xi, k)\mathring{\Gamma}^{(d)}_{a_l\tilde{a}_j}(\xi, k, \omega) \tag{61}$$

  where $\mathring{\Gamma}_{a_i a_j}(\xi, k)$ is the static two-point vertex function of the GLW model and $\mathring{\Omega}_{a_i\tilde{a}_j}$ and $\mathring{\Gamma}^{(d)}_{a_i\tilde{a}_j}$ are purely dynamic functions. We expect that this structure also holds in higher loop order although this has not been proven. Quite analogous as discussed in the mentioned sections, the singularities at $d = 3$ have been absorbed by introducing the parameter $\mathring{r}_c$ for the T_c-shift and the correlation length $\xi(\mathring{r} - \mathring{r}_c)$. Therefore, ξ enters as an argument in all functions.
- The dynamic vertex functions $\mathring{\Gamma}_{\tilde{a}_i\tilde{a}_j}$ can be expressed by the functions $\mathring{\Omega}_{a_i\tilde{a}_j}$ and $\mathring{\Gamma}^{(d)}_{a_i\tilde{a}_j}$ via the relation

$$\mathring{\Gamma}_{\tilde{a}_i\tilde{a}_j}(k, \omega) = -2\sum_l \mathrm{Re}\big[\mathring{\Omega}_{a_i\tilde{a}_i}(k, \omega)\mathring{\Gamma}^{(d)}_{a_i\tilde{a}_j}(k, \omega)\big]. \tag{62}$$

Thus, the knowledge of the two functions $\mathring{\Omega}_{a_i\tilde{a}_j}$ and $\mathring{\Gamma}_{a_i\tilde{a}_j}$ completely determines the matrix of vertex functions in (59).

6.3. Lowest order of the dynamic vertex functions

In lowest order, the dynamic functions appearing in (61) are

$$\mathring{\Omega}^{(0)}_{a_i\tilde{a}_j}(k, \omega) = \Delta_{ij}(k, \omega) \tag{63}$$

with

$$\Delta_{ij}(k, \omega) = \begin{cases} \delta_{ij} & \text{for any real densities } a_i, \tilde{a}_j \\ 1 - \delta_{ij} & \text{for every pair of conjugated densities } a_i, \tilde{a}_j = \tilde{a}_i^+ \end{cases} \tag{64}$$

and

$$\mathring{\Gamma}^{(d)(0)}_{a_i\tilde{a}_j}(k, \omega) = \mathring{L}_{ij}(k). \tag{65}$$

In section 3, the structure of $\mathring{L}_{ij}$ has been discussed. For the (Fourier transformed) KCs, one has

$$\mathring{L}_{ij}(k) = \begin{cases} \mathring{\Lambda}_{ij}k^2 & \text{for any conserved real densities } a_i, a_j \\ \mathring{\Lambda}_{ij} & \text{for any non-conserved real densities } a_i, a_j \\ (1 - \delta_{ij})2\mathring{\Lambda}_i & \text{for any pair of non-conserved densities } a_i, a_j = a_i^+. \end{cases} \tag{66}$$

The lowest order of the static vertex function is simply

$$\mathring{\Gamma}^{(s)(0)}_{a_i a_j}(k) = \mathring{\chi}^{-1}_{ij}(k) \tag{67}$$

with

$$\mathring{\chi}_{ij}^{-1}(k) = \begin{cases} (\mathring{r} + k^2) & \text{if } a_i = a_j = \phi \text{ is the real OP} \\ (1 - \delta_{ij})\frac{1}{2}(\mathring{r} + k^2) & \text{if } \{a_i, a_j\} = \{\psi, \psi^+\} \text{ correspond to a complex OP} \\ \delta_{ij} & \text{for any secondary densities } a_i, a_j\ . \end{cases} \tag{68}$$

Thus the zeroth order of the response vertex functions is

$$\mathring{\Gamma}^{(0)}_{a_i\tilde{a}_j}(k,\omega) = -\mathrm{i}\omega\Delta_{ij} + \sum_l \mathring{\chi}^{-1}_{il}\mathring{L}_{lj}(k). \tag{69}$$

From relations (62) and (69), one obtains

$$\mathring{\Gamma}^{(0)}_{\tilde{a}_i\tilde{a}_j}(k,\omega) = -2\,\mathrm{Re}[\mathring{L}_{ij}(k)]. \tag{70}$$

Inserting (69) and (70) into (59) leads to the zeroth order of the correlation matrix which represents the dynamic propagators of the system.

6.4. Simplifications of the structure in special models

In section 6.2, we have considered the general expressions of the dynamic vertex functions and the structures therein. In concrete models considered in this review, the matrices simplify considerably for several reasons.

Models without secondary densities. Some of the models (A, B, J) include only the order parameter. In this case, (59) reduces to a relation between two-dimensional matrices for a real OP and four-dimensional matrices for a complex OP. In both cases, the connection between the dynamic correlation function and the dynamic vertex functions is

$$\mathring{C}_{\varphi\varphi^+}(\xi,k,\omega) = -\frac{\mathring{\Gamma}_{\tilde{\varphi}\tilde{\varphi}^+}(\xi,-k,-\omega)}{|\mathring{\Gamma}_{\varphi\tilde{\varphi}^+}(\xi,-k,-\omega)|^2}. \tag{71}$$

From (61) and (62) follows for the structure of the dynamic vertex functions

$$\mathring{\Gamma}_{\varphi\tilde{\varphi}^+}(\xi,k,\omega) = -\mathrm{i}\omega\mathring{\Omega}_{\varphi\tilde{\varphi}^+}(\xi,k,\omega) + \mathring{\Gamma}^{(s)}_{\varphi\varphi^+}(\xi,k)\mathring{\Gamma}^{(d)}_{\varphi\tilde{\varphi}^+}(\xi,k,\omega) \tag{72}$$

and

$$\mathring{\Gamma}_{\tilde{\varphi}\tilde{\varphi}^+}(\xi,k,\omega) = -2\,\mathrm{Re}\big[\mathring{\Omega}_{\varphi\tilde{\varphi}^+}(\xi,k,\omega)\mathring{\Gamma}^{(d)}_{\varphi\tilde{\varphi}^+}(\xi,k,\omega)\big]. \tag{73}$$

So far in the static and dynamic functions only ξ, k and ω have been mentioned explicitly as arguments for convenience. Of course, these functions also depend on the model parameters, which are the static couplings $\mathring{u}, \mathring{\gamma}$, the kinetic coefficients $\mathring{\Lambda}_{ij}$ and mode coupling parameters $\mathring{g}_i$. The latter are parameters defined from (2) and describe the reversible part of the dynamic equations. In the dynamic models considered in this review, the term $\delta Q_{ij}/\delta a_j^+$ in (2) does not contribute. In this case, the mode coupling parameters are defined by $Q_{ij} = k_B T\{a_i, a_j^+\} = g_{ij} f(\{a\})$, where $f(\{a\})$ contains secondary densities which may appear in the Poisson bracket (see also section 7.2). The couplings g_{ij} are divided into sets including mode couplings with the same cut-off dimension. Each set is represented by a mode coupling $\mathring{g}_i$. A closer look at the two dynamic functions $\mathring{\Omega}_{\varphi\tilde{\varphi}^+}$ and $\mathring{\Gamma}^{(d)}_{\varphi\tilde{\varphi}^+}$ as functions of the model parameters reveals a further general structure valid in all dynamic models, which is important for the determination of the dynamic exponent z_φ in the subsequent sections. $\mathring{\Omega}_{\varphi\tilde{\varphi}^+}$ can be written as

$$\mathring{\Omega}_{\varphi\tilde{\varphi}^+} = 1 + \mathring{\Omega}_R(\mathring{u}^2) + \sum_i \mathring{\gamma}_i \mathring{W}^{(i)}_{\varphi\tilde{\varphi}^+}(\mathring{u}, \{\mathring{\gamma}_l\}, \{\mathring{\Lambda}_{kl}\}, \{\mathring{g}_l\}). \tag{74}$$

In the above expression, even the case of the existence of several static couplings $\{\mathring{\gamma}_i\}$ has been incorporated. The function $\mathring{\Omega}_R$ only contains contributions from the static coupling $\mathring{u}$ and represents the result for model A/B in the case of a non-conserved/conserved OP. All other contributions are proportional to the static couplings $\mathring{\gamma}_i$. This means that in all models without static couplings $\mathring{\gamma}_i$ the function $\mathring{\Omega}_{\varphi\tilde{\varphi}^+} = 1 + \mathring{\Omega}_R(\mathring{u}^2)$ is simply determined by model A/B although these models may include mode couplings $\{\mathring{g}_i\}$. This is in contrast to the structure of $\mathring{\Gamma}^{(d)}_{\varphi\tilde{\varphi}^+}$ which is determined by the mode couplings $\{\mathring{g}_i\}$. The kinetic coefficient $\mathring{\Lambda}_{\varphi\varphi^+}$ for the OP is usually denoted by $\mathring{\Lambda}_{\varphi\varphi^+} = 2\mathring{\Gamma}$ in the case of a complex OP and $\mathring{\Lambda}_{\phi\phi} = \mathring{\Gamma}$ for a real OP. Using this notation, one obtains

$$\mathring{\Gamma}^{(d)}_{\varphi\tilde{\varphi}^+} = 2\mathring{\Gamma}k^a + \sum_i \mathring{g}_i \mathring{G}^{(i)}_{\varphi\tilde{\varphi}^+}(\mathring{u}, \{\mathring{\gamma}_l\}, \{\mathring{\Lambda}_{kl}\}, \{\mathring{g}_l\}). \tag{75}$$

The exponent a in the first term of (75) is 0 for a non-conserved and 2 for a conserved OP. All nontrivial contributions to the function are proportional to the mode couplings, thus this function is simply $2\mathring{\Gamma}k^a$ in all models without mode couplings. The explicit expressions of the functions $\mathring{W}^{(i)}_{\varphi\tilde{\varphi}^+}$ and $\mathring{G}^{(i)}_{\varphi\tilde{\varphi}^+}$ depend of course on the considered dynamic model. For conserved OPs ($a = 2$), the function $\mathring{G}^{(i)}_{\varphi\tilde{\varphi}^+}$ can be written as

$$\mathring{G}^{(i)}_{\varphi\tilde{\varphi}^+} = 2\mathring{\Gamma}k^2 \mathring{\tilde{G}}^{(i)}_{\varphi\tilde{\varphi}^+} \tag{76}$$

where $\mathring{\tilde{G}}^{(i)}_{\varphi\tilde{\varphi}^+}$ is finite at $k = 0$. Therefore, the dynamic vertex function (75) is proportional to k^2 and can be written as

$$\mathring{\Gamma}^{(d)}_{\varphi\tilde{\varphi}^+} = 2\mathring{\Gamma}k^2 \left[1 + \sum_i \mathring{g}_i \mathring{\tilde{G}}^{(i)}_{\varphi\tilde{\varphi}^+}(\mathring{u}, \{\mathring{\gamma}_l\}, \{\mathring{\Lambda}_{kl}\}, \{\mathring{g}_l\})\right] \tag{77}$$

for conserved OPs.

Models with decoupled dissipation of OP and secondary densities. The OP and the secondary densities are considered as dynamically decoupled if the matrix of the KCs (66) contains no cross coefficients $L_{\varphi\alpha_k}$ between them. There are two classes of models in which the OP and the secondary densities decouple:

- Models with relaxing OP (models C, E, F, G). Kinetic cross coefficients cannot exist between relaxing and conserved densities and the secondary densities are always conserved.
- Models with conserved scalar OP and the conserved secondary density being a vector or vector component (model H). Kinetic cross coefficients exist only for densities which have the same behaviour regarding the time inversion. The scalar OP is invariant (even) under time inversion while vectors like magnetizations or current densities change sign (odd).

In these cases, the structure of the matrices in (59) allows the separation into submatrices only containing the OP functions and submatrices only containing the functions corresponding to the secondary densities. The OP functions fulfil the same relations (71)–(75) as described above. The correlation functions of the secondary densities can then be calculated within the subspace of the secondary densities analogous to (59) with

$$\begin{pmatrix} [\mathring{C}_{\beta_i\beta_j}](k,\omega) & [\mathring{C}_{\tilde{\beta}_i\beta_j}](k,\omega) \\ [\mathring{C}_{\beta_i\tilde{\beta}_j}](k,\omega) & [0] \end{pmatrix} = \begin{pmatrix} [0] & [\mathring{\Gamma}_{\beta_i\tilde{\beta}_j}](-k,-\omega) \\ [\mathring{\Gamma}_{\tilde{\beta}_i\beta_j}](-k,-\omega) & [\mathring{\Gamma}_{\tilde{\beta}_i\tilde{\beta}_j}](-k,-\omega) \end{pmatrix}^{-1}, \tag{78}$$

where β is a placeholder for any secondary density m_{i0} or j_0. The dynamic response vertex functions of the secondary densities have the general structure

$$\mathring{\Gamma}_{\beta_i\tilde{\beta}_j}(\xi,k,\omega) = -\mathrm{i}\omega\mathring{\Omega}_{\beta_i\tilde{\beta}_j}(\xi,k,\omega) + \sum_l \mathring{\Gamma}^{(s)}_{\beta_i\beta_l}(\xi,k)\mathring{\Gamma}^{(d)}_{\beta_l\tilde{\beta}_j}(\xi,k,\omega). \tag{79}$$

The sum covers the number of secondary densities. $\mathring{\Gamma}_{\beta_i\beta_l}(\xi,k)$ are components of the matrix of the static two-point vertex functions calculated with the extended static functional (48) as described in section 5.2. A relation corresponding to (73) also holds for the dynamic vertex functions of the secondary densities. It reads

$$\mathring{\Gamma}_{\tilde{\beta}_i\tilde{\beta}_j}(\xi,k,\omega) = -2\sum_l \mathrm{Re}\left[\mathring{\Omega}_{\beta_l\tilde{\beta}_i}(\xi,k,\omega)\mathring{\Gamma}^{(d)}_{\beta_l\tilde{\beta}_j}(\xi,k,\omega)\right]. \tag{80}$$

Considering the dependence on the model parameters, an analogous structure to (74) and (75) can be found. One has

$$\mathring{\Omega}_{\beta_i\tilde{\beta}_j} = \delta_{ij} + \mathring{\gamma}_i\mathring{W}_{\tilde{\beta}_j}(\mathring{u},\{\mathring{\gamma}_l\},\{\mathring{\Lambda}_{kl}\},\{\mathring{g}_l\}) \tag{81}$$

and

$$\mathring{\Gamma}^{(d)}_{\beta_i\tilde{\beta}_j} = \mathring{\Lambda}_{ij}k^2 + \mathring{g}_i\mathring{G}_{\tilde{\beta}_j}(\mathring{u},\{\mathring{\gamma}_l\},\{\mathring{\Lambda}_{kl}\},\{\mathring{g}_l\}). \tag{82}$$

Like the corresponding dynamic OP functions these functions again have the same feature that the static couplings $\mathring{\gamma}_i$ and the mode couplings $\mathring{g}_i$ determine which of the two functions in (81) and (82) is trivial. In systems without static couplings (models E, G, H), we have simply $\mathring{\Omega}_{\beta_i\tilde{\beta}_j} = \delta_{ij}$. In contrast, in systems without mode couplings (model C) it follows from (82) that $\mathring{\Gamma}^{(d)}_{\beta_i\tilde{\beta}_j} = \mathring{\Lambda}_{ij}k^2$. The functions $\mathring{W}_{\tilde{\beta}_j}$ and $\mathring{G}_{\tilde{\beta}_j}$ depend on the precise dynamic model which is considered. The dynamic vertex functions (82) are proportional to k^2 and can be written quite analogously to (77) as

$$\mathring{\Gamma}^{(d)}_{\beta_i\tilde{\beta}_j} = k^2[\mathring{\Lambda}_{ij} + \mathring{g}_i\mathring{\hat{G}}_{\tilde{\beta}_j}(\mathring{u},\{\mathring{\gamma}_l\},\{\mathring{\Lambda}_{kl}\},\{\mathring{g}_l\})] \tag{83}$$

with finite functions $\mathring{\hat{G}}_{\tilde{\beta}_j} = \mathring{G}_{\tilde{\beta}_j}/k^2$ at $k = 0$. In the current review, we consider dynamic models with one or two secondary densities. If only one secondary density is present, the corresponding kinetic coefficient $\mathring{\Lambda}_{11}$ will be denoted by $\mathring{\lambda}$. In the case of two secondary densities, the notation used in the following depends on whether the two densities are coupled ($\mathring{\Lambda}_{12} \neq 0$) or not ($\mathring{\Lambda}_{12} = 0$) in their dissipative modes. Secondary densities of different vector type, as for instance energy density (scalar) and a magnetization (vector), do not couple dissipatively thus the kinetic coefficients $\mathring{\Lambda}_{ii}$ are denoted by λ_e, λ_m and so on. In the case of two scalar secondary densities, the dissipative coupling exists and a matrix

$$[\mathring{\Lambda}_{ij}] = \begin{pmatrix} \mathring{\lambda} & \mathring{L} \\ \mathring{L} & \mathring{\mu} \end{pmatrix} \equiv \mathring{\mathbf{\Lambda}} \tag{84}$$

will be used.

6.5. Relation to experimentally measurable quantities

In the previous section, we have discussed the structure of the unrenormalized dynamic vertex functions in an abstract manner. These functions are important because they are on the one hand directly calculable in perturbation theory and on the other hand related to experimentally accessible quantities. Basically there are two fields where a connection to experimental quantities exists.

Correlation functions. In scattering experiments usually correlation functions $\langle a_i(k,\omega)a_j(-k,-\omega)\rangle_c$ at finite k and ω can be measured. This may be the OP correlation function, as for instance the spin correlation in magnets measured with neutron scattering

experiments, or the mass density correlation in liquids at the gas/liquid critical point measured with light scattering. But also correlation functions corresponding to secondary densities may be measured by inelastic light scattering like the density correlation in ^{4}He at the superfluid transition. Within the theoretical approach, the relation between dynamic vertex functions and correlation functions is generally given by (59) and for special cases in (71) and (78).

Hydrodynamic modes. In the case of conserved densities, the generalized Poisson brackets in the dynamic equations (1) are constructed in a way that they also define the corresponding reversible hydrodynamic equations. The same is true for the dissipative part where the structure of the Onsager coefficients in hydrodynamics determines the structure of the KCs in the matrix L_{ij}. The main difference between hydrodynamic equations and the dynamic equations (1) is that the latter use a non-Gaussian static functional, which also includes gradient terms, leading to nonlinear terms in the dynamic equations. With a purely Gaussian functional $H = \int \mathrm{d}^d x \sum_i a_i^2/2$, equations (1) reduce to the corresponding hydrodynamic equations. Accordingly, the lowest order of the dynamic vertex functions reflects the Fourier-transformed hydrodynamic equations (see section 6.3). The determinant of the coefficient matrix Δ_H of the Fourier-transformed linearized (in the densities) hydrodynamic equations can be factorized into dissipative modes [73]. These modes have to be compared with the modes resulting from the matrix of dynamic vertex functions $\mathring{\Gamma}_{a_i\tilde{a}_j}$. Typical dissipative modes are as follows:

(i) The diffusion process with diffusion coefficient D. It is determined by the equation

$$\frac{\partial a(x,t)}{\partial t} = D\nabla^2 a(x,t) \qquad \text{or} \qquad (-\mathrm{i}\omega + Dk^2)a(k,\omega) = 0 \tag{85}$$

leading to a hydrodynamic determinant $\Delta_H = -\mathrm{i}\omega + Dk^2$. The diffusion coefficient D does not depend on k and ω. One has to compare (85) with

$$\mathring{\Gamma}_{a\tilde{a}}(\xi,k,\omega) = -\mathrm{i}\omega\mathring{\Omega}_{a\tilde{a}}(\xi,k,\omega) + \mathring{\Gamma}^{(s)}_{aa}(\xi,k)\mathring{\Gamma}^{(d)}_{a\tilde{a}}(\xi,k,\omega) \tag{86}$$

taken in the hydrodynamic limit. The functions $\mathring{\Omega}_{a\tilde{a}}$ and $\mathring{\Gamma}^{(d)}_{a\tilde{a}}$ have special properties in the limit $\omega \to 0, k \to 0$ when a is a conserved density. At first (77) and (83) imply that we can write

$$\mathring{\Gamma}^{(d)}_{a\tilde{a}}(\xi,k,\omega) = k^2 \mathring{f}^{(d)}_{a\tilde{a}}(\xi,k,\omega) \tag{87}$$

where $\mathring{f}^{(d)}_{a\tilde{a}}(\xi,0,0)$ is a finite function. And secondly the function $\mathring{\Omega}_{a\tilde{a}}(\xi,k,\omega)$ has the property

$$\mathring{\Omega}_{a\tilde{a}}(\xi,0,0) = 0. \tag{88}$$

Thus, in the hydrodynamic limit (86) reduces to

$$\mathring{\Gamma}_{a\tilde{a}}(\xi,k,\omega) = -\mathrm{i}\omega + \mathring{\Gamma}^{(s)}_{aa}(\xi,0)\mathring{f}^{(d)}_{a\tilde{a}}(\xi,0,0)k^2. \tag{89}$$

Comparing with (85) immediately leads to

$$D = \mathring{\Gamma}^{(s)}_{aa}(\xi,0)\mathring{f}^{(d)}_{a\tilde{a}}(\xi,0,0) = \left.\frac{\partial\mathring{\Gamma}_{a\tilde{a}}(\xi,k,0)}{\partial k^2}\right|_{k=0}. \tag{90}$$

The above equation relates an experimental diffusion coefficient D to unrenormalized response vertex functions.

For several coupled diffusive processes, the procedure is quite analogous with the difference that the hydrodynamic determinant is a more complex expression. Considering the system of equations

$$\frac{\partial a_i(x,t)}{\partial t} = -\sum_j D_{ij}\nabla^2 a_j(x,t) \qquad \text{or} \qquad \sum_j(-\mathrm{i}\omega\delta_{ij} + D_{ij}k^2)a_j(k,\omega) = 0 \tag{91}$$

where D_{ij} is a nondiagonal matrix, the hydrodynamic determinant is now written in terms

of the eigenvalues λ_i of the matrix D_{ij}. With an orthogonal transformation determined by the eigenvectors, the matrix D_{ij} turns into a diagonal matrix. Assuming that there are r eigenvalues, the determinant is simply

$$\Delta_H = (-\mathrm{i}\omega + \lambda_1 k^2)(-\mathrm{i}\omega + \lambda_2 k^2)\cdots(-\mathrm{i}\omega + \lambda_r k^2) \tag{92}$$

where the eigenvalues $\lambda_i = \lambda_i(\{D_{ij}\})$ are functions of the diffusion coefficients. This has to be compared with the determinant calculated from the matrix

$$\begin{aligned}\mathring{\Gamma}_{a_i\tilde{a}_j}(\xi,k,\omega) &= -\mathrm{i}\omega\delta_{ij} + \sum_l \mathring{\Gamma}^{(s)}_{a_i a_l}(\xi,0)\,\mathring{f}^{(d)}_{a_l\tilde{a}_j}(\xi,0,0)k^2 \\ &= -\mathrm{i}\omega\delta_{ij} + \left.\frac{\partial\mathring{\Gamma}_{a_i\tilde{a}_j}(\xi,k,0)}{\partial k^2}\right|_{k=0} k^2. \end{aligned}\tag{93}$$

(ii) In order to obtain the critical behaviour of the sound velocity and sound attenuation, extended dynamic models (not considered explicitly in this review) may be introduced. They include additional dynamic equations for variables, which are necessary for sound propagation. In systems with a dynamics based on hydrodynamic equations these are for instance the equations for the mass density ρ and the longitudinal mass current j_l. Such extended models have been established in ^{4}He [35] and ^{3}He–^{4}He mixtures at the λ-transition [74] or in liquids at the gas/liquid transition and binary mixtures at the gas/liquid and liquid/liquid transition [34]. The additional equations lead to a dissipative mode of the form $\omega^2 + \mathrm{i}\omega D_s k^2 - c_s^2 k^2$. The coefficient c_s denotes the sound velocity and D_s is related to the sound attenuation.

In these extended models, a new type of dynamic response vertex functions appears which is different from (87) in its k-dependence. The dynamic vertex functions $\mathring{\Gamma}_{a_i\tilde{j}_l}$ and $\mathring{\Gamma}_{j_l\tilde{a}_i}$ corresponding to j_l have the structure

$$\mathring{\Gamma}^{(d)}_{j_l\tilde{a}_i}(\xi,k,\omega) = \mathrm{i}k\,\mathring{f}^{(d)}_{j_l\tilde{a}_i}(\xi,k,\omega), \tag{94}$$

$$\mathring{\Gamma}^{(d)}_{a_i\tilde{j}_l}(\xi,k,\omega) = \mathrm{i}k\,\mathring{f}^{(d)}_{a_i\tilde{j}_l}(\xi,k,\omega), \tag{95}$$

where a_i denotes any scalar density in the considered model. Again $\mathring{f}^{(d)}_{j_l\tilde{a}_i}(\xi,0,0)$ and $\mathring{f}^{(d)}_{a_i\tilde{j}_l}(\xi,0,0)$ are finite functions.

Thus, in general the dissipative modes for conserved densities may have the structure

$$\Delta_H = (-\mathrm{i}\omega + \lambda_1 k^2)\cdots(-\mathrm{i}\omega + \lambda_r k^2)\left(\omega^2 + D_s\mathrm{i}\omega k^2 - c_s^2 k^2\right) \tag{96}$$

when the hydrodynamic equations include r diffusion modes and one sound mode. Therefore, it is obvious to compare the coefficients in the hydrodynamic modes with the corresponding expressions calculated from the matrix of dynamic vertex functions. Of course, this leads to more complex relations (see for instance [34]) between experimental quantities and field-theoretic vertex functions compared to (90).

7. Renormalization and field-theoretic functions

So far we have given a survey over the definitions and properties of the unrenormalized functions and parameters usually appearing in models describing the critical dynamic behaviour. Experimentally accessible quantities can be related to unrenormalized dynamic vertex functions or correlation functions, which once again are related to dynamic vertex functions within the considered approach. By introducing the T_c-shift and the correlation function in the static functions as well as in the dynamic functions and applying the general structure (61) and (62) within dynamics, all functions are in a form ready to apply any field-theoretic renormalization scheme.

Several field-theoretic renormalization approaches are available in the literature. They can be roughly separated into two classes. The approaches in the first class use ε-expansion ($\varepsilon = 4 - d$) and extrapolate the obtained expressions to $\varepsilon = 1$ ($d = 3$). For the method using normalization conditions see [75], for the minimal subtraction scheme see [76]. The approaches in the second class avoid the ε-expansion and calculate all functions directly at $d = 3$ where the theory is super-renormalizable [64]. A renormalization scheme using the minimal subtraction scheme while calculating the finite amplitudes at $d = 3$ has been developed in [66].

7.1. Renormalization of the static parameters

GLW functional. The renormalization of the Ginzburg–Landau–Wilson functional (24) is well known within different renormalization schemes [64, 66, 75, 76]. Assuming in general a complex OP $\vec{\varphi}$, we define its renormalization constant (RC) Z_φ by

$$\vec{\varphi}_0 = Z_\varphi^{1/2}\vec{\varphi}, \qquad \vec{\varphi}_0^+ = Z_\varphi^{1/2}\vec{\varphi}^+ \tag{97}$$

where Z_φ is a real quantity and identical to the RC Z_ϕ for a real OP $\vec{\phi}$. For the renormalization of the fourth-order coupling u appearing in (24), the RC Z_u is introduced as

$$\mathring{u} = \kappa^\varepsilon Z_\varphi^{-2} Z_u u A_d^{-1}, \tag{98}$$

where κ represents a free wave number scale. For convenience we have introduced the geometry factor

$$A_d = \Gamma\left(1 - \frac{\varepsilon}{2}\right)\Gamma\left(1 + \frac{\varepsilon}{2}\right)\frac{\Omega_d}{(2\pi)^d} \tag{99}$$

with d the spatial dimension,

$$\Omega_d = 2\pi^{d/2}/\,\Gamma(d/2) \tag{100}$$

the surface of the d-dimensional unit sphere and $\Gamma(x)$ the Euler Γ-function. The RCs introduced so far are not enough in order to make all static vertex functions finite. Vertex functions with $|\varphi|^2$-insertions contain poles which cannot be absorbed by Z_φ and Z_u. Thus, a Z_φ-factor

$$|\varphi_0|^2 = Z_{\varphi^2}|\varphi|^2 \tag{101}$$

is necessary to renormalize vertex functions containing $|\varphi|^2$-insertions. At least the correlation function $\langle|\varphi_0|^2|\varphi_0|^2\rangle_c$, which represents the specific heat within the GLW model, needs an additive renormalization $A_{\varphi^2}(u)$.

The renormalization described so far is not restricted to a special approach. The RCs may be determined by normalization conditions or within the minimal subtraction scheme. We want to remark that the usage of the minimal subtraction scheme as a renormalization approach makes it necessary to introduce a RC Z_r for the parameter $\mathring{r}$ which is

$$\mathring{r} - \mathring{r}_c = Z_\varphi^{-1} Z_r r. \tag{102}$$

If the T_c-shift $\mathring{r}_c(\mathring{u})$ and the correlation length $\xi^{-2}(\mathring{r} - \mathring{r}_c, \mathring{u})$ have been introduced, the RC Z_r is determined by the condition that $\xi^{-2}(r, u)$ does not contain any ε-poles. The renormalization of r in (102) is connected to the renormalization of the $\frac{1}{2}|\varphi|^2$-insertions by the relation

$$Z_{\varphi^2} = Z_\varphi^{-1} Z_r. \tag{103}$$

As a consequence, one does not need to consider correlation or vertex functions containing $\frac{1}{2}|\varphi|^2$-insertions explicitly within the minimal subtraction scheme apart from the additive renormalization $A_{\varphi^2}(u)$ of the specific heat, which can be written as

$$A_{\varphi^2}(u) = -\frac{\kappa^\varepsilon}{4}\left[Z_{\varphi^2}^2\langle|\varphi_0|^2|\varphi_0|^2\rangle_c\right]_S A_d^{-1} \tag{104}$$

in this renormalization approach. The bracket $[\cdot]_S$ denotes the singular part containing only ε-poles of the embraced function.

Extended static functional. The renormalization of the general form (48) of the extended functional is equal to the renormalization of the extended functional (40) which includes only one scalar secondary density. This has two reasons. The first one is that secondary densities without a static coupling γ need no renormalization because they contribute only trivially to the loop expansion of the vertex functions. The second one is that even when more than one scalar secondary density is present, the corresponding static functional is equivalent to (47) where only one secondary density couples to the OP. The renormalization of the extended static functional including one scalar secondary density (40) has been considered in detail in [21] using the normalization condition approach and in [77, 78] within the minimal subtraction scheme. The justification of several relations between the static Z-factors mentioned below can also be found therein.

Although one may introduce RCs for $\mathring{\tau}$ and $\mathring{\tilde{u}}$ quite analogous to (102) and (98) it is not necessary to consider them explicitly here. The complete renormalization of the extended model is determined by the RCs of the GLW model and the additional parameters in (40). The latter require the introduction of further RCs. The secondary density m_0 and the coupling parameter $\mathring{\gamma}$ between OP and secondary density will be renormalized analogously to (97) and (98) by

$$m_0 = Z_m m, \qquad \mathring{\gamma} = \kappa^{\varepsilon/2} Z_\varphi^{-1} Z_m^{-1} Z_\gamma \gamma A_d^{-1/2}. \tag{105}$$

Note that we have introduced the Z-factor Z_m instead of $Z_m^{1/2}$ contrary to most of the definitions in the literature. Our definition is more convenient if one wants to maintain consistency with the definitions useful in model C′ [71] or model F′ [72] where a renormalization matrix $\boldsymbol{Z}_m$ has to be introduced.

Since the extended static functional is a Gaussian extension of the GLW model, no new independent RCs are necessary. Both new RCs Z_m and Z_γ introduced in (105) are related to renormalizations in the GLW model. First, the RC of the static coupling γ is determined by

$$Z_\gamma = Z_m^2 Z_\varphi Z_{\varphi^2}. \tag{106}$$

Inserting this into (105) gives

$$\mathring{\gamma} = \kappa^{\varepsilon/2} Z_{\varphi^2} Z_m \gamma A_d^{-1/2}. \tag{107}$$

Second, the renormalization factor Z_m of the secondary density is determined by the additive renormalization $A_{\varphi^2}(u)$ of the specific heat in the GLW model with the structure

$$Z_m^{-2}(u, \gamma) = 1 + \gamma^2 A_{\varphi^2}(u). \tag{108}$$

7.2. Renormalization of the dynamic parameters

In this subsection, we will discuss all dynamic renormalizations necessary for the different models. The RCs necessary in dynamics and their properties can be classified into three groups, namely the RCs of the auxiliary densities, the KCs and the mode coupling parameters. All three groups will be discussed in general including all dynamic models.

Auxiliary densities. In the dynamic functional (23) auxiliary densities $\tilde{a}_i$ have been introduced. How they renormalize depends mainly on the conservation property of the corresponding density a_i.

In all dynamic models at least the OP $\vec{\varphi}_0$ is present and a corresponding auxiliary density $\vec{\tilde{\varphi}}_0$ appears in the dynamic functional. The renormalization of the auxiliary density is usually written as

$$\vec{\tilde{\varphi}}_0 = Z_{\tilde{\varphi}}^{1/2}\vec{\tilde{\varphi}}, \qquad \vec{\tilde{\varphi}}_0^{+} = Z_{\tilde{\varphi}^+}^{1/2}\vec{\tilde{\varphi}}^{+}. \tag{109}$$

In contrast to Z_φ in statics $Z_{\tilde{\varphi}}$ may be a complex quantity and in such a case we have $Z_{\tilde{\varphi}^+} = Z_{\tilde{\varphi}}^{+}$. Concerning the structure of $Z_{\tilde{\varphi}}$ we may distinguish two cases:

- *Conserved OP.* In all dynamic models with a conserved OP (models B, H, J) the function $\mathring{\Omega}_{\varphi\tilde{\varphi}^+}$ in the dynamic OP vertex function (72) does not contain any new ε-poles which could not be removed with the remaining RCs. Therefore, one has

  $$Z_{\tilde{\varphi}} = Z_{\varphi}^{-1}. \tag{110}$$

  As a consequence, $Z_{\tilde{\varphi}}$ is always real in such models.
- *Non-conserved OP.* In all dynamic models with a non-conserved OP (models A, C, E, F, G, SSS, DP) the factor $Z_{\tilde{\varphi}}$ is a new independent renormalization. From (74) immediately follows that it has the structure

  $$Z_{\tilde{\varphi}} = Z_{\tilde{\varphi}}^{(A^\star)} Z_{\tilde{\varphi}}^{(\gamma)} \tag{111}$$

  where $Z_{\tilde{\varphi}}^{(A^\star)}$ is the RC of the auxiliary density in model A*, a generalization of model A to a complex KC Γ. Only dynamic models with a coupling γ in their static functional (models C, F) have a nontrivial RC $Z_{\tilde{\varphi}}^{(\gamma)}$. Otherwise (models A, E, G) one has simply $Z_{\tilde{\varphi}}^{(\gamma)} = 1$.

Only the one secondary density m_0 with a static coupling γ to the OP needs a renormalization as discussed in the previous subsection. The same is true for the corresponding auxiliary density $\tilde{m}_0$. Thus, we have

$$\tilde{m}_0 = Z_{\tilde{m}}\tilde{m} \tag{112}$$

and $\tilde{m}_0 = \tilde{m}$ for all other secondary densities without a static coupling to the OP. Secondary densities are always conserved therefore no new independent RC $Z_{\tilde{m}}$ is needed for $\tilde{m}_0$. Analogous to (110), it is simply renormalized with

$$Z_{\tilde{m}} = Z_m^{-1}. \tag{113}$$

Kinetic coefficients. In all models, a kinetic coefficient Γ of the OP is present and it renormalizes as

$$\mathring{\Gamma} = Z_\Gamma \Gamma. \tag{114}$$

From (72) follows that Z_Γ contains contributions from the renormalization of the dynamic functions $\mathring{\Omega}_{\varphi\tilde{\varphi}^+}$ and $\mathring{\Gamma}^{(d)}_{\varphi\tilde{\varphi}^+}$ as well as static contributions. Generally, we can write

$$Z_\Gamma = Z_\varphi^{1/2} Z_{\tilde{\varphi}^+}^{-1/2} Z_\Gamma^{(d)}, \tag{115}$$

where $Z_\Gamma^{(d)}$ contains the poles of $\mathring{\Gamma}^{(d)}_{\varphi\tilde{\varphi}^+}$. The above relation (115) may simplify in different models for the following reasons:

- In all dynamic models without mode coupling parameters g (models A, B, C), we simply have $Z_\Gamma^{(d)} = 1$. This follows from the general structure (75) of $\mathring{\Gamma}^{(d)}_{\varphi\tilde{\varphi}^+}$ where all contributions of the loop expansion are proportional to g.
- In models with conserved OP (models B, H, J), we can insert (110) into (115) and obtain

  $$Z_\Gamma = Z_\varphi Z_\Gamma^{(d)}. \tag{116}$$

  In model B where also no mode couplings are present, this relation simplifies further to $Z_\Gamma = Z_\varphi$ (see first item).

- In models with non-conserved OP where no static coupling γ is present (models A, E, G), it follows from (74) that $Z_{\tilde{\varphi}} = Z_{\tilde{\varphi}}^{(A^\star)}$ for the renormalization factors of the OP auxiliary density. Inserting into (115) leads to

$$Z_\Gamma = Z_\varphi^{1/2}\big(Z_{\tilde{\varphi}^+}^{(A^\star)}\big)^{-1/2} Z_\Gamma^{(d)}, \tag{117}$$

  which further reduces to $Z_\Gamma = Z_\varphi^{1/2}\big(Z_{\tilde{\varphi}^+}^{(A^\star)}\big)^{-1/2}$ in model A* due to the absence of mode couplings.

If secondary densities are present the corresponding KCs also need a renormalization. Considering at first models with one secondary density the KC renormalizes as

$$\mathring{\lambda} = Z_\lambda \lambda. \tag{118}$$

The structure of Z_λ now depends on the existence of a static coupling γ and a mode coupling g. The RC Z_λ can always be separated into a product of a static and a dynamic Z-factor, that is

$$Z_\lambda = Z_m^2 Z_\lambda^{(d)}. \tag{119}$$

In dynamic models where a static coupling γ and a mode coupling g is present (model F), Z_m is the static RC defined in (105) and $Z_\lambda^{(d)}$ contains purely dynamic contributions. In most dynamic models either a static coupling or a mode coupling is present. Then several simplifications in (119) take place:

- In dynamic models without a mode coupling g (model C), the dynamic RC is $Z_\lambda^{(d)} = 1$. Therefore, the renormalization of the kinetic coefficient is determined by statics and (119) reduces to

$$Z_\lambda = Z_m^2. \tag{120}$$

- In dynamic models without a static coupling γ (models E, G, H), the secondary density needs not be renormalized, thus $Z_m = 1$ and (119) reduces to

$$Z_\lambda = Z_\lambda^{(d)}. \tag{121}$$

In dynamic models with two secondary densities (models C′, E′, F′) three KCs are present, which can be written as a matrix

$$\mathring{\mathbf{\Lambda}} = \begin{pmatrix} \mathring{\lambda} & \mathring{L} \\ \mathring{L} & \mathring{\mu} \end{pmatrix}. \tag{122}$$

Analogous to (118), the coefficients renormalize as

$$\mathring{\lambda} = Z_\lambda \lambda, \qquad \mathring{L} = Z_L L, \qquad \mathring{\mu} = Z_\mu \mu. \tag{123}$$

Although initially both secondary densities couple with parameters γ_1 and γ_2 to the OP, the static functional can always be transformed to a form in which only one secondary density has a coupling γ (see the discussion in section 5.2). Assuming that the second secondary density, which corresponds to $\mathring{\mu}$, couples to the OP, the Z-factors in (123) separate into a static and a dynamic part as follows:

$$Z_\lambda = Z_\lambda^{(d)}, \qquad Z_L = Z_m Z_L^{(d)}, \qquad Z_\mu = Z_m^2 Z_\mu^{(d)}. \tag{124}$$

Such a separation (124) occurs for instance in model F′. The simplifications in cases where either static couplings or mode couplings are present remain the same as discussed above for

the case of one secondary density. Without static couplings (model E′) we have $Z_m = 1$, and without mode couplings (model C′) we have $Z_\lambda^{(d)} = Z_L^{(d)} = Z_\mu^{(d)} = 1$.

Mode couplings. Models with a nonvanishing reversible part (2) contain mode coupling parameters. As already outlined in section 6.4, the mode coupling parameters are defined from (3) by the Poisson bracket relation

$$Q_{ij} = k_B T \left\{ a_i, a_j^+ \right\} = \mathring{g} f(\{a\}). \tag{125}$$

The renormalization of a mode coupling $\mathring{g}$ is introduced as

$$\mathring{g} = \kappa^{\varepsilon/2} Z_g g A_d^{-1/2}. \tag{126}$$

Z_g is determined by the condition that the Poisson bracket relations should be invariant under renormalization. This leads to the different renormalizations of $\mathring{g}$ in the models considered.

- *Model J (Heisenberg ferromagnet).* In this model one looks at a lattice of classical three-component spin vectors where S_i^α should be the αth component of the spin vector on lattice site i. The generalized Poisson bracket relations between the spin components are easily derived either from quantum theory by using the correspondence principle or from infinitesimal rotations in spin space where $\vec{S}$ is their generator [57]. Both methods lead to

  $$\left\{ S_i^\alpha, S_j^\beta \right\} = \varepsilon_{\alpha\beta\gamma} S_i^\gamma \delta_{ij}. \tag{127}$$

  The magnetization density

  $$\vec{\phi}_0(x) = \sum_i \vec{S}_i \delta(x - x_i) \tag{128}$$

  represents the OP of the system in this model. The OP is the only dynamic variable and the corresponding Poisson bracket relations (125) follow by inserting (127) into the definition of the OP. One obtains for (3)

  $$Q_{\phi^\alpha(x)\phi^\beta(x')} = k_B T \left\{ \phi_0^\alpha, \phi_0^\beta \right\} = \mathring{g} \varepsilon_{\alpha\beta\gamma} \phi_0^\gamma(x) \delta(x - x'). \tag{129}$$

  Inserting the renormalized quantities with relations (97) and (126), one immediately has

  $$Z_g = Z_\phi^{1/2} \tag{130}$$

- *Model G (Heisenberg antiferromagnet).* In the antiferromagnet, two sublattices A and B with spins are considered. Let $S_{i_A}^\alpha$ be the αth component of the spin vector on lattice site i of lattice A and $S_{i_B}^\beta$ the βth component of the spin vector on lattice site i of lattice B. According to (127), the Poisson bracket relations for the spins are now

  $$\begin{aligned} \left\{ S_{i_A}^\alpha, S_{j_A}^\beta \right\} &= \varepsilon_{\alpha\beta\gamma} S_{i_A}^\gamma \delta_{i_A j_A}, \\ \left\{ S_{i_B}^\alpha, S_{j_B}^\beta \right\} &= \varepsilon_{\alpha\beta\gamma} S_{i_B}^\gamma \delta_{i_B j_B}, \\ \left\{ S_{i_A}^\alpha, S_{j_B}^\beta \right\} &= 0. \end{aligned} \tag{131}$$

  Introducing sublattice magnetization densities

  $$\vec{M}_A(x) = \sum_i \vec{S}_{i_A} \delta(x - x_i), \qquad \vec{M}_B(x) = \sum_i \vec{S}_{i_B} \delta(x - x_i), \tag{132}$$

  the OP $\vec{\phi}_0(x)$ of the model is defined by the staggered magnetization density

  $$\vec{\phi}_0(x) = \vec{M}_A(x) - \vec{M}_B(x), \tag{133}$$

  while the magnetization density

  $$\vec{m}_0(x) = \vec{M}_A(x) + \vec{M}_B(x) \tag{134}$$

represents a secondary density. Inserting (131)–(134) into (3) leads to the following Poisson bracket relations:

$$Q_{\phi^\alpha\phi^\beta} = k_B T\left\{\phi_0^\alpha(x), \phi_0^\beta(x')\right\} = \mathring{g}_\phi \varepsilon_{\alpha\beta\gamma}\phi_0^\gamma(x)\delta(x-x'), \tag{135}$$

$$Q_{m^\alpha m^\beta} = k_B T\left\{m_0^\alpha(x), m_0^\beta(x')\right\} = \mathring{g}\varepsilon_{\alpha\beta\gamma}m_0^\gamma(x)\delta(x-x'), \tag{136}$$

$$Q_{\phi^\alpha m^\beta} = k_B T\left\{\phi_0^\alpha(x), m_0^\beta(x')\right\} = \mathring{g}\varepsilon_{\alpha\beta\gamma}\phi_0^\gamma(x)\delta(x-x'). \tag{137}$$

An analysis of the naive dimensions reveals that the mode coupling $\mathring{g}_\phi$ in (135) is irrelevant and therefore has to be neglected in the following. For the dynamic critical behaviour only the Poisson bracket relations (136) and (137) have to be considered. Inserting the renormalized quantities by using (97), (105) and (126) leads to the relation

$$Z_g = Z_m. \tag{138}$$

The secondary density is a vector therefore $\gamma = 0$ and $Z_g = Z_m = 1$.

- *Model E (planar ferromagnet).* In a planar ferromagnet, the spin vectors order in a plane in spin space. The components of a three-dimensional magnetization density vector are

$$M^x(x) = \sum_i S_i^x \delta(x - x_i), \qquad M^y(x) = \sum_i S_i^y \delta(x - x_i), \tag{139}$$

$$M^z(x) = \sum_i S_i^z \delta(x - x_i). \tag{140}$$

Assuming that the ferromagnetic arrangement occurs in the x–y-plane a complex OP

$$\psi_0(x) = M^x(x) - \mathrm{i}M^y(x) \tag{141}$$

can be defined. Then, the z-component of the magnetization represents the secondary density

$$m_0(x) = M^z(x). \tag{142}$$

The only existing Poisson bracket relation, which does not vanish, is

$$Q_{\psi m} = k_B T\{\psi_0(x), m_0(x')\} = -\mathrm{i}\mathring{g}\psi_0(x)\delta(x-x'). \tag{143}$$

Quite analogous to model G, the relation

$$Z_g = Z_m = 1 \tag{144}$$

can be obtained by inserting the renormalization relations (97), (105) and (126). The last equality is valid because m_0 is a vector component which has no static OP coupling γ in the extended functional.

- *Model H (critical point in fluids).* In order to describe the critical behaviour of the thermal conductivity and the shear viscosity at the gas/liquid critical point in fluids, the dynamic equations for the entropy density per volume $s(x)$ and the transverse momentum current density $\vec{j}_t(x)$ have to be considered. Generalized Poisson brackets can now only be derived from infinitesimal translations as presented in [57] because the entropy density has no quantum theoretical counterpart. Only Poisson brackets with the momentum density being the generator of the translations are different from zero. They are

$$\left\{s(x'), j_t^\alpha(x)\right\} = s(x)\nabla^\alpha\delta(x-x'), \tag{145}$$

$$\left\{j_t^\alpha(x'), j_t^\beta(x)\right\} = j_t^\alpha(x)\nabla^\beta\delta(x-x') - j_t^\beta(x')\nabla^\alpha\delta(x-x'). \tag{146}$$

The OP is apart from constant factors determined by the entropy density thus we have $\phi_0(x) \sim s(x)$. The transverse momentum density represents a secondary density without static coupling γ. The above generalized Poisson brackets lead to the relations

$$Q_{\phi j_t^\alpha} = k_B T \left\{\phi_0(x'), j_t^\alpha(x)\right\} = \mathring{g}\phi_0(x)\nabla^\alpha \delta(x - x'). \tag{147}$$

$$Q_{j_t^\alpha j_t^\beta} = k_B T \left\{j_t^\alpha(x'), j_t^\beta(x)\right\} = \mathring{g}\left[j_t^\alpha(x)\nabla^\beta \delta(x - x') - j_t^\beta(x')\nabla^\alpha \delta(x - x')\right]. \tag{148}$$

Taking into account the renormalization of the OP (97) and the property that $\vec{j}_t$ does not renormalize, one immediately obtains from (147) and (148)

$$Z_g = 1. \tag{149}$$

In liquid mixtures at the gas/liquid transition (plait point) or the demixing transition (consolute point), an additional scalar density has to be incorporated. This is the concentration of one of the two components of the mixture $c(x)$. It leads to model H′ which includes the further Poisson bracket

$$\left\{c(x'), j_t^\alpha(x)\right\} = c(x)\nabla^\alpha \delta(x - x'). \tag{150}$$

The scalar concentration represents an additional secondary density $m_0(x) \sim c(x)$ compared to model H but with a coupling γ in the extended static functional and a RC $Z_m \neq 1$. The corresponding additional Poisson bracket relation reads

$$Q_{m j_t^\alpha} = k_B T \left\{m_0(x'), j_t^\alpha(x)\right\} = \mathring{g} m_0(x)\nabla^\alpha \delta(x - x') \tag{151}$$

in accordance with (149).

- *Model F (superfluid transition in ^{4}He).* Here, the situation is more complex than in the previous models. Although it is enough to take into account only the equations for the macroscopic wavefunction of the Bose-condensed state $\psi_0(x)$ as OP and the entropy density per mass $\sigma(x)$ as secondary density in order to obtain the critical behaviour of the thermal conductivity, at the level of Poisson brackets the whole set of dynamic variables has to be considered. This includes apart from $\psi_0(x)$ the entropy per volume $s(x)$, the mass density $\rho(x)$ and the momentum current density $\vec{j}(x)$. Because the hydrodynamics of ordinary fluids is included in the hydrodynamics of superfluids, the infinitesimal translations lead to the same Poisson brackets (145) and (146). Additionally, one obtains the Poisson bracket

$$\{\rho(x'), j^\alpha(x)\} = \rho(x)\nabla^\alpha \delta(x - x'), \tag{152}$$

which would also be present in an extended dynamic model for simple fluids incorporating critical behaviour of sound propagation. In the current model, the generator of infinitesimal translations also acts on the OP leading to a Poisson bracket

$$\{\psi_0(x'), j^\alpha(x)\} = -\delta(x - x')\nabla'^\alpha \psi_0(x') + \tfrac{1}{2}\psi_0(x')\nabla^\alpha \delta(x - x'), \tag{153}$$

which of course does not exist in simple fluids. The mass density $\rho(x)$ is the generator of phase transformations of $\psi_0(x)$. Infinitesimal phase transformations lead to a further Poisson bracket

$$\{\psi_0(x'), \rho(x)\} = -\mathrm{i}\frac{m_4}{\hbar}\psi_0(x)\delta(x - x') \tag{154}$$

distinguishing the superfluid hydrodynamics from the one of a simple fluid. In (154), m_4 is the ^{4}He atomic mass and $\hbar$ is Planck's constant divided by 2π. The Poisson brackets

lead to different mode coupling parameters. The corresponding relations are

$$Q_{sj^\alpha} = k_B T\{s(x'), j^\alpha(x)\} = \mathring{g}_j s(x)\nabla^\alpha \delta(x - x'), \tag{155}$$

$$Q_{\rho j^\alpha} = k_B T\{\rho(x'), j^\alpha(x)\} = \mathring{g}_j \rho(x)\nabla^\alpha \delta(x - x'), \tag{156}$$

$$Q_{j^\alpha j^\beta} = k_B T\{j^\alpha(x'), j^\beta(x)\} = \mathring{g}_j [j^\alpha(x)\nabla^\beta \delta(x - x') - j^\beta(x')\nabla^\alpha \delta(x - x')], \tag{157}$$

$$Q_{\psi j^\alpha} = k_B T\{\psi_0(x'), j^\alpha(x)\} = -\mathring{g}_1 \delta(x - x')\nabla'^\alpha \psi_0(x') + \mathring{g}_2 \psi_0(x')\nabla^\alpha \delta(x - x'), \tag{158}$$

$$Q_{\psi\rho} = k_B T\{\psi_0(x'), \rho(x)\} = -\mathrm{i}\mathring{g}\psi_0(x)\delta(x - x'). \tag{159}$$

A dimensional analysis in the corresponding dynamic equations reveals that the mode couplings $\mathring{g}_j, \mathring{g}_1$ and $\mathring{g}_2$ are irrelevant and therefore have to be neglected. Only the last relation (159) is relevant for the critical dynamics of ^{4}He at the superfluid transition. Introducing a secondary density which is proportional to the entropy per mass $m_0(x) \sim s(x)/\rho(x)$, the Poisson bracket relation (159) and therefore the relevant mode coupling $\mathrm{i}\mathring{g}$ couples to the dynamic equation for $m_0(x)$. After the neglection of all irrelevant couplings, the additional densities $\rho(x)$ and $\vec{j}(x)$ appear only in quadratic order in the dynamic functional. Since they are not necessary for the critical dynamics of the heat mode, they are eliminated by integration leading to a model at constant pressure instead of constant mass density. The resulting dynamic functional and the corresponding dynamic equations are known as model F. The mode coupling term therein is consistent with a Poisson bracket relation

$$Q_{\psi m} = k_B T\{\psi_0(x'), m_0(x)\} = -\mathrm{i}\mathring{g}\psi_0(x)\delta(x - x') \tag{160}$$

from which immediately

$$Z_g = Z_m \tag{161}$$

follows. In contrast to model E Z_m is now a nontrivial RC because the scalar secondary density (entropy per mass) couples with γ to the OP in the extended static functional.

7.3. ζ-functions

The ζ-functions defined from the renormalization factors introduced in sections 7.1 and 7.2 are not uniformly defined. In the literature different definitions are used depending on the authors. In the following, we will use in statics and dynamics the uniform definition

$$\zeta_{x_i}(\{y_j\}) = \frac{\mathrm{d}\ln Z_{x_i}^{-1}}{\mathrm{d}\ln\kappa} \tag{162}$$

where $\{y_j\} = \{u, \gamma, \Gamma, \Lambda_{ij}, g_i\}$ is the set of static and dynamic model parameters. x_i stands for any density $a_i, \tilde{a}_i$ or any model parameter y_i. Note that the κ-derivative is always taken at fixed bare parameters $\{\mathring{y}_j\}$. The only exception in the definition of the ζ-functions is the additive renormalization A_{φ^2} of the specific heat introduced in (108), which leads to

$$B_{\varphi^2}(u) = \kappa^\varepsilon Z_{\varphi^2}^2 \kappa \frac{\mathrm{d}}{\mathrm{d}\kappa}\left(Z_{\varphi^2}^{-2}\kappa^{-\varepsilon} A_{\varphi^2}\right). \tag{163}$$

Relations (106) and (108) between the static Z-factors mentioned in section 7.1 also lead to relations between the ζ-functions, which are

$$\zeta_\gamma(u, \gamma) = 2\zeta_m(u, \gamma) + \zeta_\varphi(u) + \zeta_{\varphi^2}(u) \tag{164}$$

and

$$\zeta_m(u, \gamma) = \tfrac{1}{2}\gamma^2 B_{\varphi^2}(u). \tag{165}$$

The second relation can be used to eliminate ζ_m in the first one. Thus, we obtain

$$\zeta_\gamma(u,\gamma) = \gamma^2 B_{\varphi^2}(u) + \zeta_\varphi(u) + \zeta_{\varphi^2}(u). \tag{166}$$

With relations (165) and (166) both ζ-functions ζ_m and ζ_γ, which appear additionally in the extended static functional compared to the GLW functional, are determined by the ζ-functions of the GLW model (24).

The ζ-function of the kinetic OP coefficient Γ follows from the Z-factor relation (115) by inserting into (162). Generally, we have

$$\zeta_\Gamma(u,\gamma,\Gamma,\Lambda_{ij},g_i) = \tfrac{1}{2}\zeta_\varphi(u) - \tfrac{1}{2}\zeta_{\tilde\varphi^+}(u,\gamma,\Gamma,\Lambda_{ij},g_i) + \zeta_\Gamma^{(d)}(u,\gamma,\Gamma,\Lambda_{ij},g_i). \tag{167}$$

The dependence of the ζ-function on the static coupling γ, KCs Λ_{ij} or mode couplings g_i is of course due to the dynamic model under consideration. All simplifications in Z_Γ for different dynamic models as discussed under the item 'kinetic coefficients' in section 7.2 also concern the ζ-functions because $Z_x = 1$ corresponds to $\zeta_x = 0$. In the case of a complex OP KC $\Gamma = \Gamma' + \mathrm{i}\Gamma''$ for the OP, as for instance in models F, F′, the relation

$$\zeta_{\Gamma^+}(u,\gamma,\Gamma,\Lambda_{ij},g_i) = \zeta_\Gamma^+(u,\gamma,\Gamma,\Lambda_{ij},g_i) \tag{168}$$

holds. In dynamic models with a secondary density from relation (119) follows

$$\zeta_\lambda(u,\gamma,\Gamma,\Lambda_{ij},g_i) = 2\zeta_m(u,\gamma) + \zeta_\lambda^{(d)}(u,\gamma,\Gamma,\Lambda_{ij},g_i). \tag{169}$$

If no static coupling γ is present, we get from relation (165) $\zeta_m = 0$. In such cases it is not necessary to distinguish between ζ_λ and $\zeta_\lambda^{(d)}$. Dynamic models with two secondary densities include a matrix (122) of KCs. The corresponding ζ-functions are

$$\zeta_\lambda(u,\gamma,\Gamma,\Lambda_{ij},g_i) = \zeta_\lambda^{(d)}(u,\gamma,\Gamma,\Lambda_{ij},g_i), \tag{170}$$

$$\zeta_L(u,\gamma,\Gamma,\Lambda_{ij},g_i) = \zeta_m(u,\gamma) + \zeta_L^{(d)}(u,\gamma,\Gamma,\Lambda_{ij},g_i), \tag{171}$$

$$\zeta_\mu(u,\gamma,\Gamma,\Lambda_{ij},g_i) = 2\zeta_m(u,\gamma) + \zeta_\mu^{(d)}(u,\gamma,\Gamma,\Lambda_{ij},g_i). \tag{172}$$

Explicit expressions of the dynamic ζ-functions mentioned above are given in appendix A for several dynamic models.

7.4. β-functions and flow equations

The flow of any model parameter y_i as a function of the flow parameter ℓ is determined by the flow equation

$$\ell\frac{\mathrm{d}y_i}{\mathrm{d}\ell} = \beta_{y_i}(\{y_j\}). \tag{173}$$

Multiplicatively renormalizable model parameters may be generally written in the form

$$\mathring{y}_i = \kappa^{c_i} Z_\varphi^{-p_i} Z_m^{-q_i} Z_{y_i} y_i \tag{174}$$

where c_i is the naive dimension of the corresponding parameter. Dependent on the actual model parameter the powers c_i, p_i, q_i have different values, which may be finite or zero. Considering for instance $y_i = u$, from (98) follows $c_i = \varepsilon$, $p_i = 2$, $q_i = 0$. Taking $y_i = \Gamma$ as a further example, one obtains from (114) $c_i = p_i = q_i = 0$. From (174) follows the general structure of the β-functions as

$$\beta_{y_i}(\{y_j\}) = y_i(-c_i - p_i\zeta_\varphi(u) - q_i\zeta_m(u,\gamma) + \zeta_{y_i}(\{y_j\})) \tag{175}$$

where the definition of the ζ-functions (162) has been used.

Statics. Within statics at most two flow equations

$$\ell \frac{\mathrm{d}u}{\mathrm{d}\ell} = \beta_u(u), \qquad \ell \frac{\mathrm{d}\gamma}{\mathrm{d}\ell} = \beta_\gamma(u,\gamma) \tag{176}$$

have to be solved. The second equation is only necessary if at least one scalar secondary density couples to the OP. From (98) and (107), one immediately obtains the β-functions

$$\beta_u(u) = u(-\varepsilon - 2\zeta_\varphi(u) + \zeta_u(u)), \tag{177}$$

$$\beta_\gamma(u,\gamma) = \gamma\left(-\frac{\varepsilon}{2} + \zeta_{\varphi^2}(u) + \frac{1}{2}\gamma^2 B_{\varphi^2}(u)\right). \tag{178}$$

In (178) relation (166) has been used. The above two relations reveal that only functions of the GLW model are necessary in order to determine the critical behaviour of the parameters even in the extended static functional. The explicit expressions of the ζ-functions of the GLW model are well known [59, 60] and currently obtained within five-loop order [79]. Within the minimal subtraction renormalization scheme, the two-loop order expressions are

$$\zeta_\varphi(u) = -\frac{n+2}{72}u^2, \tag{179}$$

$$\zeta_u(u) = \frac{n+8}{6}u - \frac{5n+22}{18}u^2, \tag{180}$$

$$\zeta_{\varphi^2}(u) = \frac{n+2}{6}u\left(1 - \frac{5}{12}u\right), \tag{181}$$

$$B_{\varphi^2}(u) = \frac{n}{2}. \tag{182}$$

The asymptotic critical region will be approached in the limit $\ell \to 0$. The parameters u and γ have to reach fixed points $u^\star$ and $\gamma^\star$ in this limit, which determine the static critical exponents and amplitude ratios. The conditions for the fixed points are

$$\ell \frac{\mathrm{d}u}{\mathrm{d}\ell} = 0 \qquad \text{or} \qquad \beta_u(u^\star) = 0 \tag{183}$$

$$\ell \frac{\mathrm{d}\gamma}{\mathrm{d}\ell} = 0 \qquad \text{or} \qquad \beta_\gamma(u^\star,\gamma^\star) = 0. \tag{184}$$

Equations (183) and (184) determine all possible fixed points in the GLW model and the extended model. The stability of a fixed point $u^\star$, $\gamma^\star$ is determined by the property that for small deviations of the model parameters from their fixed-point values $\Delta u = u - u^\star$, $\Delta\gamma = \gamma - \gamma^\star$, the flow has to drive back the parameters to their fixed-point values, independent of the direction of the deviations. Expanding the β-functions around the fixed point, one obtains

$$\beta_u(u^\star + \Delta u) = \left(\frac{\partial\beta_u}{\partial u}\right)\Bigg|_{u=u^\star}(u - u^\star), \tag{185}$$

$$\beta_\gamma(u^\star + \Delta u, \gamma^\star + \Delta\gamma) = \left(\frac{\partial\beta_\gamma}{\partial u}\right)\Bigg|_{\substack{u=u^\star\\ \gamma=\gamma^\star}}(u - u^\star) + \left(\frac{\partial\beta_\gamma}{\partial\gamma}\right)\Bigg|_{\substack{u=u^\star\\ \gamma=\gamma^\star}}(\gamma - \gamma^\star). \tag{186}$$

The fixed point is stable if the eigenvalues ω_i of the matrix

$$\left(\frac{\partial\beta_{y_j}}{\partial y_i}\right)\Bigg|_{\{y\}=\{y^\star\}} = \begin{pmatrix} \left(\frac{\partial\beta_u}{\partial u}\right) & \left(\frac{\partial\beta_\gamma}{\partial u}\right) \\ 0 & \left(\frac{\partial\beta_\gamma}{\partial\gamma}\right) \end{pmatrix}\Bigg|_{\substack{u=u^\star\\ \gamma=\gamma^\star}} \tag{187}$$

are positive. The eigenvalues are usually denoted as transient exponents. For the above matrix (187), the conditions for a stable fixed point read

$$\omega_u = \left(\frac{\partial \beta_u}{\partial u}\right)\Bigg|_{u=u^\star} > 0, \qquad \omega_\gamma = \left(\frac{\partial \beta_\gamma}{\partial \gamma}\right)\Bigg|_{\substack{u=u^\star \\ \gamma=\gamma^\star}} > 0. \tag{188}$$

The transient exponents also determine how fast a fixed point will be approached. The smaller the transient exponents, the longer non-asymptotic effects are observable in the critical behaviour of different quantities. A closer examination of the β-functions reveals that for u two fixed points exist. The Gaussian fixed point $u^\star = 0$ and the Heisenberg fixed point $u^\star = u_H$ with a finite non-zero value u_H. From the stability condition for u in (188), it follows that for $d < 4$ the Gaussian fixed point is unstable and the Heisenberg fixed point is always stable. Inserting u_H into (184), the resulting equation

$$\beta_\gamma(u_H, \gamma^\star) = 0 \tag{189}$$

has two solutions, namely $\gamma^\star = 0$ and $\gamma^\star = \gamma_C$, where γ_C is finite. In contrast to u now the stability of $\gamma^\star$ depends on the number n of OP components. In two-loop order, the stability condition for γ in (188) leads to the following result:

$$\gamma^\star = \gamma_C \text{ is stable} \qquad \text{for} \quad n = 1. \tag{190}$$

$$\gamma^\star = 0 \text{ is stable} \qquad \text{for} \quad n = 2, 3. \tag{191}$$

In the above relations, we have considered only values for n which are of physical relevance. A general comprehensive discussion of the static fixed points in the whole n–d-plane can be found in [80]. The explicit values of u_H and γ_C depend on how the flow equations and the β-functions therein are treated. There are two major ways to proceed:

(i) Linearizing the β-functions around the fixed points as done in (185) and (186), inserting into the flow equations and using ε-expansion. This leads to ε-expanded values for u_H and γ_C. The resulting flow is only valid in the asymptotic region.

(ii) Calculating the flow from the nonlinear equations and solving them for $\ell \to 0$ in order to obtain $u^\star$ and $\gamma^\star$. The resulting flow is also valid in the non-asymptotic region. Such nonlinear flow equations can be established by different approaches:

- The straightforward approach is to insert the ζ-functions (179)–(182) into the β-functions (177) and (178) and treat the flow equations (176) as nonlinear equations. Within this method, a major problem arises with the flow equation for u in (176). The equation $\beta_u(u^\star) = 0$, which is in two-loop order a simple quadratic equation, has no real solution for u_H. The corresponding nonlinear flow $u(\ell)$ would have no real fixed point to approach in the asymptotic region. The linearized flow equations of (i) lead to an ε-expanded value for u_H. If non-asymptotic effects should be taken into account, a cumbersome ε-expansion of the flow equation with the correct ε-expanded fixed point should be constructed.
- One possibility to circumvent this problem is to avoid the explicit flow equations but reconstruct the flows out of experimental quantities [81]. The flow of the parameters is obtained from experimentally measured thermodynamic quantities by using relations between thermodynamic derivatives and static vertex functions. Originally, this approach has been introduced in order to obtain the non-asymptotic static flow in ^{4}He at the superfluid transition. There the flow of $u(\ell)$ can be calculated from the experimentally measured specific heat C_P at constant pressure P above and below T_λ, while $\gamma(\ell)$ is determined by $u(\ell)$ and the specific heat above T_λ. The necessary relations are given in [78].

This method has also been applied for an analysis at several phase transitions: (i(a)) at the superfluid transition in ^{4}He [78]; (i(b)) in ^{3}He–^{4}He mixtures [69], where the flow has been calculated from the specific heat C_{PX} at constant pressure P and mole fraction X; (ii(a)) at the gas/liquid critical point [34]; (ii(b)) and in binary liquid mixtures at the plait point and at the consolute point [16] and (iii) it has also been adapted in [82] to uniaxial dipolar systems (ferromagnets and ferroelectrics) where the non-asymptotic flow $u(\ell)$ has been calculated from the corresponding magnetic or electric susceptibilities above and below T_c (the critical dimension is $d_c = 3$ and the stable fixed point is $u^\star = 0$ in such systems).

The calculation of the corresponding amplitudes of vertex functions for systems with an n-component OP has been improved over the time. Amplitude functions of the static thermodynamic quantities (susceptibility, specific heat, etc) have been calculated within this approach above [83] and below [84] the critical temperature. A four-loop calculation of the free energy above and below the critical temperature can be found in [79, 85]. In general resummation procedures are necessary since the loop expansion is only an asymptotic one (see the next item).

Although this method delivers good results in different systems, it has its limits for several reasons. Firstly, for the calculation of $u(\ell)$ experimental results have to be present with enough accuracy above and below the critical temperature. This is not the case in many systems. Secondly, all experimentally measured quantities contain a noncritical background temperature behaviour which is not covered by the critical theory where only the contributions of the fluctuations to the temperature behaviour are determined. Therefore, the background contributions should be small in the considered quantities in order to obtain a reliable flow. Thirdly on the theoretical side the ϕ^4-model is used, which itself has limited applicability when going into the background.

- Another approach is to improve the expressions for the flow equations by applying some summation procedure [61, 86–88] with the result that a stable fixed point is reached. Formerly released calculations of the behaviour of the GLW model in high-order perturbation expansion are either restricted to Ising like models [89] or use other renormalization schemes such as normalization conditions or the Callan–Symanzik method [90–92]. In high-order calculations within the minimal subtraction scheme, the Borel resummation is applied to the fixed-point values of u and the critical exponents [93, 94]. In [66, 95], the Borel resummation procedure is applied to the ζ- and β-functions obtained within minimal subtraction scheme. The result can be written within the accuracy in the simple form

$$\zeta_{\varphi^2}(u) = 4(n+2)\frac{u}{4!}\left(1 - 10\frac{u}{4!}\right) + a_1\left(\frac{u}{4!}\right)^3 - a_2\left(\frac{u}{4!}\right)^4, \tag{192}$$

$$\zeta_{\varphi}(u) = -\frac{n+2}{72}u^2 + a_3\left(\frac{u}{4!}\right)^3 \tag{193}$$

and

$$\beta_u(u) = -\frac{u}{4!} + 40\left(\frac{u}{4!}\right)^2 \frac{\left(1 + a_4\frac{u}{4!}\right)}{\left(1 + a_5\frac{u}{4!}\right)}. \tag{194}$$

The coefficients a_1, a_2, a_3, a_4, a_5 have been calculated in [66] (see table 2 therein) for several n. When $u(\ell)$ is calculated from (194), it is possible to calculate $\gamma(\ell)$ either by using the two-loop expression (181) or the Borel-summed expression (192) for $\zeta_{\varphi^2}(u)$. This leads to a slightly different flow of γ in the noncritical background. The

u contributions of the function $B_{\psi^2}(u) = n/2 + \mathcal{O}(u^2)$ are negligible [79] at the current order of calculation, thus we simply can insert $B_{\psi^2}(u) = n/2$ into (178) also in this case.

Effective critical exponents visible in the experimentally accessible temperature region can be calculated from such a non-asymptotic flow by inserting the flow for special initial conditions into the corresponding ζ-functions. This might explain differences of measured critical 'exponents' when the measurements have not been made in the asymptotic region.

Dynamics. The critical flow of KCs has the property that it either diverges or goes to zero, depending on the existence of mode coupling parameters. In dynamic models with at least one secondary density usually time scale ratios will be introduced, which may stay finite at the fixed point. For dynamic models with one secondary density (models C, E, F, G, H), one time scale ratio

$$w \equiv \frac{\Gamma}{\lambda} \tag{195}$$

can be defined. This parameter is of course always positive and its numerical range lies between 0 and ∞. The corresponding flow equation reads

$$l\frac{\mathrm{d}w}{\mathrm{d}l} = \beta_w(u, \gamma, w, F) \qquad \text{with} \qquad F \equiv \frac{g}{\lambda}. \tag{196}$$

The β-function of the time scale ratio w follows from its definition (195). According to (175), it can be written as

$$\beta_w(u, \gamma, w, F) = w(-c_w + \zeta_\Gamma(u, \gamma, w, F). - \zeta_\lambda(u, \gamma, w, F)) \tag{197}$$

In the above equation, the general structures (167) and (169) of the ζ-functions may be inserted leading to simplifications in different dynamic models. The naive dimension c_w depends on the dynamic model. In models C, E, F, G we have $c_w = 0$ while in model H we have $c_w = 2$.

If one secondary density is present also at most one mode coupling g may exist (models E, F, G, H). Instead of the mode coupling parameters g or F

$$f \equiv \frac{F}{\sqrt{w'}} = \frac{g}{\sqrt{\Gamma'\lambda}} \tag{198}$$

will be usually introduced. This has been done in (196) and (197). Which of the two parameters F or f is more convenient depends on the actual dynamic model and the features considered therein. For the presentation of explicit results of ζ-functions in some models F it is more appropriate (see appendix A) while for fixed-point discussions usually f is preferred because it has finite fixed-point values. In (198), the most general definition with complex w has been presented. In dynamic models with real Γ and therefore real w, we have of course $w' = w$. The flow equation of the mode coupling parameter reads

$$l\frac{\mathrm{d}F}{\mathrm{d}l} = \beta_F(u, \gamma, w, F) \qquad \text{or} \qquad l\frac{\mathrm{d}f}{\mathrm{d}l} = \beta_f(u, \gamma, w, f). \tag{199}$$

The β-functions can be expressed by ζ-functions using the general structure (175) and the definitions (199) of the mode coupling parameters. The naive dimension is always $c_F = \varepsilon/2$ in the dynamic models which include secondary densities. Thus, the β-functions can be written as

$$\beta_F(u, \gamma, w, F) = -F\Big(\frac{\varepsilon}{2} - \zeta_g(u, \gamma) + \zeta_\lambda(u, \gamma, w, F)\Big) \tag{200}$$

or

$$\beta_f(u, \gamma, w, f) = -f\left(\frac{\varepsilon}{2} - \zeta_g(u, \gamma) + \frac{1}{2}\zeta_\lambda(u, \gamma, w, f) + \frac{1}{2}\,\mathrm{Re}\left[\frac{\Gamma}{\Gamma'}\zeta_\Gamma(u, \gamma, w, f)\right]\right). \tag{201}$$

The above β-function is needed in model F where Γ is complex and $\zeta_g(u,\gamma) = \zeta_m(u,\gamma)$. From the renormalization of the mode coupling g discussed in the previous section follows that in the models E, G, H $\zeta_g(u,\gamma) = 0$. Furthermore, Γ is a real parameter in these models. Thus, (200) can be reduced to

$$\beta_f(u,\gamma,w,f) = -\frac{f}{2}(\varepsilon + \zeta_\lambda(u,\gamma,w,f) + \zeta_\Gamma(u,\gamma,w,f)) \tag{202}$$

in those cases.

The list of arguments (u,γ,w,F) in (196)–(202) describes the most general case. Except for model F all other models include only a subset of parameters because in some of them the mode coupling F or the static coupling γ may not be present.

In dynamic models with two secondary densities (models C′, E′, F′, H′), three time scale ratios

$$w_1 \equiv \frac{\Gamma}{\lambda}, \qquad w_2 \equiv \frac{\Gamma}{\mu}, \qquad w_3 \equiv \frac{L}{\sqrt{\lambda\mu}} \tag{203}$$

may exist. For complex Γ the time scale ratios w_1 and w_2 are also complex quantities. Quite analogous to w, the numerical values of the real part range from 0 to ∞. The time scale ratio w_3 determines the dissipative coupling between the two secondary densities. Its numerical values lie in a restricted range. Considering the square, the lower border is $w_3^2 = 0$, which is the case if the dissipative processes of the two secondary densities decouple. The other border value is $w_3^2 = 1$ describing total coupling in the sense that the dissipation of two secondary densities is determined only by one density. In the totally coupled case a transformation to new secondary densities can be found where the first one fulfils a dynamic equation with a diffusion term while the dynamics of the second one is determined by a time-reversible equation without any dissipation. The values of w_3^2 cannot exceed 1 because the matrix (122) of dynamic coefficients has to be positive definite.

Models with two secondary densities may also have two mode coupling parameters (model F′) which are defined as

$$F_1 \equiv \frac{g_1}{\lambda} \qquad \text{or} \qquad f_1 \equiv \frac{F_1}{\sqrt{w_1'}} = \frac{g_1}{\sqrt{\Gamma'\lambda}}, \tag{204}$$

$$F_2 \equiv \frac{g_2}{\mu} \qquad \text{or} \qquad f_2 \equiv \frac{F_2}{\sqrt{w_2'}} = \frac{g_2}{\sqrt{\Gamma'\mu}}. \tag{205}$$

The flow equations for the time scale ratios are analogous to (196)

$$l\frac{\mathrm{d}w_i}{\mathrm{d}l} = \beta_{w_i}(u,\gamma,\{w_j\},\{F_j\}) \tag{206}$$

where $i = 1, 2, 3$ and with β-functions

$$\beta_{w_1} = w_1\big(-c_{w_1} + \zeta_\Gamma - \zeta_\lambda\big), \tag{207}$$

$$\beta_{w_2} = w_2\big(-c_{w_2} + \zeta_\Gamma - \zeta_\mu\big), \tag{208}$$

$$\beta_{w_3} = w_3\big(-c_{w_3} + \zeta_L - \tfrac{1}{2}(\zeta_\lambda + \zeta_\mu)\big). \tag{209}$$

For simplicity, we dropped the argument list $(u,\gamma,\{w_i\},\{F_i\})$ in the above equations. The naive dimensions are $c_{w_1} = c_{w_2} = c_{w_3} = 0$ in models C′, E′, F′, while in model H′ one has $c_{w_1} = 2$, $c_{w_2} = 0$ and $c_{w_3} = 0$. The flow equations for the mode coupling parameters are

$$l\frac{\mathrm{d}F_i}{\mathrm{d}l} = \beta_{F_i}(u,\gamma,\{w_j\},\{F_j\}) \qquad \text{or} \qquad l\frac{\mathrm{d}f_i}{\mathrm{d}l} = \beta_{f_i}(u,\gamma,\{w_j\},\{f_j\}) \tag{210}$$

where $i = 1, 2$. The corresponding β-functions read

$$\beta_{F_1} = -F_1\left(\frac{\varepsilon}{2} + \zeta_\lambda\right), \tag{211}$$

$$\beta_{F_2} = -F_2\left(\frac{\varepsilon}{2} - \zeta_{g_2} + \zeta_\mu\right). \tag{212}$$

or

$$\beta_{f_1} = -\frac{f_1}{2}\left(\varepsilon + \zeta_\lambda + \mathrm{Re}\left[\frac{\Gamma}{\Gamma'}\zeta_\Gamma\right]\right), \tag{213}$$

$$\beta_{f_2} = -\frac{f_2}{2}\left(\varepsilon - 2\zeta_{g_2} + \zeta_\mu + \mathrm{Re}\left[\frac{\Gamma}{\Gamma'}\zeta_\Gamma\right]\right). \tag{214}$$

Only the second secondary density has a static coupling γ to the OP therefore we have always $\zeta_{g_1} = 0$, which is already taken into account in (211) and (213). From the renormalization of the mode coupling parameters in section 7.2 follows that ζ_{g_2} is either 0 or ζ_m in the different dynamic models. Explicit expressions for dynamic ζ-functions in two-loop order are presented in appendix A.

An exception of the considerations so far is model J (Heisenberg ferromagnet). This model includes a conserved OP with a kinetic coefficient Γ and a mode coupling g. No secondary density is present. Thus, there is only one mode coupling parameter and we denote it by

$$F \equiv \frac{g}{\Gamma}. \tag{215}$$

The naive dimension of F is $c_F = (6 - d)/2$ instead of $(4 - d)/2$ in all other models. The corresponding β-function reads

$$\beta_F(u, F) = -F\left(\frac{6-d}{2} - \zeta_g(u) + \zeta_\Gamma(u, F)\right). \tag{216}$$

From (130) it immediately follows $\zeta_g(u) = \zeta_\varphi(u)/2$ leading to

$$\beta_F(u, F) = -F\left(\frac{6-d}{2} - \frac{1}{2}\zeta_\varphi(u) + \zeta_\Gamma(u, F)\right). \tag{217}$$

The static flow equations (176) and dynamic flow equations (196)–(210) describe the critical behaviour of the corresponding parameters. Starting from initial values $y_i(\ell_0)$, the asymptotic critical region can be reached by integrating the flow equations and performing the limit $\ell \to 0$. The flow parameter can be related by means of a so-called 'matching condition' to the correlation length $\xi^{-2}(t)$, depending on the relative temperature $t = (T - T_c)/T_c$ (T_c denotes the critical temperature of the considered system), to the wave vector k and the frequency ω. This matching condition is chosen in such a way that the integral expressions of the amplitudes of the vertex functions remain finite in the asymptotic critical limit. The matching condition defines generally a path $\ell(t, k, \omega)$ in the ω–k–ξ^{-2}-space. But in most cases only the paths in a subspace are needed. These are for instance as follows:

- $k = 0, \omega = 0$. This path is used to calculate the critical temperature behaviour of quantities such as specific heat, susceptibility, thermal conductivity, mass diffusion coefficient or thermodiffusion ratio. All functions depend only on ξ^{-2} and the matching condition reads

$$\frac{\xi^{-2}(t)}{(\kappa\ell)^2} = 1. \tag{218}$$

From the matching condition, a function $\ell(t)$ is obtained which transforms all model parameters $y_i(\ell(t))$ to functions of the relative temperature. In most cases, the asymptotic correlation length

$$\xi(t) = \xi_0 t^{-\nu} \tag{219}$$

is used and $\kappa = \xi_0^{-1}$ has been chosen. Then, the matching condition (218) reduces to $\ell(t) = t^{\nu}$. But for $\xi(t)$ also any other function which includes a more realistic background behaviour may be used in (218) leading to non-asymptotic effects in the functions $y_i(\ell(t))$.

- $\xi^{-2} = 0, \omega = 0$. This path is taken for the critical k-dependence of shape functions or the characteristic frequency (see the next section) when only their k-dependence is of interest. The amplitude functions, which are only a function of k in this case, stay finite in the critical limit with the matching condition

$$\frac{k}{\kappa\ell} = 1 \tag{220}$$

which relates the flow parameter ℓ to the wave vector k. Inserting $\kappa = \xi_0^{-1}$ we obtain $\ell(k) = \xi_0 k$ and all model parameters become functions $y_i(\ell(k))$.

- $\xi^{-2} = 0, k = 0$. Considering critical sound propagation, the critical frequency dependence of the sound velocity and sound attenuation is of interest. Moving along this path, all amplitudes are functions of ω and they stay finite with the matching condition

$$\frac{\omega}{2\Gamma'(\ell)(\kappa\ell)^{2+a}} = 1 \tag{221}$$

leading to a function $\ell(\omega)$. The above relation is written in a general form. For systems with a real OP kinetic coefficient, we have $\Gamma'(\ell) = \Gamma(\ell)$. The parameter a is equal to 0 for a non-conserved OP (model F/F′ for instance) and 2 for a conserved OP (model H/H′ for instance). With the flow parameter $\ell(\omega)$, the model parameters $y_i(\ell(\omega))$ are functions of the frequency.

In cases where more then one variable is different from zero, the matching condition is generalized and may depend on the classical dynamical critical exponent z (for an example see (360)).

7.5. *Dynamic stability*

The stability of the dynamic fixed point follows from the dynamic stability matrix obtained in the same way as the static stability matrix (187). One has to expand around the fixed point. A dynamic fixed point is then stable if the eigenvalues of the stability matrix (we consider as an example the case of one mode coupling f and one time scale ratio w)

$$\left(\frac{\partial\beta_{y_j}}{\partial y_i}\right)\Bigg|_{\{y\}=\{y^\star\}} = \left(\begin{array}{cc} \left(\frac{\partial\beta_f}{\partial f}\right) & \left(\frac{\partial\beta_w}{\partial f}\right) \\ \left(\frac{\partial\beta_f}{\partial w}\right) & \left(\frac{\partial\beta_w}{\partial w}\right) \end{array}\right)\Bigg|_{\substack{u=u^\star,\gamma=\gamma^\star \\ w=w^\star,f=f^\star}} \tag{222}$$

are positive. These eigenvalues which give the dynamical transient exponents are

$$\omega_\pm = \frac{1}{2}\left(\frac{\partial\beta_f}{\partial f} + \frac{\partial\beta_w}{\partial w}\right) \times \left(1 \pm \sqrt{1 - 4\left(\frac{\partial\beta_f}{\partial f}\frac{\partial\beta_w}{\partial w} + \frac{\partial\beta_w}{\partial f}\frac{\partial\beta_f}{\partial w}\right) \Big/ \left(\frac{\partial\beta_f}{\partial f} + \frac{\partial\beta_w}{\partial w}\right)^2}\right)\Bigg|_{\substack{u=u^\star,\gamma=\gamma^\star \\ w=w^\star,f=f^\star}}. \tag{223}$$

It is a general feature of the eigenvalue ω_- that for $w^\star \to 0$ one finds $\omega_- \to 0$ if the β-functions are well behaved. This is the case for all models considered here (see the explicit discussion for the SSS model, section 15.1). This feature ensures that the existence boundary of the fixed point with finite $w^\star$ agrees with the stability boundary of the fixed point with finite $w^\star$ and the stability boundary of the fixed point with $w^\star = 0$. This guarantees that dynamic scaling holds with well-defined dynamical critical exponents (see section 8.3) in the d–n-plane (so-called 'phases'; see especially the discussion for model C and the SSS model).

8. Dynamic scaling and asymptotic exponents

8.1. Scaling of the dynamic correlation function

The dynamic scaling assumption states [96] that the dynamic correlation function $\mathring{C}_{\varphi\varphi^+}(\xi, k, \omega)$ of the OP introduced in (71) is a homogeneous function of its arguments in the asymptotic region. It can be written in the form

$$\mathring{C}_{\varphi\varphi^+}(\xi, k, \omega) = \frac{\mathring{C}^{(s)}_{\varphi\varphi^+}(\xi, k)}{\omega_c(\xi, k)} \mathcal{F}\left(\frac{\omega}{\omega_c(\xi, k)}, k\xi\right) \tag{224}$$

with

$$\mathring{C}^{(s)}_{\varphi\varphi^+}(\xi, k) = \left\langle \varphi_0(k)\varphi_0^+(-k)\right\rangle_c(\xi) = \left[\mathring{\Gamma}^{(s)}_{\varphi\varphi^+}(\xi, k)\right]^{-1} \tag{225}$$

as the static correlation function (see also equation (31)) and $\mathcal{F}$ the dynamic shape function. The scaling form of the static correlation function is

$$\mathring{C}^{(s)}_{\varphi\varphi^+}(\xi, k) = k^{-2+\eta} g(k\xi). \tag{226}$$

The characteristic frequency ω_c (for which we take the half width at half height of the dynamic correlation function) is also a homogeneous function of k. Dynamic critical scaling assumes

$$\omega_c(\xi, k) = A_\phi k^{z_\varphi} f(k\xi) \tag{227}$$

with z_φ as the only new dynamic critical exponent. The frequency is measured in an appropriate time scale. The shape function $\mathcal{F}(y, x)$ fulfils the relations

$$\int \mathrm{d}y\, \mathcal{F}(y, x) = 2\pi \qquad \text{and} \qquad \mathcal{F}(1, x) = \frac{1}{2}\mathcal{F}(0, x) \tag{228}$$

where the scaling variables

$$x = k\xi, \qquad y = \frac{\omega}{\omega_c(\xi, k)} \tag{229}$$

have been introduced. The large y-behaviour of $\mathcal{F}$ at T_c ($\xi^{-1} = 0$) is proportional to $y^{-\upsilon_\varphi}$.

The limiting behaviour of the dynamic correlation function (224) for $k \to 0$ is different for conserved and non-conserved OPs. In the case of a conserved OP the dynamic correlation function has to be proportional to k^2, while in the non-conserved case it goes to a constant value. Inserting the scaling forms (226) and (227) into (224), one obtains for large y

$$\frac{k^{-2+\eta}}{k^{z_\varphi}} \left(\frac{\omega}{k^{z_\varphi}}\right)^{-\upsilon_\varphi} \sim k^2 \qquad \text{for a conserved OP,} \tag{230}$$

$$\frac{k^{-2+\eta}}{k^{z_\varphi}} \left(\frac{\omega}{k^{z_\varphi}}\right)^{-\upsilon_\varphi} \sim k^0 \qquad \text{for a non-conserved OP.} \tag{231}$$

Table 2. Dynamical critical exponent ζ_φ and ζ_m of the dynamic OP and secondary density shape function in different models in $d = 3$ calculated from the dynamic critical exponents z_φ and z_m (see table 3) according to (232) and (239).

Model	Remark	υ_φ	υ_m
A		$\frac{4-(1-c)\eta}{2+c\eta} \sim 2$	–
B		2	–
C	$n = 1$	$\frac{4+\alpha/\nu-\eta}{2+\alpha/\nu} \sim 1.89$	$\frac{4+\alpha/\nu}{2+\alpha/\nu} \sim 1.86$
C	$n > 1$	$\frac{4-(1-c)\eta}{2+c\eta} \sim 2$	2
E	Scaling FP	$\frac{7-2\eta}{3} \sim 2.3$	$\frac{7-2\eta}{3} \sim 2.3$
G		$\frac{7-2\eta}{3} \sim 2.3$	$\frac{7-2\eta}{3} \sim 2.3$
H		$\frac{8-2\eta-x_\lambda}{4-\eta-x_\lambda} \sim 2.3$	
J		$\frac{13-3\eta}{5-\eta} \sim 2.6$	–

Therefore, the exponent υ_φ has to fulfil the relation

$$\upsilon_\varphi = \frac{z_\varphi + 4 - \eta}{z_\varphi} \qquad \text{for a conserved OP,} \tag{232}$$

$$\upsilon_\varphi = \frac{z_\varphi + 2 - \eta}{z_\varphi} \qquad \text{for a non-conserved OP.} \tag{233}$$

If a secondary density is present, the corresponding dynamic correlation function $\mathring{C}_{mm}(\xi, k, \omega)$ (see (78) for a single density $\beta_i = \beta$) fulfils a scaling relation analogous to (224). One has

$$\mathring{C}_{mm}(\xi, k, \omega) = \frac{\mathring{C}^{(s)}_{mm}(\xi, k)}{\omega_c^{(m)}(\xi, k)} \mathcal{F}_m \left(\frac{\omega}{\omega_c^{(m)}(\xi, k)}, k\xi \right) \tag{234}$$

where $\mathcal{F}_m$ is the corresponding shape function. The function

$$\mathring{C}^{(s)}_{mm}(\xi, k) = \langle m_0(k) m_0(-k) \rangle_c(\xi) = \left[\mathring{\Gamma}^{(s)}_{mm}(\xi, k) \right]^{-1} \tag{235}$$

is the static correlation function (see also equation (52)) of the secondary density. The scaling form of the static correlation function is simply

$$\mathring{C}^{(s)}_{mm}(\xi, k) = g_m(k\xi). \tag{236}$$

The characteristic frequency $\omega_c^{(m)}$ fulfils a scaling relation

$$\omega_c^{(m)}(\xi, k) = k^{z_m} f_m(k\xi) \tag{237}$$

analogous to (227). Assuming that the large y-behaviour of the shape function $\mathcal{F}_m$ at T_c is proportional to $y^{-\upsilon_m}$, we obtain the relation

$$\frac{1}{k^{z_m}} \left(\frac{\omega}{k^{z_m}} \right)^{-\upsilon_m} \sim k^2 \qquad \text{for a conserved OP} \tag{238}$$

when (236) and (237) are inserted into (234). The right-hand side of (238) follows from the fact that the secondary densities are always conserved. The exponent υ_m is therefore

$$\upsilon_m = \frac{z_m + 2}{z_m}. \tag{239}$$

8.2. The static critical exponents

GLW model. The connection between the fixed-point values of the static ζ-functions of the GLW model and the static critical exponents is well established [59, 75] and will not be repeated comprehensively in this review. In the current notation, the anomalous dimension η appearing in the scaling form of the static OP correlation function (see equation (226)) is

$$\zeta_\varphi^\star \equiv \zeta_\varphi(u^\star) = -\eta. \tag{240}$$

The critical exponent ν of the correlation length (219) is defined by the relation

$$\zeta_{\varphi^2}^\star \equiv \zeta_{\varphi^2}(u^\star) = 2 - \frac{1}{\nu}. \tag{241}$$

The remaining static exponents are then determined by familiar scaling relations [59]. The asymptotic behaviour, above T_c, of the specific heat $C_+(t)$ ($t = |T - T_c|/T_c$) and the susceptibility $\chi_+(t)$ is

$$C_+(t) = C_0 t^{-\alpha}, \qquad \chi_+(t) = \chi_0 t^{-\gamma}. \tag{242}$$

Note that the critical exponent γ above should not be confused with the renormalized static coupling γ of the extended static functional in (107). The exponents α and γ are related to η and ν by

$$2 - \alpha = d\nu, \qquad \gamma = (2 - \eta)\nu. \tag{243}$$

Approaching the critical point T_c from below, the asymptotic critical behaviour of the OP is

$$\varphi(t) = \varphi_0 |t|^\beta \tag{244}$$

where the exponent β fulfils the relation

$$\alpha + 2\beta + \gamma = 2. \tag{245}$$

Finally moving along the critical isotherm to the critical point, the external field J conjugated to the OP, which is for instance the magnetic field in the case of magnets or the chemical potential in the case of fluids, behaves like

$$J(\varphi) \sim \varphi^\delta. \tag{246}$$

The exponent δ can be calculated from β and γ by

$$\beta(\delta - 1) = \gamma. \tag{247}$$

Thus, all static exponents can be determined from η and ν or $\zeta_\varphi^\star$ and $\zeta_{\varphi^2}^\star$ correspondingly.

Extended static model. If at least one scalar secondary density is present, the additional ζ-function ζ_m is also related to static critical exponents. Of course, these exponents cannot be new and independent because the whole static critical behaviour is contained in the GLW model. The stable fixed point $\gamma^\star$, which depends on n as can be seen from (190) and (191), determines how $\zeta_m^\star$ is related to critical exponents. We obtain

$$\zeta_m^\star = \frac{\alpha}{2\nu} \qquad \text{for} \quad n = 1 \ (\gamma^\star \neq 0), \tag{248}$$

$$\zeta_m^\star = 0 \qquad \text{for} \quad n = 2, 3 \ (\gamma^\star = 0). \tag{249}$$

8.3. The dynamic critical exponent z

Order parameter. In order to connect the dynamic critical exponent z_φ with the ζ-functions introduced above, we consider the critical frequency $\omega_c(\xi, k)$ in (227) near T_c. The asymptotic form at T_c according to scaling is

$$\omega_c(\infty, k) = A_\varphi k^{z_\varphi}. \tag{250}$$

On the other hand, for the dynamic models introduced above the characteristic frequency can be written as

$$\omega_c(\infty, k) = \Gamma(\ell) k^{2+a} \tag{251}$$

where the flow parameter ℓ is connected to the wave vector via the matching condition $\ell = k/k_0$ (220) and $a = 0$ for non-conserved and $a = 2$ for conserved OP. $\Gamma(\ell)$ is determined by the flow equation

$$\ell \frac{\mathrm{d}\Gamma}{\mathrm{d}\ell} = \Gamma \zeta_\Gamma. \tag{252}$$

In the asymptotic region, it is assumed that the static and dynamic model parameters have reached their fixed-point values, thus we can write $\zeta_\Gamma^\star \equiv \zeta_\Gamma(\{y_i^\star\})$. Inserting into (252) the asymptotic solution of the flow equation leads to

$$\Gamma(\ell) = \Gamma(\ell_0) \ell^{\zeta_\Gamma^\star}. \tag{253}$$

Inserting this solution into (251) and using the matching condition (220), one finds the asymptotic behaviour of the critical frequency as

$$\omega_c(\infty, k) \sim \Gamma(\ell_0) k^{2+a+\zeta_\Gamma^\star}. \tag{254}$$

Comparing (250) and (254), one concludes that the dynamic critical exponent z_φ of the OP is

$$z_\varphi = 2 + a + \zeta_\Gamma^\star. \tag{255}$$

Inserting the relation between the RCs (115) into the definition of the ζ-functions, (162) ζ_Γ can be expressed as

$$\zeta_\Gamma^\star = \tfrac{1}{2}\zeta_\varphi^\star - \tfrac{1}{2}\zeta_{\tilde{\varphi}^+}^\star + \zeta_\Gamma^{(d)\star}. \tag{256}$$

Secondary density. If at least one secondary density is present, a corresponding critical frequency $\omega_c^{(m)}$ can be introduced (see equation (234)). According to (250), the asymptotic behaviour of the critical frequency is

$$\omega_c^{(m)}(\infty, k) = A_m k^{z_m}. \tag{257}$$

From dynamic models on the other hand the characteristic frequency can be written as

$$\omega_c^{(m)}(\infty, k) = \lambda(\ell) k^2. \tag{258}$$

The flow equation for the kinetic coefficient λ reads

$$\ell \frac{\mathrm{d}\lambda}{\mathrm{d}\ell} = \lambda \zeta_\lambda \tag{259}$$

with the asymptotic solution

$$\lambda(\ell) = \lambda(\ell_0) \ell^{\zeta_\lambda^\star}. \tag{260}$$

Inserting (260) into (258) leads to

$$\omega_c^{(m)}(\infty, k) \sim \lambda(\ell_0) k^{2+\zeta_\lambda^\star} \tag{261}$$

where again the matching condition (220) has been used. Within theory, the dynamic critical exponent z_m is therefore

$$z_m = 2 + \zeta_\lambda^\star. \tag{262}$$

From relation (119), it follows for ζ_λ

$$\zeta_\lambda = 2\zeta_m + \zeta_\lambda^{(d)}. \tag{263}$$

Using this relation at the fixed point, the dynamic exponent z_m can be written as

$$z_m = 2 + 2\zeta_m^\star + \zeta_\lambda^{(d)\star}. \tag{264}$$

Strong dynamical scaling states that there is only one dynamic exponent z. Thus in all correlation functions (of the OP and the other slow densities), the characteristic time scales with this one dynamic exponent z. Therefore, one has the relation between the differently defined exponents $z_\varphi = z_m$ corresponding to a relation of the ζ-functions at the fixed point. Weak dynamic scaling allows different time scales for the OP and the other conserved densities. Thus, one has in this case at least two different dynamic exponents z_φ and z_m. There may be a decoupling of the OP from a secondary density. Then, the decoupled density has no influence on the asymptotics and its characteristic time scale is trivial. The dynamic exponents of the decoupled densities are their classical ones, i.e. $z = 2$ since they are conserved. This region is called the decoupled region. Strong-scaling, weak-scaling and decoupled regions are related to different stable fixed points as will be shown in the following.

In contrast to the static critical exponents, which can only be determined at least in a loop expansion with a subsequent ε-expansion or $d = 3$ calculation, the dynamic exponents of most dynamic models can be derived exactly by using general arguments. In the following, we will consider the different models explicitly.

8.4. Dynamic exponent z of models without mode coupling terms

In models without mode coupling parameters g_i, or $F_i(f_i)$ correspondingly, the dynamic RCs of the KCs are simply 1 as discussed in section 7.2. Therefore, the corresponding ζ-functions vanish. That is

$$\zeta_\Gamma^{(d)} = 0, \qquad \zeta_\lambda^{(d)} = 0. \tag{265}$$

The dynamic exponents (256) and (264) reduce to

$$z_\varphi = 2 + a + \zeta_\Gamma^\star = 2 + a + \tfrac{1}{2}\zeta_\varphi^\star - \tfrac{1}{2}\zeta_{\tilde\varphi^+}^\star \tag{266}$$

and

$$z_m = 2 + \zeta_\lambda^\star = 2 + 2\zeta_m^\star. \tag{267}$$

Model A. This model includes only a non-conserved OP thus we have $a = 0$. The function $\zeta_{\tilde\varphi^+}(u, \Gamma)$ is nontrivial and can only be calculated in loop expansion. In two-loop order, one can write $\zeta_\Gamma^\star = \zeta_\Gamma^{(A)}(u^\star) = c\eta$ in both the real model A and the complex model A* because $\Gamma'^\star = 0$. The coefficient c depends on the order of the loop expansion. Although separating η is trivial, it turns out that c is independent of n at least up to three-loop order (see [97, 98] and section 9). In two-loop order, $\zeta_\Gamma^{(A)}(u)$ is given in appendix A. Inserting into (266), a dynamic critical exponent

$$z_\varphi = 2 + c\eta \tag{268}$$

is obtained.

Model B. This model includes only a conserved OP thus we have $a = 2$. From relation (110), it immediately follows $\zeta_{\tilde\varphi^+}^\star = -\zeta_\varphi^\star$. This leads to a dynamic exponent

$$z_\varphi = 4 + \zeta_\varphi^\star = 4 - \eta \tag{269}$$

where in the last equality (240) has been used. In contrast to model A, this result is valid for all orders of loop expansion. The dynamic exponent is determined by statics.

Model C. A more complicated situation is found in model C where a non-conserved OP ($a = 0$) is coupled in the static functional to a conserved secondary density (energy). The critical dynamic exponents depend on the stable fixed points of the static coupling γ and the time scale ratio w. From (197), the relation for the fixed point of w follows as

$$\beta_w(u^\star, \gamma^\star, w^\star) = 0 = w^\star(\zeta_\Gamma^\star - \zeta_\lambda^\star). \tag{270}$$

For this equation several solutions are possible.

(i) $w^\star \neq 0$: then the relation $\zeta_\Gamma^\star = \zeta_\lambda^\star$ must hold which is only possible if also $\gamma^\star \neq 0$. From $\zeta_\lambda^\star = 2\zeta_m^\star$ and (248) follows

$$\zeta_\Gamma^\star = \zeta_\lambda^\star = 2\zeta_m^\star = \frac{\alpha}{\nu}. \tag{271}$$

The dynamical critical exponents (265) and (267) are then

$$z_\varphi = z_m = 2 + \frac{\alpha}{\nu}. \tag{272}$$

The critical frequencies are getting equal in the asymptotic region therefore the fixed point $\gamma^\star \neq 0$, $w^\star \neq 0$ is called the scaling fixed point, which is stable for $n = 1$.

(ii) $w^\star = 0$: ζ_Γ in model C has the property $\zeta_\Gamma(u, \gamma, w = 0) = \zeta_\Gamma^{(A)}(u)$ (see appendix A). At the fixed point, we have therefore $\zeta_\Gamma^\star = \zeta_\Gamma^{(A)}(u^\star) = c\eta$. The critical dynamical exponent for the OP,

$$z_\varphi = 2 + c\eta, \tag{273}$$

is identical to model A. z_m depends on the fixed-point value of γ due to (248) and (249). Inserting into (267) leads to

$$z_m = \begin{cases} 2 + \dfrac{\alpha}{\nu} & \text{for} \quad \gamma^\star \neq 0, \\ 2 & \text{for} \quad \gamma^\star = 0. \end{cases} \tag{274}$$

The fixed point $w^\star = 0$, $\gamma^\star \neq 0$ is denoted as weak-scaling fixed point[3], while $w^\star = 0$, $\gamma^\star = 0$ is the decoupling fixed point. For the integer OP dimensions $n = 2, 3$, the weak-scaling fixed point is stable. A comprehensive discussion of the stability regions of model C in the whole n–d-plane is given in [80].

8.5. Dynamic exponent z of models with mode coupling terms

In models which include mode coupling parameters, the purely dynamic ζ-functions $\zeta_\Gamma^{(d)}$ and $\zeta_\lambda^{(d)}$ are different from zero and give a contribution to the dynamic exponents. Apart from model F, all models of this type (models E, G, H, J) do not contain a static coupling γ, thus we have $\zeta_m = 0$ in these cases. The OP in model F has a component number $n = 2$. From (249), we know that the stable fixed point is $\gamma^\star = 0$ for $n = 2$. Thus in model F the relation $\zeta_m^\star = 0$ is valid at the fixed point, which means that γ does not influence the fixed-point discussion. Therefore in all models with mode couplings, the dynamic critical exponent of the secondary densities is

$$z_m = 2 + \zeta_\lambda^\star = 2 + \zeta_\lambda^{(d)\star}. \tag{275}$$

[3] At the strong-scaling fixed-point dynamic scaling involves only one dynamic exponent z whereas at the weak-scaling fixed point two different dynamic exponents are necessary.

Models E, G, SSS, DP. All models include a non-conserved OP ($a = 0$) and a conserved secondary density. The equations for the fixed point have the same structure and will be discussed together leading to the same critical dynamic exponents. The dynamic fixed points are determined by the equations

$$\beta_w(u^\star, w^\star, f^\star) = 0 = w^\star\left(\zeta_\Gamma^\star - \zeta_\lambda^{(d)\star}\right) \tag{276}$$

and

$$\beta_f(u^\star, w^\star, f^\star) = 0 = -\frac{f^\star}{2}\left(\varepsilon + \zeta_\Gamma^\star + \zeta_\lambda^{(d)\star}\right). \tag{277}$$

The fixed point $f^\star \neq 0$ is stable therefore from (277) follows immediately

$$\zeta_\Gamma^\star + \zeta_\lambda^{(d)\star} = -\varepsilon. \tag{278}$$

The dynamical critical exponent now depends on the fixed point $w^\star$.

(i) $w^\star \neq 0$: at the scaling fixed point, the ζ-functions fulfil the relation

$$\zeta_\Gamma^\star = \zeta_\lambda^{(d)\star} \tag{279}$$

which follows from (276). Inserting into (278) leads to

$$\zeta_\Gamma^\star = \zeta_\lambda^{(d)\star} = -\frac{\varepsilon}{2}. \tag{280}$$

The critical dynamic exponents are obtained by inserting (280) into (255) and (275). This gives

$$z_\varphi = z_m = \frac{d}{2} \tag{281}$$

which is an exact result valid in all orders of loop expansion.

(ii) $w^\star = 0$: at the weak-scaling fixed point nothing can be concluded from (276), thus only relation (278) is valid from which a weak-scaling fixed-point value $f^\star = f_{\mathrm{WSC}}$ may be calculated in every order of loop expansion. Inserting $w^\star = 0$, $f^\star = f_{\mathrm{WSC}}$ into the ζ-functions of (255) and (275) leads to loop expanded critical dynamic exponents (see [99, 100]).

One can define the stability exponent $\omega_w^{\mathrm{WSC}} = \zeta_\Gamma^\star - \zeta_\lambda^{(d)\star}$ at the weak-scaling fixed point. Then, using (280) the critical dynamic exponents read [4]

$$z_\varphi = \frac{d}{2} + \omega_w^{\mathrm{WSC}}/2, \qquad z_m = \frac{d}{2} - \omega_w^{\mathrm{WSC}}/2. \tag{282}$$

Thus, the two dynamic exponents differ by the correction exponent. Near the stability borderline between the scaling and the weak-scaling fixed point ω_w^{WSC} is very small and $w^\star$ is very small or zero. Both situations lead to the same effects in the critical behaviour of dynamic quantities. The most prominent effect is the non-universal behaviour of the universal amplitude of the thermal conductivity and second sound damping at the superfluid transition (see the discussion below).

Model F. As mentioned at the beginning of this section, the static coupling γ does not influence the fixed-point discussion in this model compared to models E, G due to $\gamma^\star = 0$. The only difference remaining to model E is then the imaginary part Γ'' present in this model. The only contributions to the imaginary part of ζ_Γ are proportional to w'', also present in the complex model C*, and from i$g\gamma$ terms. At the fixed point $\gamma^\star = 0$, the latter contributions vanish and the imaginary part of ζ_Γ is only generated by w'' like in model C*. From there it is known that $w''^\star = 0$. Thus, model F reduces completely to model E at the fixed point. As a consequence, also the critical dynamic exponents are like in model E.

Model H. The dynamic equations include a conserved OP ($a = 2$) and a conserved secondary density. The time scale ratio $w = \Gamma/\lambda$ has a naive dimension -2 and is therefore irrelevant.

Table 3. The dynamical critical exponent for different dynamic models. The expression c, the transient ω_w^{WSC} and the exponent of the shear viscosity x_η have to be calculated from a dynamical loop expansion. Exponents η, α and ν are the static critical exponents of the correlation function at the critical point, of the specific heat and of the correlation length, respectively.

Model	Name	z_{OP} (in $d = 3$)	z_m
Relaxation	A	$2 + c\eta$	–
Diffusion	B	$4 - \eta$	–
Relaxation	C	$2 + \alpha/\nu$ $(n = 1)$	$2 + \alpha/\nu$ $(n = 1)$
Relaxation	C	$2 + c\eta$ $(n \geqslant 2)$	2 $(n \geqslant 2)$
Relaxation	C′	Same as model C	Same as model C
Symmetric planar m	E	$3/2$ or $3/2 - \omega_w^{\mathrm{WSC}}/2$	$3/2$ or $3/2 + \omega_w^{\mathrm{WSC}}/2$
E′	Same as model E	Same as model E	
Asymmetric planar m	F	Same as model E	Same as model E
F′	Same as model E	Same as model E	
Antiferromagnet	G	$3/2$	–
Fluid	H	$3 + x_\eta$	$2 - x_\eta$
Mixture	H′	$3 + x_\eta$	$2 - x_\eta$
Ferromagnet	J	$1/2(5 - \eta)$	–
DP model	DP	$3/2$ or $3/2 - \omega_w^{\mathrm{WSC}}/2$	$3/2$ or $3/2 + \omega_w^{\mathrm{WSC}}/2$

Thus, only a weak-scaling fixed point $w^\star = 0$ exists in this model. The only remaining dynamic fixed-point equation is equal to (277) leading to the same relation

$$\zeta_\Gamma^\star + \zeta_\lambda^{(d)\star} = -\varepsilon \tag{283}$$

as in (278). The difference now is the conserved OP from which $\zeta_{\tilde{\varphi}^+}^\star = -\zeta_\varphi^\star = \eta$ follows (see also model B). This gives $\zeta_\Gamma^\star = -\eta + \zeta_\Gamma^{(d)\star}$. Inserting into (283) leads to the relation

$$\zeta_\Gamma^{(d)\star} + \zeta_\lambda^{(d)\star} = -(\varepsilon - \eta). \tag{284}$$

This relation is consistent with the exponent relation

$$x_\lambda + x_\eta = \varepsilon - \eta \tag{285}$$

found in [101] where x_λ is the dynamical critical exponent of the thermal conductivity (denoted by λ therein) and x_η accordingly of the shear viscosity (denoted by η in this reference). The field-theoretic functions in the present approach are related to the exponents introduced in [101] by the relations $\zeta_\Gamma^{(d)\star} = -x_\lambda$ and $\zeta_\lambda^{(d)\star} = -x_\eta$. These two dynamic exponents have to be calculated in loop expansion in order to determine the dynamic exponents

$$z_\varphi = 4 - \eta - x_\lambda = d + x_\eta, \qquad z_m = 2 - x_\eta. \tag{286}$$

In the second equality of the first equation relation (285) has been used.

Model J. This model includes only a conserved OP ($a = 2$) without any secondary density. From (217) follows at the fixed point

$$\beta_F(u^\star, F^\star) = 0 = -F^\star \left(\frac{6-d}{2} - \frac{1}{2}\zeta_\varphi^\star + \zeta_\Gamma^\star \right). \tag{287}$$

For $F^\star \neq 0$, one gets from the above equation

$$\zeta_\Gamma^\star = -\frac{6-d}{2} + \frac{1}{2}\zeta_\varphi^\star = -\frac{6-d+\eta}{2}. \tag{288}$$

Inserting this into (255), the critical dynamic exponent reads

$$z_\varphi = \frac{2+d-\eta}{2}. \tag{289}$$

The critical exponent z has been derived directly above T_c (see also [102]) without using dynamic scaling and the propagating mode below T_c [96]. Note that in all cases the naive dimension of the mode coupling F is $(6-d)/2$. Thus, the static upper borderline dimension $d_c = 4$ for the irrelevance of the static coupling u is different from $d_c = 6$ for the irrelevance of the mode coupling F.

We may conclude that in many cases the asymptotic dynamical power laws can be found without explicit perturbational calculations, which are necessary for the relaxational model A, the liquid–gas critical point model H and for the superfluid transition described by model E or F if the weak-scaling fixed point is stable (which seems to be the case). As we shall see below perturbational calculations are necessary anyway for calculating dynamical correlation functions or the crossover from background behaviour to the asymptotic behaviour of transport coefficients.

9. Model A (relaxational dynamics)

Model A is the simplest dynamical model which may apply to uniaxial magnetic systems [20, 50]. It describes the dynamics of a non-conserved OP relaxing to an equilibrium fixed by the static functional $\mathcal{H}$ of the GLW model (24). The most general form, denoted as model A* in the following, includes a complex OP $\vec{\varphi}_0$ with $n/2$-components, which fulfils the equations [97]

$$\frac{\partial \vec{\varphi}_0}{\partial t} = -2\mathring{\Gamma}\frac{\delta \mathcal{H}}{\delta \vec{\varphi}_0^+} + \vec{\theta}_\varphi, \qquad \frac{\partial \vec{\varphi}_0^+}{\partial t} = -2\mathring{\Gamma}^+\frac{\delta \mathcal{H}}{\delta \vec{\varphi}_0} + \vec{\theta}_\varphi^+ \tag{290}$$

with a complex relaxation rate $\mathring{\Gamma} = \mathring{\Gamma}' + \mathrm{i}\mathring{\Gamma}''$ (a real OP leads necessarily to a real relaxation rate). The field-theoretic ζ-function $\zeta_\Gamma(u, \Gamma)$ of model A* is complex. Although the model has been treated in [97], no explicit result can be found therein. The reason is that the real and imaginary parts of the corresponding functions have been calculated separately which is a cumbersome procedure. A two-loop calculation with the complex relaxation rate is relatively simple and can be found in appendix A (see (A.1)). The fixed-point value of the imaginary part $\mathring{\Gamma}''$ is zero and the asymptotic behaviour of model A* is identical to model A described by

$$\frac{\partial \vec{\phi}_0}{\partial t} = -\mathring{\Gamma}\frac{\delta \mathcal{H}}{\delta \vec{\phi}_0} + \vec{\theta}_\phi \tag{291}$$

with a real n-component OP $\vec{\phi}_0$ and a real kinetic coefficient Γ. The static functional $\mathcal{H}$ (24) has to be taken for $\vec{\varphi}_0 = \vec{\varphi}_0^+ = \vec{\phi}_0$.

The dynamical critical exponent z_φ for model A is usually written in the form $z_\varphi = 2 + c\eta$ (268) with the static exponent η in three-loop order and ε-expanded

$$\eta = \frac{n+2}{2(n+8)}\varepsilon^2\left(1 + \frac{-n^2+56n+272}{4(n+8)^2}\varepsilon\right). \tag{292}$$

For the expansion up to fifth-loop order see [60], for the Ising model ($n = 1$) a numerical estimate $\eta = 0.0364(5)$ has been given [103] where summation techniques have been used. The dynamical part c of z reads up to three-loop order in ε-expansion [98]:

$$c = 0.726(1 - 0.1885\varepsilon). \tag{293}$$

A surprising feature of this decomposition in the ε-expansion is the independence of the dynamic factor c from n. The n-dependence is up to this order only contained in the static exponent η. Taking the result for c at $\varepsilon = 1$ together with the best value for η from above leads to $z = 2.021$ for the Ising model. Earlier results [97] contained an error. Comparing with

Table 4. Different values for the dynamical critical exponent z_φ for the three-dimensional Ising model for which the models apply.

Reference	z_φ	Method
[50]	2.121	Two-loop ε-expansion
[98]	2.021	Three-loop ε-expansion
[105]	2.017	Four loop in $d = 3$ Padé Borel summed
[106]	2.017	Padé estimation
[107]	2.04 ± 0.03	MC simulation
[108]	2.032 ± 0.004	MC simulation
[109]	2.10 ± 0.02	MC simulation

the expansion given in footnote 4 the ε-expanded result of (293), it is in agreement with the $1/n$-expansion. In contrast, the earlier result of [97] does not agree with the $1/n$-expansion. Within the fixed dimension approach z has been calculated for $n = 1$ in three-loop [104] and four-loop order [105]. The question of the n-dependence has not been touched in this four-loop approach.

In order to improve the value of z for the Ising model ($n = 1$) in $d = 3$, an interpolation between the value obtained from an ε-expansion of the interface dynamics and the two-loop order result has been suggested [106]

$$z = 2 + \frac{6c(4-d)^2(d-1)}{(2+60c) - (4+3c)d + (2-3c)d^2}. \tag{294}$$

The value obtained in this way is in very good agreement with the four-loop calculation mentioned above (see also table 4).

Recently, the structure factor of the Ising model has been calculated in two-loop order [109]. As expected, only a slight deviation from the Lorentzian shape valid for the Gaussian model is found. In order to get the shape function in its scaling variables, one has to define the characteristic frequency ω_c or time scale τ_c. Several definitions are possible like half width at half height or a median frequency (see equation (3.19) in [1] for ω_c) or different autocorrelation times (see equations (13) or (14) in [109]). All these characteristic frequencies have the same asymptotic scaling behaviour as (251).

The theoretical results may be compared with computer simulations (for a review see [110]) which lead to estimates for the dynamical critical exponent z. The values reported in [111, 112] were smaller than 2, thus below the borderline value $z = 2$ for $n \geqslant 1$ according to (294) (see figure 1 in [106]). Later in simulations for larger systems values larger than 2 were found [107, 109, 113]. In table 4, we list the values for the dynamical critical exponents estimated by different methods for the three-dimensional Ising model. More values for z calculated by other methods may be found in [114] (see table 3 there).

It was argued [115] that the dynamical critical behaviour described by model A is stable with respect to all dynamical perturbations, including those of non-equilibrium nature, provided the dynamics is (i) local, (ii) does not conserve the order parameter or any other

[4] The lowest order of the $1/n$-expansion reads [50]

$$c = \frac{4}{4-d}\left(\frac{\mathrm{d}B(d/2-1, d/2-1)}{8\int_0^{1/2}\mathrm{d}x[x(2-x)]^{d/2-3}} - 1\right).$$

This also corrects a misprint in [1].

secondary density and (iii) respects the discrete symmetry of the equilibrium Ising model. Later it was shown that the last condition is not necessary [116].

We shortly mention that model A has also been considered below T_c [117] where the singular behaviour of the Goldstone mode has to be treated properly.

10. Models B and D (diffusive dynamics)

If the OP is a conserved quantity, the irreversible dynamics is determined by diffusion (see the discussion in section 3). Assuming an n-component real OP $\vec{\phi}_0$ the dynamic equation reads

$$\frac{\partial \vec{\phi}_0}{\partial t} = \mathring{\Gamma}\nabla^2 \frac{\delta \mathcal{H}}{\delta \vec{\phi}_0} + \vec{\theta}_\phi. \tag{295}$$

Due to the conservation property relation (110) holds (no new dynamic pole terms in $\mathring{\Omega}_{\varphi\tilde{\varphi}^+}$ of the vertex function (72)). The dynamic critical exponent z_φ remains the one found in conventional theory (see (269)),

$$z = 4 - \eta. \tag{296}$$

If there is another conserved density beside the OP, it might be considered as belonging to the set of slow variables (model D). It is easy to show that the static coupling to such a density is irrelevant and the critical dynamical behaviour is determined by the fixed point of model B.

This might be different if one abolishes the local conservation property, keeps the global conservation and allows long-range transport for the conserved density [51, 118]. Under such a case Fick's law is no longer valid. Then in Fourier space the generalized equation of motion would read

$$\left(\frac{1}{\mathring{\lambda} k^\sigma} + \frac{1}{\mathring{\Gamma}}\right) \frac{\partial \vec{\phi}_0(k,t)}{\partial t} = \frac{\delta \mathcal{H}}{\delta \vec{\phi}_0(k,t)} + \vec{\theta}_\phi(k,t), \tag{297}$$

where a value of $\sigma \neq 2$ and $\sigma > 0$ simulates non-locality and ensures conservation, respectively. Recently, a system of two dynamic equations of this type with a static functional $\mathcal{H} = \mathcal{H}_\varphi + \mathcal{H}_m^{(1s)}$ (see (38) and (40)) has been considered [119]. This amounts to adding an equation for a scalar density similar to (297)

$$\left(\frac{1}{\mathring{\lambda} k^\mu} + \frac{1}{\mathring{\Gamma}}\right) \frac{\partial m_0(k,t)}{\partial t} = \frac{\delta \mathcal{H}}{\delta m_0(k,t)} + \theta_m(k,t). \tag{298}$$

Under certain conditions, a 'true model-D-like region' exists in the σ–μ-space where σ and correspondingly μ are the exponents characterizing the non-locality of the OP and the coupling secondary density.

11. Model C and generalizations (model C′)

11.1. Model C/C and its 'phase diagram'*

In order to study the effect of energy conservation on the critical behaviour of a non-conserved OP, the basic equations of motion were set up in [20]. The model contains in addition to the OP equation (290) of model A* a model B-like equation for a secondary density m_0, which may be the energy density. So, we have for model C*

$$\frac{\partial \vec{\varphi}_0}{\partial t} = -2\mathring{\Gamma} \frac{\delta \mathcal{H}}{\delta \vec{\varphi}_0^+} + \vec{\theta}_\varphi, \qquad \frac{\partial \vec{\varphi}_0^+}{\partial t} = -2\mathring{\Gamma}^+ \frac{\delta \mathcal{H}}{\delta \vec{\varphi}_0} + \vec{\theta}_\varphi^+. \tag{299}$$

$$\frac{\partial m_0}{\partial t} = \mathring{\lambda}\nabla^2 \frac{\delta \mathcal{H}}{\delta m_0} + \theta_m \tag{300}$$

with an $n/2$-component complex OP $\vec{\varphi}_0$ and a complex kinetic coefficient $\mathring{\Gamma}$. The coupling of both equations is accomplished by a coupling $\mathring{\gamma}$ in the static functional $\mathcal{H} = \mathcal{H}_\varphi + \mathcal{H}_m^{(1s)}$ (see (38) and (40)). The dynamical parameter of interest is the time scale ratio $w = \Gamma/\lambda = w' + \mathrm{i}w''$ which is also a complex quantity. The explicit two-loop expressions of the ζ-functions ζ_Γ and ζ_λ are presented in (A.8) and (A.10). It turns out [80] that the fixed-point value of the imaginary part w'' of the time scale ratio is always zero leading to an asymptotic behaviour identical to model C. However, the imaginary generalization is an important limiting case of model F (see below). Model C is restricted to a real n-component OP $\vec{\phi}_0$ and a real kinetic coefficient $\mathring{\Gamma}$. The dynamic equations (299) reduce to

$$\frac{\partial \vec{\phi}_0}{\partial t} = -\mathring{\Gamma}\frac{\delta \mathcal{H}}{\delta \vec{\phi}_0} + \vec{\theta}_\phi. \tag{301}$$

The dynamic equation for the secondary density (300) remains unchanged. In order to discuss the fixed points and the asymptotic critical behaviour of this model, it is convenient to introduce beside the time scale ratio $w = \Gamma/\lambda$, which is now a real quantity, the parameter

$$\rho = \frac{w}{1+w}. \tag{302}$$

It maps the values $0 \leqslant w \leqslant \infty$ to the finite interval $0 \leqslant \rho \leqslant 1$. Three types of fixed-point values have been found [20] in one-loop order $w^\star = 0, w_c, \infty$ (or $\rho^\star = 0, \rho_c, 1$) corresponding to a situation where the OP time scale and the energy density time scale differ (weak scaling), where both have the same time scale (strong scaling) and where the conserved density is slower than the OP (anomalous fixed point with breakdown of scaling). It was not clear if and where in the d–n-plane the infinite fixed point is stable. Subsequent two-loop considerations [120] and calculation [121] could not clarify the situation, although a reestablishment of scaling in the anomalous region was found in [122].

The situation was clarified only recently [23, 80] by (i) calculating the two-loop field-theoretic functions and (ii) discussing the possible fixed-point values and their stability. It turned out that the cumbersome fixed point $w^\star = \infty$ ($\rho^\star = 1$) is unstable in the whole d–n-plane and the two other fixed points are stable in certain regions. However, this result cannot be obtained within the usual ε-expansions since a non-analytic ε-dependence of the finite fixed-point value appears in a certain region of the d–n-plane.

Considering the fixed point $\rho^\star(\varepsilon, n)$ as a function of the spatial dimension d and the component number n of the OP, one finds in the vicinity of 1 the deviation as

$$\rho^\star_{\mathrm{as}}(\varepsilon, n) = 1 - 0.5\,\mathrm{e}^{-a(\varepsilon,n)/\gamma^{\star 2}} \equiv 1 - x \tag{303}$$

with (L_A defined by (A.2))

$$a(\varepsilon, n) = \frac{n}{2} - 1 + \frac{n+2}{6}u^\star(1 - L_A) + \frac{\gamma^{\star 2}}{2}\left(\frac{n}{2} - 1 - \frac{(n+2)L_A}{2}\right) - \frac{(n+2)u^{\star 2}}{72\gamma^{\star 2}}(2L_A - 1) \tag{304}$$

proving it to be smaller than 1. Since $\gamma^{\star 2} \sim \varepsilon$, the fixed point $\rho^\star_{\mathrm{as}}(\varepsilon, n)$ cannot be represented in the usual ε-expansion. Figure 1 (right part) verifies the crossover of the numerical solution for $\rho^\star(\varepsilon, n)$ to the asymptotic solution (303), but even in this enlarged figure, the difference of $\rho^\star$ from 1 cannot be seen. This feature persists in a self-similar way even for higher magnifications.

Using the non-analytic fixed point (303) in calculating the stability regions, one comes to the 'phase diagram' in the d–n-plane as shown in figure 2. There exist three regions:

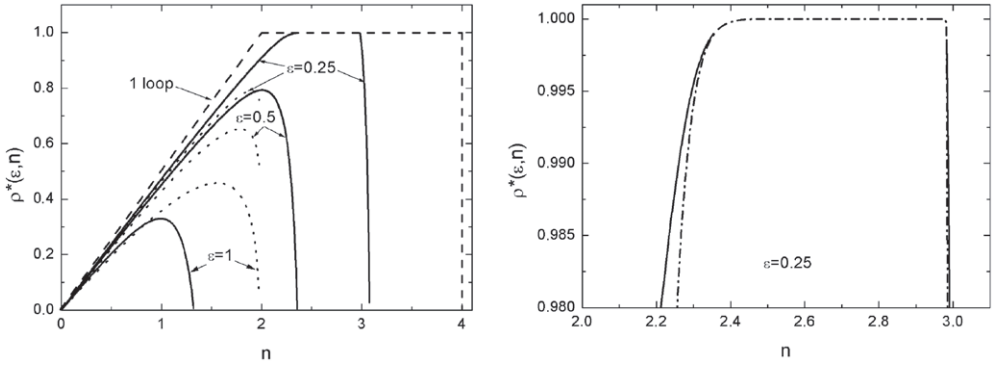

Figure 1. Left: fixed-point function $\rho^\star(\varepsilon, n)$ (n OP dimension) at different spatial dimensions d ($\varepsilon = 4 - d$); solid curve: numerical solution. The maximum of the function is always *smaller* than 1 (see (303)) but this is not visible for ε close zero. Dotted curves are calculated from strict ε-expansions, which break down at $n = 2$. Right: enlargement of the region near $\rho^\star(\varepsilon, n) = 1$. Shown here is the merging of the numerical solution (solid curve) into the analytic solution (303) (dashed-dotted curve) valid near $\rho^\star(n) = 1$. Even at this resolution, one cannot see that the fixed-point function does not reach the value 1 (from [23]).

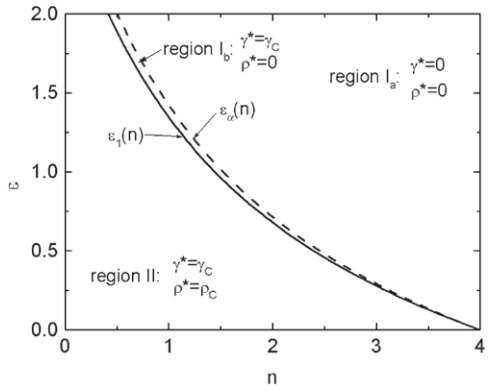

Figure 2. Regions of existence of different fixed points: $\varepsilon_\alpha(n)$ separates the region with non-diverging ($\gamma^\star \equiv 0$, right) from those with diverging ($\gamma^\star \neq 0$, left) specific heat (dashed curve). The solid curve $\varepsilon_1(n)$ separates the region I where the fixed point $\rho^\star(\varepsilon, n) \equiv 0$ is stable (right) from that where it is unstable (left).

- *Decoupled region I_a.* Right of $\varepsilon_\alpha(n)$ with $(u^\star = u_H, \gamma^\star = 0, \rho^\star = 0)$ stable; the asymptotic dynamical critical exponents are $z_\varphi = 2 + c\eta$ for the OP and $z_m = 2$ for the secondary density m.
- *Weak-scaling region I_b.* Between $\varepsilon_1(n)$ and $\varepsilon_\alpha(n)$ with $(u^\star = u_H, \gamma^\star = \gamma_C, \rho^\star = 0)$ stable; the asymptotic dynamical critical exponents are $z_\varphi = 2 + c\eta$ for the OP, $z_m = 2 + \alpha/\nu$ for the secondary density m
- *Strong-scaling region II.* Left of $\varepsilon_1(n)$ with $(u^\star = u_H, \gamma^\star = \gamma_C, \rho^\star = \rho_C)$ stable; the asymptotic dynamical critical exponents are $z_\varphi = z_m = 2 + \alpha/\nu$ for the OP and the secondary density m

The borderlines of the different boundaries are

$$\varepsilon_\alpha(n) = \frac{(4-n)(n+8)^2}{(n+2)(13n+44)}, \tag{305}$$

Table 5. Values for the dynamical critical exponent z in the different regions of the d–n-plane for the OP and the secondary density m.

	Region		
	I_a	I_b	II
z_φ	$2+c\eta$	$2+c\eta$	$2+\alpha/\nu$
z_m	2	$2+\alpha/\nu$	$2+\alpha/\nu$

where the static coupling goes to zero, and

$$\varepsilon_1(n) = \frac{(4-n)(n+8)}{(n+2)\left(\frac{13n+44}{n+8} + \left(L_A - \frac{1}{2}\right)\right)} \tag{306}$$

where w or ρ goes to zero.

The corresponding asymptotic dynamical critical exponents are collected in table 5. They are obtained from the ζ_Γ- and ζ_λ-function (see (A.8) and (A.10)) inserting the appropriate values for the fixed points. In the case of strong scaling ($w^\star \neq 0$), the fixed-point values $\zeta_\Gamma^\star = \zeta_\lambda^\star$ and can be expressed exactly by the static exponents α/ν (271).

From the two modes of model C, a dimensionless amplitude ratio can be defined [19]

$$\mu = \lim_{q\to 0}\left(\frac{\omega_m(q)}{\omega_\phi(q)(q\xi)^2}\right). \tag{307}$$

The amplitude was calculated within the Wilson–Feynman graph expansion in one-loop order [120]. Inserting the fixed-point values for $n = 1$ in the strong-scaling region in $\mathcal{O}(\varepsilon)$, one obtains

$$\mu = 1 + 0.5004\varepsilon. \tag{308}$$

So far no field-theoretic calculation of this ratio has been performed.

11.2. Flow of model C and effective dynamic exponent

The neighbourhood of the borderlines $\varepsilon_1(n)$ and $\varepsilon_\alpha(n)$ of the different regions in $d = 3$ for the cases $n = 1$ and $n = 2$ leads to the existence of small dynamical transient exponents. In fact one has the values 0.045 ($n = 1$), 0.0145 ($n = 2$) and 0.015 ($n = 3$) (see figure 3(*a*) in [80]). Therefore, one might expect that the non-asymptotic behaviour dominates and the dynamical behaviour is described by an effective exponent z_φ^{eff} instead of the asymptotic z_φ even for $n = 3$. The effective dynamic exponent for the OP is defined as

$$z_\varphi^{\text{eff}} = 2 + \zeta_\Gamma(u, \gamma; w) \tag{309}$$

extending the asymptotic definition (255). The values of the couplings u, γ and time ratio w are taken from the corresponding solution of the flow equations (see (176)–(178) and (196), (197) shown in the left part of figure 3). Inserting this flow into (309) gives the effective dynamical critical exponent. The right part of figure 3 displays two examples of z_φ^{eff} for each value of $n = 1, 2, 3$. The interesting general feature is that the effective exponents might be larger than the asymptotic values. The maximum decreases when the initial value of the fourth-order coupling u reaches its fixed-point value.

Comparing the flow of w in the left part of figure 3 and z_φ^{eff} in the right part of figure 3, one observes that the effective exponent might be near its fixed-point value although the time scale ratio w is far from its fixed-point value. This can be explained by looking at the expression for ζ_Γ (see (A.8)). One notes that ζ_Γ depends on the product $\gamma^2 w$. Therefore, if

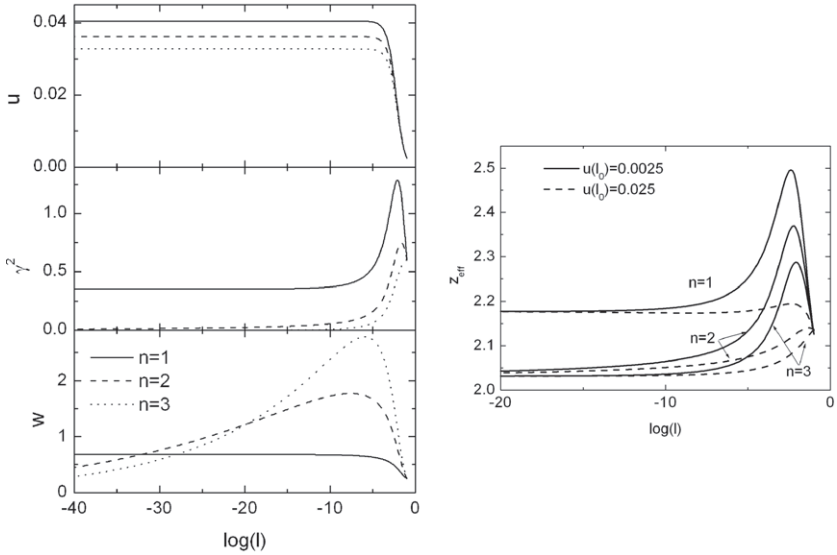

Figure 3. Left: flow of the static fourth-order coupling u, the static coupling γ^2 and the time scale ratio w at $\varepsilon = 1$ ($d = 3$) at three physically relevant OP component numbers $n = 1, 2, 3$. The initial values $u = 0.0025$, $\gamma^2(l_0) = 0.6$ and $w(l_0) = 0.25$ are the same in all three cases. Right: effective dynamical critical exponent for three physically relevant OP component numbers $n = 1, 2, 3$ calculated from the flow of figure 3. In order to demonstrate the dependence of z_φ^{eff} on the initial conditions two different initial values of u were chosen.

γ^2 reaches its fixed-point value $\gamma^{\star 2} = 0$ the time scale ratio w may be far from its fixed-point value $w^\star = 0$ but $\zeta_\Gamma \sim \zeta_\Gamma^\star$. This is the case for $n = 2, 3$. In the case $n = 1$, both γ^2 and w have to reach their fixed-point values in order to obtain the asymptotic result.

11.3. Computer simulations

Computer simulations have been performed in [123] for the Ising antiferromagnet with fixed magnetization well represented by model C [20]. For the Ising case, one expects $z = 2 + \alpha/\nu \sim 2.158$ much larger than the value expected for model A where $z \sim 2.05$. From simulations, a value of $z \sim 2.28$ was estimated. Surprisingly, a much larger exponent, $z \sim 3.3$, was found for the Ising ferromagnet with energy conservation which also belongs to the model C class [124].

11.4. Models C′ and C′*

Model C or C* may be generalized to the case where two conserved densities couple to the OP [71] indicated by the prime. This leads to dynamic equations

$$\frac{\partial \vec{\varphi}_0}{\partial t} = -2\mathring{\Gamma}\frac{\delta \mathcal{H}}{\delta \vec{\varphi}_0^+} + \vec{\theta}_\varphi, \qquad \frac{\partial \vec{\varphi}_0^+}{\partial t} = -2\mathring{\Gamma}^+\frac{\delta \mathcal{H}}{\delta \vec{\varphi}_0} + \vec{\theta}_\varphi^+, \tag{310}$$

$$\frac{\partial \boldsymbol{m}_0}{\partial t} = \mathring{\boldsymbol{\Lambda}} \cdot \nabla^2 \frac{\delta \mathcal{H}}{\delta \boldsymbol{m}_0} + \boldsymbol{\theta}_m. \tag{311}$$

The static functional $\mathcal{H} = \mathcal{H}_\varphi + \mathcal{H}_m^{(Ms)}$ is given by (38) and (47) for $M = 2$. The KCs of the two secondary densities are now represented by the matrix $\mathring{\mathbf{\Lambda}}$ introduced in (84). Note that apart from the static coupling to the OP $\mathring{\gamma}$ the conserved densities are diffusively coupled by $\mathring{L}$. The explicit two-loop results for the ζ-functions of the KCs are presented in (A.53) and (A.56).

The main result of the analysis of this model is that it can be related asymptotically to the simpler model C. Defining three time scale ratios $w_1 = \Gamma/\lambda$, $w_2 = \Gamma/\mu$ and $w_3 = L/(\lambda\mu)^{1/2}$ (see (203)), the fixed-point values can be related to the fixed-point value of model C, since only one of the time scale ratios, in our case w_2, may have a non-zero value. Introducing

$$\rho_2 = \frac{w_2}{1 + w_2} \tag{312}$$

quite analogous to (302), the finite fixed point can be written as

$$\rho_2^\star = \rho^\star \frac{1 - w_3^2}{1 - \rho^\star w_3^2} \tag{313}$$

where $\rho^\star$ is the model C fixed point. Inserting the ζ-functions (A.56) into (209), the flow equation for w_3 reduces to

$$\ell \frac{\mathrm{d}w_3}{\mathrm{d}\ell} = \beta_{w_3} = 0. \tag{314}$$

Thus, we have $w_3(\ell) = w_3(\ell_0)$. w_3 stays constant and acts as parameter in the flow of the remaining time scale ratios and mode coupling parameters. Thus, one has a line of fixed points according to (313). w_3 determines the dissipative coupling between the two secondary densities. Its values may range from $w_3 = 0$ on the one hand, which is the case of a decoupling of the dissipative processes of the two secondary densities, to $w_3 = \pm 1$ on the other hand, describing total coupling in the sense that the dissipation of two secondary densities is determined only by one density. For $w_3 = 0$, one of the secondary densities (namely m_1) is completely decoupled from the OP and model C is in fact recovered. In the case $w_3^2 = 1$, a transformation to new secondary densities can be found where the first one fulfils a dynamic equation with a diffusion term while the dynamics of the second one is determined by a time-reversible equation without any dissipation. The values of w_3^2 cannot exceed 1 because the matrix (84) of dynamic coefficients has to be positive definite.

The dynamical critical exponent z_φ for the finite fixed point $\rho_2^\star$ is independent of w_3 always given by $z_\varphi = 2 + \alpha/\nu$. This connection to model C can also be seen for the subleading exponents (for more details see [71]) and in conclusion the same phase diagram (with the same equations for the borderlines in d–n-space) as for model C is obtained. Thus, there exist the same three regions as for model C:

- *Decoupled region I_a.* Right of $\varepsilon_\alpha(n)$ now with ($u^\star = u_H$, $\gamma^\star = 0$, $\rho_1^\star = 0$, $\rho_2^\star = 0$) stable; in consequence, the asymptotic dynamical critical exponents are $z_\varphi = 2 + c\eta$ for the OP and formally $z_{m_1} = z_{m_2} = 2$ for the decoupled densities.
- *Weak-scaling region I_b.* Between $\varepsilon_1(n)$ and $\varepsilon_\alpha(n)$ with ($u^\star = u_H$, $\gamma^\star = \gamma_C$, $\rho_1^\star = 0$, $\rho_2^\star = 0$) stable; in consequence, the asymptotic dynamical critical exponents are $z_\varphi = 2 + c\eta$ for the OP, $z_{m_2} = 2 + \alpha/\nu$ for the coupling density m_2 and formally $z_{m_1} = 2$ for the decoupled density m_1.
- *Strong-scaling region II.* Left of $\varepsilon_1(n)$ with ($u^\star = u_H$, $\gamma^\star = \gamma_C$, $\rho_1^\star = 0$, $\rho_2^\star \neq 0$) stable; in consequence, the asymptotic dynamical critical exponents are $z_\varphi = z_{m_2} = 2 + \alpha/\nu$ for the OP and the coupling density m_2 formally $z_{m_1} = 2$ for the decoupled density m_1.

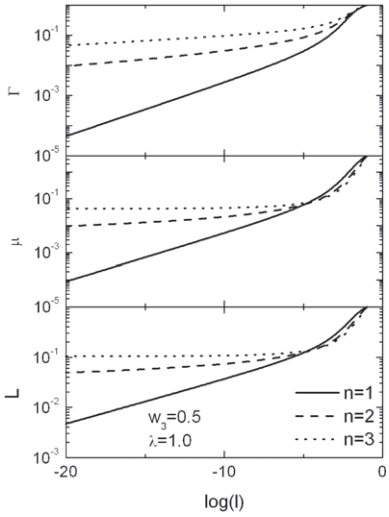

Figure 4. Flow of the dimensionless KCs of model C′ for the static flow of figure 3 and the initial values $w_1(l_0) = 1$ and $w_2(l_0) = 0.25$. Note that for $n = 2$ contrary to $n = 3$ the KCs L and μ have not reached their constant asymptotic values due to the small transient exponent (see table 6).

Table 6. Overview of the dynamical critical and transient exponents of model C′ in the different regions of the n–d-plane (see figure 2). Since $\zeta_\lambda = 0$ λ is a constant. The exponent $\omega_\rho^{(C)}$ is the transient of model C.

n	$\zeta_\Gamma^\star$	$\zeta_\mu^\star$	$\zeta_L^\star$	ω_+	ω_-
1	α/ν	α/ν	$\alpha/(2\nu)$	α/ν	$\omega_\rho^{(C)}$
2, 3	$c\eta$	0	0	$c\eta$	$c\eta$

11.5. Effective behaviour of model C′

In the asymptotic region, the flow of the parameters reaches their fixed-point values and the KCs of model C′ behave according to the power laws

$$\Gamma(\ell) \sim \ell^{\zeta_\Gamma^\star} \qquad \mu(\ell) \sim \ell^{\zeta_\mu^\star}, \tag{315}$$

$$\lambda(\ell) \sim \ell^{\zeta_\lambda^\star} \qquad L(\ell) \sim \ell^{\zeta_L^\star}. \tag{316}$$

For the exponents and also for the dynamical transient exponents see table 6.

Since the transient exponents are in part the same as in model C, where they are rather small, we also expect in model C′ that the asymptotic behaviour may be seen only very close to T_c. One has to distinguish between the different parameters and the corresponding effective behaviour, e.g., of the KCs, in the non-asymptotic region. The parameters may reach their asymptotic values at different distances from the critical point as has been discussed above. Here, we compare the effective behaviour of the KCs Γ, μ and L for the same static initial conditions but at different numbers of OP components (see figure 4). For $n = 1$, we are in the strong-scaling region and the KCs reach the power laws according to table 6. Thus, one finds for the KCs $\Gamma \sim \mu \sim L^2$ as can be easily seen in figure 4 (note the different scale for L). For $n = 2, 3$, the KC $\Gamma \sim \ell^{c\eta}$, while μ and L should be constant since they decouple. This is only seen for $n = 3$ whereas for $n = 2$ the effective behaviour shows a decrease of the kinetic

coefficient. The difference comes about by the slower decrease of the static parameter γ^2 for $n = 2$ compared to $n = 3$ (see figure 3). The value of the time scale ratio w_2 (or ρ_2) is far from its fixed-point value quite the same as w for model C in figure 3.

All KCs decrease due to fluctuation effects (in the classical van Hove theory they would be constant). This is not a general feature since for systems with mode coupling terms (compare the situation in model F′ below) the kinetic coefficient diverges due to fluctuation effects. Thus, critical slowing down may be enhanced or reduced by fluctuations.

12. Model E/E′ (planar ferromagnet)

The planar ferromagnet includes a two-component non-conserved OP describing the magnetization in a plane and a conserved secondary density which represents the magnetization perpendicular to the ferromagnetic plane. The two-component OP is usually written as a complex density ψ_0, the secondary density m_0 is a vector component. The critical dynamics of such a system is described by the dynamic equations

$$\frac{\partial \psi_0}{\partial t} = -2\mathring{\Gamma}\frac{\delta \mathcal{H}}{\delta \psi_0^+} + \mathrm{i}\psi_0 \mathring{g}\frac{\delta \mathcal{H}}{\delta m_0} + \theta_\psi, \tag{317}$$

$$\frac{\partial \psi_0^+}{\partial t} = -2\mathring{\Gamma}\frac{\delta \mathcal{H}}{\delta \psi_0} - \mathrm{i}\psi_0^+ \mathring{g}\frac{\delta \mathcal{H}}{\delta m_0} + \theta_\psi^+, \tag{318}$$

$$\frac{\partial m_0}{\partial t} = \mathring{\lambda}\nabla^2\frac{\delta \mathcal{H}}{\delta m_0} + 2\mathring{g}\,\mathrm{Im}\left[\psi_0\frac{\delta \mathcal{H}}{\delta \psi_0}\right] + \theta_m, \tag{319}$$

which are denoted as model E in the literature. The static functional $\mathcal{H} = \mathcal{H}_{\mathrm{GLW}} + \mathcal{H}_m^{(1v)}$ is determined by (24) and (41). The kinetic coefficient of the OP $\mathring{\Gamma}$ is real.

12.1. Superfluid transition in ^{4}He

Beside the critical behaviour of planar ferromagnets, model E can be used to describe the critical behaviour of ^{4}He at the superfluid transition in the very asymptotic region. The reason for this is that model F (see the next section), which is the complete model for ^{4}He at the superfluid transition, turns at the fixed points into model E. Thus, the whole asymptotic behaviour represented by the critical dynamic exponents z_i and the transient exponents ω_i is equal in both models. This has been used in the past to study the fixed points and to determine the transient exponents for the superfluid transition within model E [4, 100]. The examination of the stability of the fixed points and the values of the transient exponents revealed that the fixed-point value of w is very small or even zero (see the discussion in section 8.5) and one transient exponent, ω_w, is very small. In consequence, the critical behaviour of the model parameters, especially the time scale ratio w, is influenced heavily by non-asymptotic effects. Therefore, it is not expected to see the asymptotic behaviour of the transport coefficients like the thermal conductivity in the experimentally accessible temperature region.

12.1.1. Thermal conductivity. Measurements of the thermal conductivity κ_T demonstrated the divergence expected from scaling theory with the dynamic exponent $z = 3/2$ (see (281))

$$\kappa_T(\xi) \sim \xi^{2-z} \sim \xi^{1/2}. \tag{320}$$

However, deviations in the power law by about $\xi^{0.1}$ [6] were already mentioned in [1]. A more sensitive quantity is the thermal conductivity amplitude defined by

$$R_\lambda^{\exp}(t) = \frac{\kappa_T(t)}{\mathring{g}\sqrt{\xi(t) k_B C_P(t)}} \tag{321}$$

calculated from the thermal conductivity $\kappa_T(t)$, the specific heat $C_P(t)$ and the correlation length $\xi(t)$ measured in experiments. The amplitude was thought to be asymptotically a universal constant independent of temperature and pressure, this turned out not to be the case [11, 127].

Because the field-theoretic functions of model E are much simpler in a two-loop calculation than those of model F, model E has been used in a first attempt to calculate the theoretical counterpart of $R_\lambda^{\exp}(t)$. Instead of using the fixed-point values in the amplitude ratio, the nonlinear flow equations according to the two-loop field-theoretic functions (A.20) and (A.21) are inserted. The amplitude has been calculated in one-loop order

$$R_\lambda^{\text{eff}}(t) = \left(\frac{K_d}{w(\ell) f^2(\ell)}\right)^{1/2} \left(1 - \frac{f^2(\ell)}{4}\right), \tag{322}$$

where w and f have been defined in (195) and (198). It has been used for a fit to the data in the experimentally accessible temperature region [11, 125]. The parameter $t = (T - T_\lambda)/T_\lambda$ is the reduced temperature which is connected to the flow parameter ℓ by the matching condition (218). Once the specific flows, e.g. at different pressures (their initial values at some relative temperature distance t_0), have been found by a fit of (322) to its experimental counterpart (321), other dynamic quantities can be calculated using these selected flows.

By this method, the second sound damping below T_λ [126] has been studied within model E. The analogous effective amplitude $R_2^{\text{eff}}(t)$ for the second sound damping (see (10)–(14) in [10]) below T_λ is a function of the dynamic parameters. Inserting the flow of the fit of $R_\lambda^{\exp}(t)$, good agreement with the experimental values of $R_2^{\exp}(|t|)$ measured in [128] was obtained. The comparison with extended experimental data [129–132] could be improved by using the flow of the more complete model F analysis of the thermal conductivity amplitude [133].

Indeed, model E can only be considered as a simplified model for the dynamics of the superfluid transition because it neglects the temperature dependence of the static entropy density correlation function due to the absence of a coupling γ to the OP. Accordingly, deviations from the temperature behaviour calculated within the complete superfluid model (model F) are expected (see below).

12.1.2. Light scattering. Within model E investigations of the light scattering amplitude have also been performed [12]. In the hydrodynamic region above T_λ, the shape of the light scattering function is given by a Lorentzian and the width at fixed wave vector k is $\omega(k, \xi) = D_T(\xi)k^2$ where $D_T = \kappa_T(\xi)/(\rho C_P(\xi))$ is the thermal diffusion coefficient. Correspondingly, below T_λ the width is related to the second sound damping. Both quantities are known from the non-asymptotic analysis of (322) and $R_2^{\text{eff}}(|t|)$ and have been compared to the experimental width (see figure 5).

So far the field-theoretical calculations have not been extended into the critical region, $k\xi \gg 1$. The hydrodynamic shape function crosses over to a non-Lorentzian shape in the critical region calculated within model E in one-loop order [100]. The shape strongly depends on fixed-point values for the time scale ratio w (or effective values found from the fit of the thermal conductivity amplitude). Small values of $w^\star$ imply a peak of the shape function at finite scaled frequency in the critical region and at T_λ. This is also a feature of the SSS model, which is a generalization of model E for $n \neq 2$ (see subsections 15.1 and 18.2). Experiments

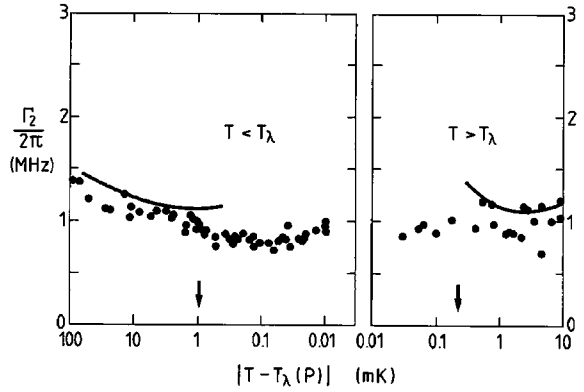

Figure 5. Halfwidth of the light scattering spectrum at $k = 1.79 \times 10^5$ cm^{-1} and $P = 23.1$ bar. Data are from [134], the solid curve is model E result for the hydrodynamic spectrum. The arrows indicate the border of the hydrodynamic region $k\xi = 1$. (from [11]).

are made in finite distance from the critical point because they are performed at finite distance from T_λ and/or at finite wave vector k. Moreover, the theoretically calculated shape has to be folded with an instrumental resolution function smearing out the specific details of the model E shape. This has been taken into account using the shape function of [100] and together with a parametrization of the thermal conductivity including the two subleading correction terms. Consistency between the thermal conductivity data and the width of light scattering over the whole temperature region of the measurements has been shown [135]. A non-asymptotic calculation of the shape and measured width in the critical region and at T_λ within model F using the flows found from an analysis of the thermal conductivity would be desirable.

13. Model F (superfluid transition in ^{4}He)

The model describing the critical dynamics in ^{4}He at the superfluid transition has been set up in [52, 136]. Although the reversible part of the dynamic equations is defined from Poisson brackets of physically different variables compared to the planar spin model (model E; see section 7.2), the dynamic equations have the same form (compare the previous subsection) apart from one difference. The kinetic coefficient $\mathring{\Gamma} = \mathring{\Gamma}' + \mathrm{i}\mathring{\Gamma}''$ is now a complex quantity.

$$\frac{\partial \psi_0}{\partial t} = -2\mathring{\Gamma}\frac{\delta \mathcal{H}}{\delta \psi_0^+} + \mathrm{i}\psi_0 \mathring{g}\frac{\delta \mathcal{H}}{\delta m_0} + \theta_\psi, \tag{323}$$

$$\frac{\partial \psi_0^+}{\partial t} = -2\mathring{\Gamma}^+\frac{\delta \mathcal{H}}{\delta \psi_0} - \mathrm{i}\psi_0^+ \mathring{g}\frac{\delta \mathcal{H}}{\delta m_0} + \theta_\psi^+, \tag{324}$$

$$\frac{\partial m_0}{\partial t} = \mathring{\lambda}\nabla^2\frac{\delta \mathcal{H}}{\delta m_0} + 2\mathring{g}\,\mathrm{Im}\left[\psi_0\frac{\delta \mathcal{H}}{\delta \psi_0}\right] + \theta_m. \tag{325}$$

Compared to model E as defined above in (317)–(319), the meaning of the densities is different. The non-conserved complex OP ψ_0 represents a macroscopic wavefunction and the secondary density m_0 represents the entropy density which is a scalar quantity. Therefore, the static functional is now $\mathcal{H} = \mathcal{H}_\varphi + \mathcal{H}_m^{(1s)}$ (see (38) and (40)) including a static coupling $\mathring{\gamma}$.

From studying the fixed points of this model, it became clear that the static coupling γ to the OP would only be relevant for the asymptotic behaviour if the fixed point $\gamma^\star \neq 0$ leading

to a diverging specific heat. An analysis of the static fixed points revealed that this is only the case for $n = 1$ (see model C). For the present model, we have $n = 2$ and therefore the value $\gamma^\star = 0$ at the stable fixed point. This leads to a finite specific heat at T_λ with a negative specific heat exponent α. There is one exception, if the stability boundary between $\gamma^\star \neq 0$ and $\gamma^\star = 0$ crosses the point $d = 3, n = 2$ the specific heat would have a logarithmic divergence ($\alpha = 0$). Measurements of the specific heat in older literature did not clarify whether the specific heat has a logarithmic divergence or a negative exponent which is very small (for an overview on the experimental situation at that time see [127]). Newer and more accurate measurements of the specific heat [8, 137] and a refined analysis of the data [7], also at higher pressures than saturated vapour pressure (SVP), confirmed that the specific heat exponent α is in fact negative but very small (a recent measurement in zero gravity found $\alpha = -0.0127$ [8]) in agreement with theoretical calculations [138]. Therefore, the flow of the static coupling $\gamma(\ell)$ is far from its fixed-point value and remains relevant in the experimental accessible region for the analysis of the static and dynamic quantities in ^{4}He.

As already mentioned, it turned out in two-loop order that model F (and E) at $n = 2, d = 3$ (see also the discussion on the 'phase diagram' of the SSS and DP models in sections 15.1 and 15.2) lies near the stability borderline between the so-called strong- and weak-scaling fixed points. This leads to the presence of a slow dynamic transient ω_w [4, 9, 100], which is defined by

$$\omega_w = \zeta_\Gamma(u^\star, \gamma^\star = 0, w^\star) - \zeta_\lambda(u^\star, \gamma^\star = 0, w^\star) \tag{326}$$

(see also section (8.5)). The position of the borderline of stability and the value of ω_w depend sensitively on the fixed-point value $u^\star$ of the static fourth-order coupling [22]. For the Borel-summed value $u^\star = 0.0362$, the weak-scaling fixed point is the stable one and the transient exponent is $\omega_w = 0.008$. But independent of the position of the stability borderline, the value of $w^\star$ and the value of ω_w are very small. This closeness of the stability boundary is the reason for the non-universal behaviour of dynamical quantities and makes it necessary to compare experimental results with the non-asymptotic RG theory calculating the effective behaviour outside the asymptotic region. For that purpose, the two-loop expressions of the field-theoretic functions of model F have to be calculated. Their correct form has been found only recently [139] after correcting errors of earlier calculations [22, 72] (see the ζ-functions (A.24) and (A.27)).

13.1. Thermal conductivity

The thermal conductivity κ_T, or the thermal diffusion coefficient D_T respectively, measured in experiments is related to the dynamic vertex functions of the secondary density by (see the discussion in section 6.5)

$$D_T = \frac{\kappa_T}{\rho C_P} = \frac{\partial}{\partial k^2} \mathring{\Gamma}_{m\tilde{m}}(\xi, k, \omega = 0)\Big|_{k=0}, \tag{327}$$

where ρ is the mass density of ^{4}He and C_P is the isobaric specific heat. The latter one is related to the static vertex function of the secondary (entropy) density by

$$C_P = \left(\mathring{\Gamma}^{(s)}_{mm}(\xi, k = 0)\right)^{-1}. \tag{328}$$

It turned out by improving and extending the measurements that $R_\lambda^{\exp}$ (321) was temperature and pressure dependent up to relative temperature distances of 10^{-9} [7, 8]. The

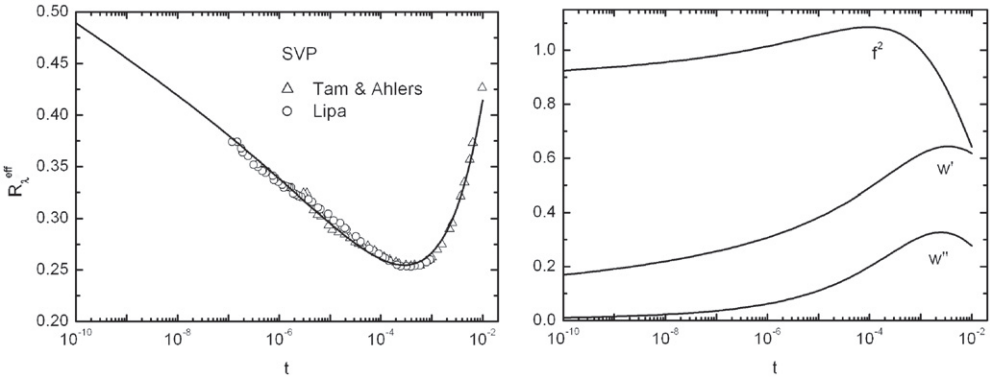

Figure 6. Left: comparison of the experimental amplitude ratio of the thermal conductivity (321) with its theoretical counterpart (329) in ^{4}He. All data (from [7, 141]) between $10^{-7} \leqslant t \leqslant 10^{-2}$ are fitted (this corrects figure 7 in [142]). Right: the flow of the fit (right) demonstrates that the time ratio w' is far from its fixed-point value $w^\star = 0$. This is due to the small dynamic transient ω_w (326).

solution to this problem was that one measures an effective (non-universal) behaviour of this ratio. The ratio has been calculated by field theory up to two-loop order in model F [140]

$$R_\lambda^{\rm eff}(t) = \frac{1 - f^2(l)/4 + f^2(\ell)M(w(\ell), f(\ell), \gamma(\ell), u(\ell))}{2\sqrt{\pi f^2(\ell)w'(\ell)(1+\gamma^2(\ell)F_+(u(\ell)))}}, \tag{329}$$

where in addition to the dynamic flow of the complex time ratio $w = w' + \mathrm{i}w''$ and f, the static flow of the fourth-order coupling u and the coupling γ appear. The function $F_+(u)$ is the static amplitude function of the specific heat above T_λ. The function M contains the two-loop contributions to $R_\lambda^{\rm eff}$. A precise comparison with experiments at different pressures has been performed in [22, 143]. Here, we show a fit of $R_\lambda^{\rm exp}$ (see figure 6) using the dynamic flow equations given by (A.24)–(A.29) in (197) and (200) and the corresponding flow at SVP. The fit fixed the initial values of the non-asymptotic flow of the dynamical parameters (mode coupling f and complex time ratio w) at $t = 10^{-2}$. The changes in the β-function of [22] due to the corrections in [72, 139] lead to a fit with only slightly changed parameters w' and f, whereas the flow of w'' is changed in the background region. Its value (the renormalized one) is now in better agreement with the unrenormalized value calculated in [144].

A test of the theoretical result consists either in a prediction of the effective behaviour in the region closer to T_λ (the quality of such a prediction can be seen by comparing a fit of the data in the region $t = 10^{-6}$ to $t = 10^{-2}$ with the data within $10^{-7} < t < 10^{-6}$, respectively, the agreement of the prediction at SVP is excellent [143]) and/or predicting other dynamical quantities of the system[5].

The dynamic flow found in the fits have been used for calculating the critical thermal boundary resistance (Kapitza resistance) [145–148], finite-size effects in the thermal conductivity [149–151] and the influence of nonlinear effects on the thermal conductivity in ^{4}He [152–155].

In order to study the Kapitza resistance between liquid ^{4}He and a solid wall, one has to extend the equations of motion by introducing a term representing the heat source on the

[5] Since the values of the dynamic parameters $w'(\ell)$ and $f(\ell)$ found by the fits to $R_\lambda^{\rm exp}$ [143] are only slightly changed compared to the flow found in [22], no changes are expected in the quantities where the flow has already been used. This also holds for the prediction of $R_\lambda^{\rm exp}$ made for temperature region in the next decades below $t = 10^{-6}$.

right-hand side of (325). The problematic input into the theoretical calculations is the correct boundary condition for the OP ψ_0 at the wall. In [145, 146], Dirichlet boundary conditions have been chosen. Good agreement with experimental results at SVP was obtained at $T < T_\lambda$. However, deviations from experimental results above T_λ remain and calculations of the Kapitza resistance remains a challenge for the theory.

At vanishing heat current, the effective correlation length diverges with the exponent ν. The presence of a finite heat current leads to an effective correlation which stays finite at T_λ. The larger the heat current the smaller the finite value at T_λ. This leads then in the thermal conductivity to finite plateau values at finite heat currents. Also the specific heat and the superfluid density will be considerably influenced by finite heat currents. This has been presented in [154] by a renormalization group treatment of the specific heat and superfluid density. The non-equilibrium conditions by a finite heat current were extended to include gravity effects in [156].

14. Model F′ (superfluid transition in ^{3}He–^{4}He mixtures)

In ^{3}He–^{4}He mixtures additional to the entropy density, one has to consider the local concentration c as a conserved density. Therefore, one has two scalar secondary densities m_{10} and m_{20} coupled to the OP. The dynamic equations are analogous to (323)–(325) in model F. The difference is that $\boldsymbol{m}_0$ is now a two-component column vector (two scalars written as a vector). Consequently, the mode coupling $\mathring{\boldsymbol{g}}$ is also a column vector and the KCs $\mathring{\boldsymbol{\Lambda}}$ define the matrix (84). The equations of motion therefore read

$$\frac{\partial \psi_0}{\partial t} = -2\mathring{\Gamma}\frac{\delta \mathcal{H}}{\delta \psi_0^+} + \mathrm{i}\psi_0 \mathring{\boldsymbol{g}} \cdot \frac{\delta \mathcal{H}}{\delta \boldsymbol{m}_0} + \theta_\psi, \tag{330}$$

$$\frac{\partial \psi_0^+}{\partial t} = -2\mathring{\Gamma}^+\frac{\delta \mathcal{H}}{\delta \psi_0} - \mathrm{i}\psi_0^+ \mathring{\boldsymbol{g}} \cdot \frac{\delta \mathcal{H}}{\delta \boldsymbol{m}_0} + \theta_\psi^+, \tag{331}$$

$$\frac{\partial \boldsymbol{m}_0}{\partial t} = \mathring{\boldsymbol{\Lambda}} \cdot \nabla^2 \frac{\delta \mathcal{H}}{\delta \boldsymbol{m}_0} + 2\mathring{\boldsymbol{g}}\,\mathrm{Im}\left[\psi_0 \frac{\delta \mathcal{H}}{\delta \psi_0}\right] + \boldsymbol{\theta}_m. \tag{332}$$

They are expected to describe all slow modes: thermal diffusion, mass diffusion and the corresponding cross phenomenon, the Sorret effect. The static functional $\mathcal{H} = \mathcal{H}_\varphi + \mathcal{H}_m^{(Ms)}$ is given by (38) and (47) for $M = 2$. Concerning the asymptotic properties of this model it reduces to model E′ since the static couplings of the conserved densities to the OP have zero fixed-point values.

14.1. Transport coefficients in mixtures

In order to understand the effective behaviour of the transport coefficients, one needs the complete information contained in the flow equations. The same argumentation as for pure ^{4}He also applies here. The static coupling is far from its fixed-point value and one has to take into account its flow. The dynamic slow transient is also present. The initial conditions in the background are concentration dependent and part of the temperature behaviour is explained by this dependence (there would also be a pressure dependence but this has not been considered so far). The limits to special values of the mole fraction X have to be considered:

- The crossover to pure ^{4}He ($X = 0$).
- The crossover to the decoupling point at about $X_D \sim 0.36$.
- The crossover to the tricritical point at about $X_t \sim 0.67$.

Each of these limits is characterized by a special behaviour of the background parameters. In case (i) one mode coupling and the time scale ratio containing the Onsager coefficient for the thermal diffusion ratio go to zero with the consequence that the non-asymptotic model F behaviour is recovered. In case (ii) also one mode coupling goes to zero but the time scale ratios stay finite. Therefore, in this case the model F behaviour is only reached in the asymptotics (for a more detailed discussion of the two cases see [157]). Case (iii) is special since it is a crossover involving the background value of static fourth-order coupling u, which goes to zero at the tricritical point, but this case will not be further discussed here (see [53, 158, 68]).

Crossover effects are most prominently observed in the thermal conductivity κ_T at zero mass current. In the mixture, this conductivity is finite at T_λ and equal to its temperature-independent value κ_{eff} below T_λ. The value below and at T_λ diverges in the limit $X \to 0$ like X^{-1}. Quite different is the behaviour of the thermal conductivity in the limit to the decoupling point X_D where it becomes temperature independent above and below T_λ.

In a first theoretical attempt, an analysis of the temperature dependence of the transport coefficients, thermal conductivity κ_T, thermal diffusion ratio k_T and mass diffusion coefficient D has been made for mole fractions $0 < X \leqslant 0.36$ within model E′ [17] in two-loop order. Analogous to model E, the static functions like specific heat or concentration susceptibility are independent of the temperature. This leads to deviations in the quantitative comparison with experiments. Most prominently this can be seen in the temperature-independent thermal conductivity κ_{eff} below T_λ which is not reproducible by model E′ where a temperature-dependent thermal conductivity is generated [159]. At the same time, a renormalization method (no scaling transformation is involved) has been applied to model F′ in [68] and the leading fluctuation effects in the transport coefficients calculated. Another attempt has been made using a hybrid model [69, 160] partly taking into account model F′ terms and model E′. Model F′ has been solved completely in one-loop order. This approach takes into account the static coupling $\gamma^2(\ell(t))$ and leads to temperature-dependent static susceptibilities. The effects of the slow transient are included by adding the two-loop model E′ results for the dynamic ζ-functions to the flow equations (then the correct two-loop asymptotics is obtained). A significant improvement has been achieved in κ_{eff} which now turns out to be temperature independent [161]. Recently, the complete model F′ has been solved in two-loop order [142]. The corresponding dynamic ζ-functions are presented in (A.65) and (A.69)–(A.71).

The comparison of results of model F′ with experimental data above T_λ for the thermal conductivity κ_T, the thermal diffusion ratio k_T and the mass diffusion coefficient D is shown in figure 7 for several mole fractions X. The relative temperature distance to T_λ is denoted by t. The connection between the experimental measurable quantities κ_T, k_T, D and the theoretical vertex functions $(\partial/\partial k^2)\mathring{\Gamma}_{m_i\tilde{m}_j}(\xi, k, \omega = 0)|_{k=0}$ is now more complex as in (327) and (328) for pure ^{4}He and will therefore not be presented explicitly here. The interested reader can find the necessary relations in [69, 160]. κ_T and k_T have been fitted in order to obtain the initial values $w_i(\ell(t_0))$, $f_i(\ell(t_0))$ for the flow of the model parameters. The fits of κ_T and k_T (solid lines in figure 7) include all data. The mass diffusion coefficient is then completely determined and the curves for D are predictions in figure 7. Fits at small mole fractions revealed that the background behaviour of k_T strongly influences the result for D. This is demonstrated at $X = 0.00095$ where less k_T data in the background are available. A second fit (dashed lines in figure 7) only down to $t = 10^{-5}$ leads to a different background behaviour of k_T. As a consequence, the result for D is considerably shifted.

The specification of the flow with the fits of κ_T and k_T also determines the effective thermal conductivity κ_{eff} below T_λ without any adjustable parameter. Calculating the thermal conductivity closer to T_λ, one observes that the values of κ_T approaching T_λ as well as κ_{eff}

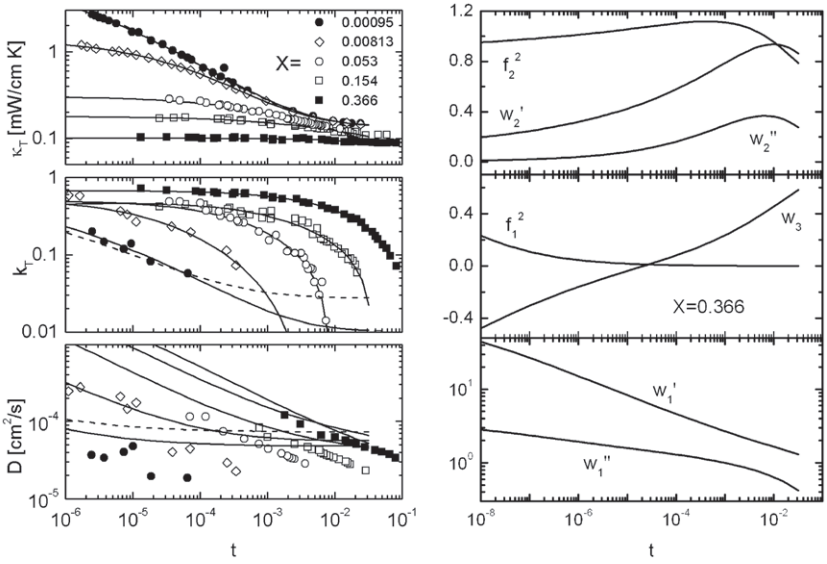

Figure 7. Left: thermal conductivity κ_T, thermal diffusion ratio k_T and mass diffusion coefficient D above T_λ at several mole fractions. The initial values for the flow are found by a fit of κ_T and k_T. D is predicted. The position of D is strongly connected with the background behaviour of k_T. This is demonstrated at $X = 0.00095$ by two fits which lead to different results for k_T in the background. The first one includes all data (solid line) the second one only data down to $t = 10^{-5}$ (dashed lines). The asymptotic behaviour of these coefficient is shown in table 7. Data from [162–164]. Right: flow of the fit at $X = 0.366$.

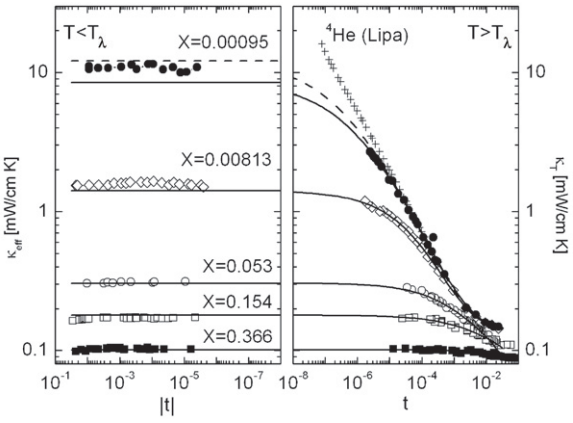

Figure 8. Thermal conductivity κ_T above and κ_{eff} below T_λ. The value of κ_{eff} is predicted by the fits of κ_T and k_T in figure 7. The plateau values of κ_T and κ_{eff} are tightly connected to the background behaviour of k_T. Now the differences of the two fits at $X = 0.00095$ with different t-intervals (see figure 7) are also visible in κ_T for values of t closer to T_λ. Data from [162–164]. This corrects figure 4 of [142].

considerably depend on the background behaviour of k_T. This is demonstrated in figure 8 where κ_T and κ_{eff} are calculated down to $t = 10^{-8}$. The dashed lines at $X = 0.00095$ correspond to the dashed curves in figure 7. The uncertainty in κ_{eff} (difference between solid and dashed lines) is a result of the uncertainty in the background behaviour of k_T.

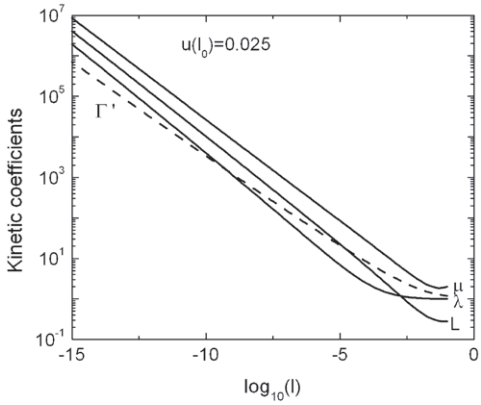

Figure 9. Kinetic coefficients for model F′ as a function of the flow parameter ℓ. Note that contrary to model C′ the KCs diverge with exponents shown in table 8.

Table 7. Asymptotic critical behaviour of the transport coefficients in ^{3}He–^{4}He mixtures and pure ^{4}He at the superfluid transition. Values calculated by RG. The thermal conductivity in the mixture is defined at zero mass current.

System	Thermal conductivity	Thermal diffusion ratio	Mass diffusion
Pure ^{4}He	$\kappa \sim \xi^{1/2+\omega_w^{(F)}/2}$	–	–
^{3}He–^{4}He mixture	Constant	see (333)	$D \sim \xi^{1/2+\omega_w^{(F)}/2-\gamma/\nu}$

Table 8. Overview of the dynamic critical exponents and transient exponents of model F′ at the scaling (SC) and at the weak-scaling (WSC) fixed point (FP). $\omega_w^{(F)} = \zeta_\Gamma^\star - \zeta_\mu^\star$ is the transient of model F. (For ω_- see (223).)

FP	$\zeta_\Gamma^\star$	$\zeta_\mu^\star$	$\zeta_L^\star$	$\zeta_\lambda^\star$	ω_-
SC	$-1/2$	$-1/2$	$-1/2$	$-1/2$	$\omega_w^{(F)}$
WSC	$-1/2+\omega_w^{(F)}$	$-1/2-\omega_w^{(F)}/2$	$-1/2-\omega_w^{(F)}/2$	$-1/2-\omega_w^{(F)}/2$	$\omega_w^{(F)}$

The thermal diffusion ratio reaches near T_λ a purely static quantity [68, 165]

$$\lim_{T\to T_\lambda} k_T = T_\lambda \left[\left(\frac{\partial c}{\partial \Delta} \right)_{\rm PT} \frac{\sigma}{c} - \left(\frac{\partial c}{\partial T} \right)_{P\Delta} \right], \tag{333}$$

where the second thermodynamic derivative is temperature dependent near T_λ. The difference of the chemical potentials of ^{4}He and ^{3}He is denoted by Δ. In the limit of zero concentration, this derivative stays finite in the low-temperature phase and at T_λ

$$\lim_{X\to 0} k_T = k_{T0} = 0.57, \qquad k_{T0} = \frac{3M_3 S_\lambda}{2M_4 R}, \tag{334}$$

but goes to zero in the background in the normal phase.

The behaviour of the KCs of the model is shown in figure 9. Contrary to model C′, the KCs diverge (see figure 4).

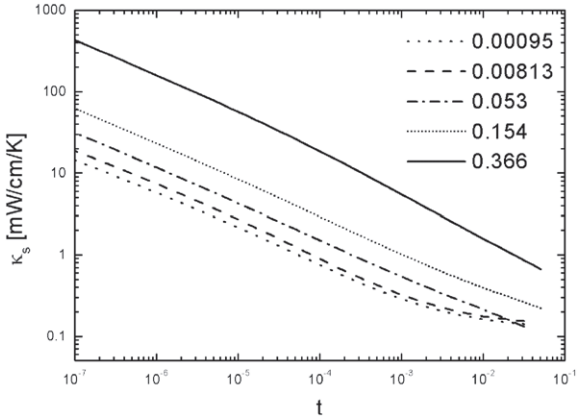

Figure 10. Singular part κ_s of the thermal conductivity at zero mass current at different concentrations according to (335). In the double logarithmic plot, the curves for different molar concentration are almost parallel indicating a divergence with the same power law. Approaching the decoupling point at X_D, the value of κ_s increases and becomes infinite at $X = X_D$. This corrects figure 6 of [142].

14.2. Singular thermal conductivity

It has been already suggested in [166] to write the thermal conductivity in the normal phase as

$$\frac{1}{\kappa_T} = \frac{1}{\kappa_\lambda} + \frac{1}{\kappa_s}, \tag{335}$$

where κ_λ is the value of the thermal conductivity at T_λ and κ_s is the divergent part. In the limit $X \to 0$, where κ_λ diverges, the singular part κ_s turns into the diverging thermal conductivity of pure ^{4}He. The singular part at finite concentration was expected to diverge as in pure ^{4}He. This was later justified by theory [17, 68, 159]. The amplitude of the divergence of κ_s depends on the concentration and goes to infinity in the limit $X \to X_D$, where the thermal conductivity κ_T becomes temperature independent and equal to κ_λ. It is the singular thermal conductivity κ_s which contains the effects of the slow dynamic transient known from pure ^{4}He. The knowledge of the theoretical expressions of the thermal conductivity and the flow allows us to extract κ_s very near to X_D for the molar concentration $X = 0.366$ where the thermal conductivity already appears to be constant (see figure 10).

14.3. Computer simulations

Since the magnetic transition of the XY-ferromagnet lies in the same dynamical universality class as the superfluid transition in ^{4}He, simulations for XY-spin systems have been performed in [167]. However because of invariance under the reflection symmetry $M_z \to -M_z$ the magnetic system is represented by the symmetric model E. Due to the additional conservation of energy in fact one has to compare with model F′ since for the energy density the reflection symmetry is absent and the static coupling between the OP and the energy might be present. Moreover, for symmetry reasons no diffusive cross term is present (in ^{3}He–^{4}He mixtures this cross term leads to the Sorret effect). Asymptotically, such a model would correspond to model E′ with $w_3 = 0$.

In the spin system, the transport coefficients corresponding to the thermal diffusion and mass diffusion in model F′ for the ^{3}He–^{4}He mixture are the thermal diffusion and the

out-of-plane magnetization diffusion, respectively. The simulations [167] show different dynamic exponents for the order parameter $z_\varphi = 1.62 \pm 0.05$ and the second conserved density $z_\varphi = 1.38 \pm 0.05$ leading to a transient exponent of about $\omega_w^{\mathrm{WSC}} = 0.24 \pm 0.1$ somewhat larger than the prediction of field theory $\omega_w^{\mathrm{WSC}} = 0.008$ [22].

15. SSS model and DP model

Two different models have been defined which can be considered as extensions of specific models applicable to physical systems. The first one (DP model) has been introduced in [99] and is a generalization of the dynamic model for the planar ferromagnet ($n = 2$, model E) introduced in [52] to arbitrary n. The other one (SSS model) has been introduced in [24] and [168] for general n and reduces to model E for $n = 2$ and to the model of the isotropic antiferromagnet (model G) [136, 52] for $n = 3$.

Among the interesting items to be studied in these generalized models are the fixed-point properties in the d–n-plane leading finally to a 'phase diagram' as it has been discussed for the simpler model C. Contrary to model C, the models considered here do not contain a static coupling $\mathring{\gamma}$ between the OP and secondary densities of the conserved quantities in their static functional but a coupling by dynamic reversible terms in the equation of motion.

15.1. SSS model

Originally, the SSS model was introduced to serve as a model for the dynamic behaviour at a structural phase transition of second order [24]. One starts from an n-component phonon system (constituting the OP and described by displacive variables) having rotational symmetry. The generators of the corresponding symmetry group are the $n(n-1)/2$ angular momenta which are conserved quantities. The corresponding Poisson brackets lead to reversible couplings between the OP and the angular momentum densities. Proceeding along the lines described in [57] (see section 7.2), one ends up at the following set of equations [168]:

$$\frac{\partial \phi_{0\alpha}}{\partial t} = -\mathring{\Gamma}\frac{\delta \mathcal{H}}{\delta \phi_{0\alpha}} + \mathring{g}\sum_\beta \phi_{0\beta}\frac{\delta \mathcal{H}}{\delta m_{0\alpha\beta}} + \theta_{\psi_\alpha}, \tag{336}$$

$$\frac{\partial m_{0\alpha\beta}}{\partial t} = \mathring{\lambda}\nabla^2\frac{\delta \mathcal{H}}{\delta m_{0\alpha\beta}} + \mathring{g}\left\{\phi_{0\alpha}\frac{\delta \mathcal{H}}{\delta \phi_{0\beta}} - \phi_{0\beta}\frac{\delta \mathcal{H}}{\delta \phi_{0\alpha}}\right\} + \theta_{m_{\alpha\beta}}. \tag{337}$$

For $n = 2$, this model describes the planar ferromagnet (model E) and for $n = 3$ the isotropic antiferromagnet. In both cases, the OP (the x, y components of the magnetization or the alternating magnetization respectively) is coupled to a conserved density (the z-component of the magnetization or the magnetization vector, respectively) by mode coupling terms.

From the dynamic ζ-functions (see (A.30) and (A.31))), the fixed-point values of the dynamic parameters—mode coupling f and time scale ratio w—can be found after inserting the fixed-point value for the static fourth-order coupling $u^\star$. Let us define $\zeta_w = \zeta_\Gamma - \zeta_\lambda$ and $\zeta_f = (\zeta_\Gamma + \zeta_\lambda)/2$. Then, the β-functions read

$$\beta_f = -f(\varepsilon/2 + \zeta_f) \qquad \text{and} \qquad \beta_w = w\zeta_w. \tag{338}$$

The existence region of the scaling fixed point (with $w_{\mathrm{SC}} \neq 0$ and finite) in the d–n-plane is found from the solution of the following set of equations:

$$\zeta_w(f_{\mathrm{SC}}, w_{\mathrm{SC}}; \varepsilon, n) = 0 \qquad \text{and} \qquad \zeta_f(f_{\mathrm{SC}}, w_{\mathrm{SC}}; \varepsilon, n) = -\varepsilon/2. \tag{339}$$

The borderline $n_c(\varepsilon)$ beyond which no non-zero solution for w_{SCc} exists is defined by

$$\zeta_w(f_{\mathrm{SC}}, w_{\mathrm{SC}} = 0; \varepsilon, n_c) = 0 \qquad \text{and} \qquad \zeta_f(f_{\mathrm{SC}}, w_{\mathrm{SC}} = 0; \varepsilon, n_c) = -\varepsilon/2 \tag{340}$$

where it is assumed $w_{\mathrm{SC}}(\varepsilon, n)$ is a continuous function.

The stability borderline $n_{\mathrm{SC}}^{\mathrm{SSS}}(\varepsilon)$ of the scaling fixed point is found from the condition that one of the eigenvalues of the dynamic stability matrix (222) goes to zero. Defining

$$\frac{1}{2}\left(-f\frac{\partial}{\partial f}\zeta_f(f, w; \varepsilon, n) + w\frac{\partial}{\partial w}\zeta_w(f, w; \varepsilon, n)\right) = a(f, w; \varepsilon, n) \tag{341}$$

and

$$\left(-f\frac{\partial}{\partial w}\zeta_f(f, w; \varepsilon, n)\frac{\partial}{\partial f}\zeta_w(f, w; \varepsilon, n)\right) - \left(-f\frac{\partial}{\partial f}\zeta_f(f, w; \varepsilon, n)\frac{\partial}{\partial w}\zeta_w(f, w; \varepsilon, n)\right) = b(f, w; \varepsilon, n), \tag{342}$$

the stability condition according to (223) reads

$$a(f_{\mathrm{SC}}, w_{\mathrm{SC}}; \varepsilon, n) - \sqrt{a^2(f_{\mathrm{SC}}, w_{\mathrm{SC}}; \varepsilon, n) - 4w_{\mathrm{SC}}b(f_{\mathrm{SC}}, w_{\mathrm{SC}}; \varepsilon, n)} > 0. \tag{343}$$

In the limit to the existence borderline where $w_{\mathrm{SC}} \to 0$, one finds that the left-hand side of (343) goes to zero like $(n-2)w_{\mathrm{SC}}(\ln w_{\mathrm{SC}}) + \mathcal{O}(w_{\mathrm{SC}})$ and not linearly with w_{SC}. This is due to the presence of $w \ln w$ terms in $\zeta_\lambda^{(d)}$ of the SSS model. Nevertheless, the stability borderline $n_{\mathrm{SC}}^{\mathrm{SSS}}(\varepsilon)$ defined in this way and the existence borderline $n_c(\varepsilon)$ of the scaling fixed point are the same.

The weak-scaling fixed point $w_{\mathrm{WSC}} = 0$ exists in the whole d–n-plane. The stability borderline of the weak-scaling fixed point $n_{\mathrm{WSC}}^{\mathrm{SSS}}$ is found from

$$\zeta_w(f_{\mathrm{WSC}}, 0; \varepsilon, n) = 0 \qquad \text{and} \qquad \zeta_f(f_{\mathrm{WSC}}, 0; \varepsilon, n) = -\varepsilon/2, \tag{344}$$

which is the same set of equations as for the existence borderline $n_c(\varepsilon)$ of the scaling fixed point w_{SC}. Thus, all borderlines agree with each other and no discontinuity appears. This resolves the difficulties reported in [25] where using the ε-expansion a region was found, where both dynamic fixed points, the scaling fixed point and the weak-scaling fixed point are stable.

The borderline of the weak-scaling fixed point found by solving these equations numerically is shown in figure 11 (left part, solid curve) (the same calculations have been done for the DP model below). These borderlines have been calculated in ε-expansion in [169, 170]

$$n_{\mathrm{WSC}}^{\mathrm{SSS}}(\varepsilon) = \tfrac{3}{2} + 0.42\varepsilon \qquad \text{and} \qquad n_{\mathrm{WSC}}^{\mathrm{DP}}(\varepsilon) = 4 - 1.80\varepsilon \tag{345}$$

where n_{DP} is the result for the DP model (see the next subsection). One observes that the ε-expansion leads to different spatial borderline dimensions at $n = 2$, which is due to neglecting $\mathcal{O}(\varepsilon^2)$ terms (see dashed lines in figure 11 (left part)). The non-expanded borderlines have the same value at $n = 2$. The value of the borderline dimension is slightly above $d = 3$. That would mean that in $d = 3$ the scaling fixed point is the stable one for $n = 2$. This is due to inserting the ε-expanded fixed-point value $u^\star = \varepsilon/[4(n+8)]$ into the dynamic ζ-functions. Using the Borel-summed fixed-point values for $n = 2$ and $n = 3$, the borderline values would be slightly shifted down (see cross in figure 11 (left part)) at these numbers of components of the OP with the consequence that at $n = 2$ the weak-scaling fixed point would be the stable one [22]. The stable fixed point for the SSS model at $n = 3$ in $d = 3$ is the scaling fixed point. The fixed-point value of the dynamical coupling f_{WSC} on the borderline is real only up to $n = 2.7$ which is due to the two-loop approximation.

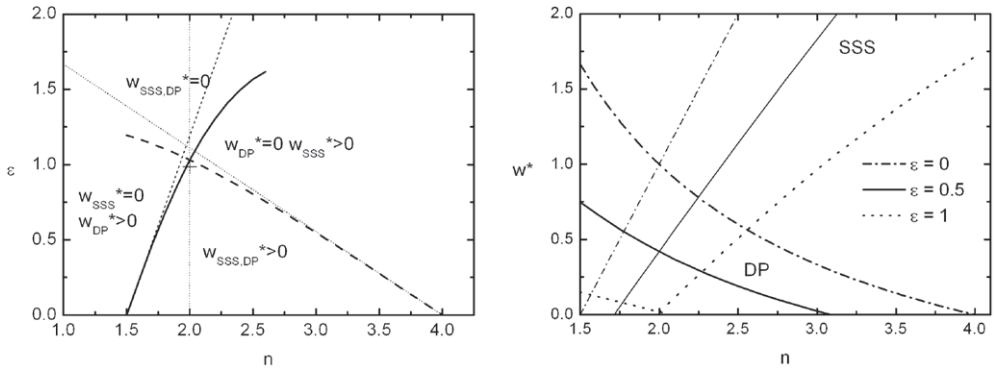

Figure 11. Left: phase diagram calculated in two-loop order for the SSS and DP models. Stability boundary of the weak-scaling fixed point for the SSS model (solid curve) and the DP model (dashed curve) compared to the result of the ε-expansion (dotted lines) for the two models. Right: fixed-point value of the time ratio $w^\star \neq 0$ for these models as a function of the number of OP components at different dimensions.

We have also plotted the fixed-point value of w as a function of n for different spatial dimensions. At $d = 4$ (dashed-dotted curves), the one-loop result $w_{\rm SC} = 2n - 3$ [168] for the SSS model is recovered at $\varepsilon = 0$. The values of $w_{\rm SC}$ decrease for increasing ε (see solid curve for $\varepsilon = 1/2$ and dashed curve for $\varepsilon = 1$) and reach zero just after $\varepsilon = 1$ (at the stability borderline of the weak-scaling fixed point).

15.2. DP model

The generalization to the DP model started from the dynamic model for the planar ferromagnets (model E) [52] by simply replacing the complex OP by an $n/2$-component complex OP and keeping the structure of the mode coupling terms [4, 99]

$$\frac{\partial\vec{\varphi}_0}{\partial t} = -2\mathring{\Gamma}\frac{\delta\mathcal{H}}{\delta\vec{\varphi}_0^+} + \mathrm{i}\mathring{g}\vec{\varphi}_0\frac{\delta\mathcal{H}}{\delta m_0} + \vec{\theta}_\varphi, \tag{346}$$

$$\frac{\partial m_0}{\partial t} = \mathring{\lambda}\nabla^2\frac{\delta\mathcal{H}}{\delta m_0} + \mathrm{i}\mathring{g}\left\{\vec{\varphi}_0\frac{\delta\mathcal{H}}{\delta\vec{\varphi}_0} - \vec{\varphi}_0^+\frac{\delta\mathcal{H}}{\delta\vec{\varphi}_0^+}\right\} + \theta_m. \tag{347}$$

In a similar manner as for the SSS model, one can look at the 'phase'-diagram for the DP model. The borderline $n_{\rm SC}^{\rm DP}$ between the scaling and the weak-scaling fixed point can be obtained by solving the corresponding equations (339), (340) and (344) now with the ζ-functions for the DP model (see (A.34) and (A.35)). The outcome is shown in figure 11. Contrary to the SSS model with $n \neq 2$, the stability exponent goes to zero linearly with $w_{\rm SC}^{\rm DP}$ since there are no $w \ln w$ terms in ζ_λ (A.35). Contrary to the SSS model for the DP model at $d = 3$ and $n = 3$, one is in the weak-scaling region. One can see this from the plot of the fixed-point value of the time scale ratio $w_{\rm SC}(\varepsilon, n)$ in figure 11 (right part). For $\varepsilon = 0$, the one-loop order fixed point value $w_{\rm SC} = (n-4)/n$ [4] is obtained (dashed-dotted line). For $\varepsilon > 0$, the value of the scaling fixed point $w_{\rm SC}$ goes to zero at the stability line of the weak-scaling fixed point.

16. Model H (gas–liquid transition in fluids)

In order to obtain the critical behaviour of the thermal transport properties of a pure fluid, one needs a conserved scalar OP ϕ_0 representing the entropy density per mass and a conserved secondary density $\vec{j}_t$ which is the transverse momentum current [52]:

$$\frac{\partial \phi_0}{\partial t} = \mathring{\Gamma} \nabla^2 \frac{\delta \mathcal{H}}{\delta \phi_0} - \mathring{g} (\vec{\nabla} \phi_0) \frac{\delta \mathcal{H}}{\delta \vec{j}_t} + \Theta_\phi, \tag{348}$$

$$\frac{\partial \vec{j}_t}{\partial t} = \mathring{\lambda}_t \nabla^2 \frac{\delta \mathcal{H}}{\delta \vec{j}_t} + \mathring{g} \overleftrightarrow{\mathcal{T}} \left[(\vec{\nabla} \phi_0) \frac{\delta \mathcal{H}}{\delta \phi_0} \right] - \mathring{g} \overleftrightarrow{\mathcal{T}} \left\{ \sum_k \left[j_{t,k} \vec{\nabla} \frac{\delta \mathcal{H}}{\delta j_{t,k}} - \nabla_k \vec{j}_t \frac{\delta \mathcal{H}}{\delta j_{t,k}} \right] \right\} + \vec{\Theta}_t. \tag{349}$$

The dissipation is determined by the corresponding KCs $\mathring{\Gamma}$ and $\mathring{\lambda}_t$ for the thermal and shear mode. The mode coupling $\mathring{g}$ follows from the Poisson brackets discussed in section 7.2. $\overleftrightarrow{\mathcal{T}}$ is a projector in the direction transverse to the propagation acting onto the vectors in (348) and (349). In Fourier space, it has the form $\mathcal{T}_{ij} = \delta_{ij} - k_i k_j / k^2$. The static functional is $\mathcal{H} = \mathcal{H}_{\mathrm{GLW}} + \mathcal{H}_j$ from (24) and (42). The above equations describe the heat conduction and the shear mode in a fluid. The couplings of all other conserved densities (mass density, longitudinal momentum current) are not relevant for the critical behaviour near the gas–liquid critical point. They have to be taken into account if one is interested in the critical behaviour of the sound mode. Model H has been extended [34, 171] to include the sound mode and study its critical properties. The couplings to these densities induce the specific critical behaviour in the sound velocity and the sound attenuation.

Field-theoretic treatments of this model with the main interest in calculating the asymptotic values of dynamic exponents for the viscosity and thermal conductivity and amplitude ratios have started in [4, 99]. A finally correct result for the necessary field-theoretic functions has been given in [172]. Field theoretic calculations at $d = 3$ have been performed in [173]. On earth in the experimental region the non-asymptotic behaviour is dominant and effects of gravity have to be taken into account. In order to incorporate such effects into the field-theoretic calculation of physical quantities, a one-loop non-asymptotic field-theoretic study has been performed in a set of papers [16, 174, 175].

Quite recently asymptotic properties of pure fluid dynamics were studied by a self-consistent theory in [176]. Comparison with the two-loop results of the field theory can be made when an ε-expansion is performed.

16.1. Asymptotic properties

The universal exponents, the exponent for the thermal conductivity x_λ and the exponent for the shear viscosity x_η, which have been presented in (285), are related according to (285). Besides these exponents, an amplitude ratio known as Kawasaki amplitude is of interest. It should be universal in the asymptotic region. The definition of the Kawasaki amplitude for pure fluids (relative to the value $R_K^{(\text{mode coupling})} = 1/(6\pi)$ of the mode coupling theory) reads

$$R_K^{(\exp)} = \frac{6\pi \bar{\eta} D_T \xi}{k_B T}, \tag{350}$$

involving the thermal diffusion coefficient D_T, the shear viscosity $\bar{\eta}$ and the correlation length ξ. It is the rewritten Kawasaki–Stokes relation [179].

The thermal diffusion coefficient D_T is related to the dynamic OP vertex functions by (compare (327) in ^{4}He at the λ-transition)

$$D_T = \frac{\kappa_T}{\rho C_P} = \frac{\partial}{\partial k^2} \mathring{\Gamma}_{\phi\tilde{\phi}}(\xi, k, \omega = 0)|_{k=0}, \tag{351}$$

Table 9. Critical exponent x_η for the shear viscosity and Kawasaki amplitude R in model H.

x_η	R_K	Reference	Remark
0.054	1.063	[181]	One loop
0.054	0.756	[52]	One loop
0.0712	0.959	[172]	Two loop
0.0679	1.174	[176]	Self-consistent
0.071	0.85	[176]	ε-expansion
0.04	1.0375	[173]	$d = 3$, one loop

while the shear viscosity at zero frequency can be calculated from

$$\bar{\eta} = \rho \frac{\partial}{\partial k^2} \mathring{\Gamma}_{j_t \tilde{j}_t}(\xi, k, \omega = 0)|_{k=0}. \tag{352}$$

After inserting the renormalized quantities and some rearrangements, the effective Kawasaki amplitude calculated within theory can be written as

$$R_K^{(\mathrm{eff})} = 6\pi A_3 \frac{\hat{\Gamma}^{(s)}_{\phi\phi}(u(\ell))}{f^2(\ell)} [1 + G(u(\ell), f(\ell))][1 + E_t(u(\ell), f(\ell))] \tag{353}$$

where $G(u(\ell), f(\ell))$ and $E_t(u(\ell), f(\ell))$ contain the loop contributions of the dynamic amplitude functions of D_T and $\bar{\eta}$. In one-loop order (ε-expanded), they read for instance

$$G(u(\ell), f(\ell)) = -\frac{f^2(\ell)}{16}, \qquad E_t(u(\ell), f(\ell)) = -\frac{f^2(\ell)}{36}. \tag{354}$$

The static OP amplitude function is in one-loop order simply

$$\hat{\Gamma}^{(s)}_{\phi\phi}(u(\ell)) = 1. \tag{355}$$

The flow parameter ℓ is via the matching condition (218) a function $\ell(t)$ of the reduced temperature t. $A_3 = 1/(4\pi)$ is the geometrical factor A_d at $d = 3$ introduced in (99). The mode coupling $f = g/\sqrt{\Gamma\lambda_t}$ is defined analogous to (198). Its flow is determined by the flow equation (199) with the β-function (202) (λ therein is now λ_t). The initial value $f(\ell(t_0))$ can be found by fitting the experimental data of the shear viscosity. The universal asymptotic value $R_K = R_K^{(\mathrm{eff})}(\ell = 0)$ for the Kawasaki amplitude is obtained by inserting the fixed-point value $f^\star$ for the mode coupling parameter.

Exponents and Kawasaki amplitude have been calculated within several approaches. In table 9, values for the exponent of the shear viscosity x_η from different approximations are summarized. In the earlier calculations of [52], a technical error in the numerical estimate of integrals occurred. This is discussed in [172] as well as in [176]. Also the results of [4] are in error, the value of the dynamic exponent z_φ as well as the stability exponents disagrees with [172]. The two-loop field-theoretic results [172] in ε-expansion read

$$z_\varphi = 4 - \frac{18\varepsilon}{19}(1 - 0.0196\varepsilon), \qquad R_K = 6\pi K_d \frac{19\varepsilon}{24}(1 - 0.054\varepsilon) \tag{356}$$

with $K_d = (2\pi^{d/2}/\Gamma(d/2))/(2\pi)^d$, ($K_4 = 1/(8\pi^2)$, $K_3 = 1/(4\pi^2)$). This can be compared with the result of [176]

$$z_\varphi = 4 - \frac{18\varepsilon}{19}(1 - 0.0205\varepsilon), \qquad R_K = \frac{3}{\pi}\frac{19\varepsilon}{24}(1 + 0.196\varepsilon). \tag{357}$$

The coefficients of the ε^2-term in the exponent z_φ and Kawasaki amplitude ratio are different but the numerical values at $d = 3$ are almost the same for the exponents and 10% different

for the Kawasaki ratios. A larger discrepancy appears if one considers the results obtained in [176] without ε-expansion. Then, the exponent is somewhat smaller but the Kawasaki ratio is much larger than the ε-expanded result (see the values collected in table 9).

The best value of the Kawasaki amplitude used in mode coupling theory as a parameter in comparison with experiment [180] turns out to be $R_K = 1.05$. This is quite the same as the value calculated in one-loop order field theory ($R_K = 1.056$ [181]). The larger value in one-loop order comes about by using a different geometrical factor in the renormalization of u as in other works. There is a freedom to choose the dimensional factor coming from the angle degrees of freedom of the unit sphere. The usual choice for this factor in field theory is

$$K_d = \Omega_d/(2\pi)^d \tag{358}$$

with Ω_d from (100) (instead of the notion K_d one finds S_d [59] but sometimes S_d means Ω_d, e.g., [172]) whereas we have chosen for the factor A_d (99) instead of K_d for all models. This choice makes no difference in the exponents, however the ε-dependence of other field-theoretic functions might be different (see the additive renormalization of the specific heat in statics [78]).

Using the minimal subtraction scheme for calculating the ζ-functions (A.38) and (A.39), the time scale ratio $w = \Gamma/\lambda_t$ (its naive dimension is -2) has to be set to zero [4]. This is not necessary if one uses the approach of [173] at $d = 3$. The ζ-functions in one-loop order then read

$$\zeta_\Gamma = -\frac{\pi}{3} f^2 \left(1 - \left(\frac{w}{1+w}\right)^2\right) \qquad \zeta_{\lambda_t} = -\frac{\pi}{80} f^2. \tag{359}$$

Since w is irrelevant its fixed-point value is zero with a transient exponent of about $\omega_w \sim 2$. A detailed discussion of the problems connected with setting the irrelevant parameter w equal to zero can be found in [172]. This is especially important if one uses formally the β-function for f and w and calculates the correction exponents ω_w.

We think it is important to obtain reliable values for the exponents and the Kawasaki amplitude within one approach. Only then a consistent picture of the dynamical behaviour of the fluid in comparison with experiments made for different quantities is achieved.

16.2. Transport coefficients and effective Kawasaki amplitude

The non-asymptotic theory has been applied to the transport coefficients near the gas–liquid phase transition in order to cope with the situations that measurements (i) are performed further away from the critical point in temperature and/or density, (ii) have to take into account gravitation [182] and (iii) are made at non-zero frequency ω (e.g., in measurements of the shear viscosity). The non-asymptotic theory also calculates a corresponding non-asymptotic Kawasaki amplitude (353). Instead of the fixed-point value of the mode coupling, the solution of the flow equation for the mode coupling appears. The flow parameter ℓ is related to the physical values of k, ξ, ω or $\Delta\rho = \rho - \rho_c$ (the deviation from critical density) by the matching condition.

The matching condition taking into account all these effects reads

$$\ell^8 = \left(\frac{\xi_0}{\xi(t, \Delta\rho)}\right)^8 + \left(\frac{2\omega\xi_0^4}{\Gamma(\ell)}\right)^2, \tag{360}$$

where $\xi(t, \Delta\rho)$ is calculated within the cubic model [183] using the heuristic expression for the correlation length given in [184]. In the corresponding limits, (360) reduces to the matching conditions (218)–(221).

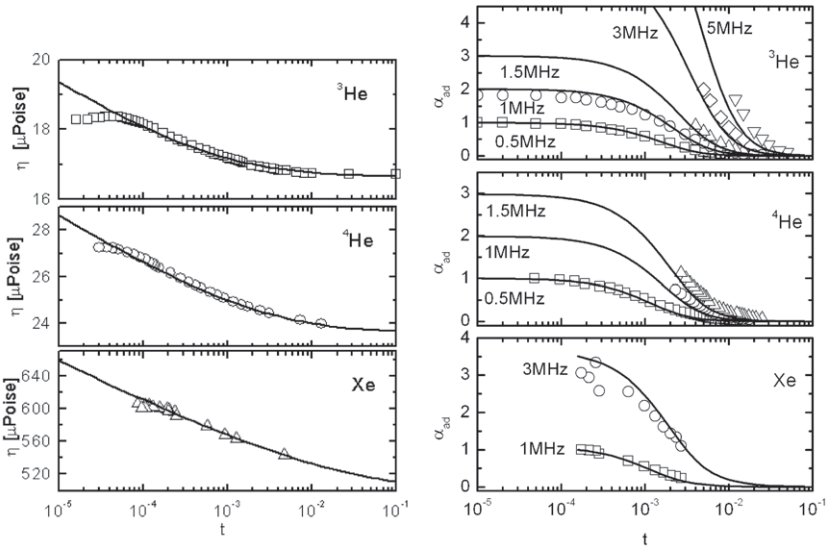

Figure 12. Left: fits (solid lines) of the shear viscosity in order to get the initial value $f(t_0)$. Data from [185] (^{3}He and ^{4}He) and from [186] (Xe). Right: adjusted sound attenuation as a function of temperature at different frequencies: theoretical result (solid lines), for details see the text. Data from [187] (^{3}He), [188] (^{4}He) and [189] (Xe).

The non-asymptotic theory permits to relate different dynamic quantities and—after the non-universal parameters have been fixed by using a certain set of data—to predict dynamic quantities in regions where one has no data or to predict other dynamic quantities. As an example, we show (figure 12) the calculation of the sound attenuation from a fit of the shear viscosity. Note that the background value of the sound attenuation has been subtracted. Therefore, the scale of the sound attenuation at the lowest frequency has been adjusted. In this respect, it compares with mode coupling theory [180].

16.2.1. Viscosity on earth and in space. Usually, the shear viscosity in a fluid is measured by the oscillating disc method where the frequencies of discs at the top and the bottom of a cell of a certain height are measured. A reliable comparison of the asymptotic critical exponent calculated for the shear viscosity is hindered by several influences. The shear viscosity is strongly affected (i) by gravity (since gravity induces a density gradient over the height of the cell) and (ii) by the finite frequency at which the experiment is performed. If one uses the facility of zero gravity in the discovery, the frequency effects can be made more visible.

Recently, such a zero gravity experiment has been performed [191] and a value $x_\eta = 0.069$ for the critical exponent of the shear viscosity has been found. This value is in good agreement with the two-loop RG result [172] and the self-consistent theory of [176] (see also table 9). The effect of higher loop terms on the exponent x_η has been considered in [192] with the result that loop orders above the two-loop order are negligible for the exponent.

As already noted in zero gravity, frequency effects can be made visible and the viscoelastic properties can be measured. At non-zero frequency, the viscosity becomes complex and both the real and imaginary parts are measured. It is the imaginary part which is related to the

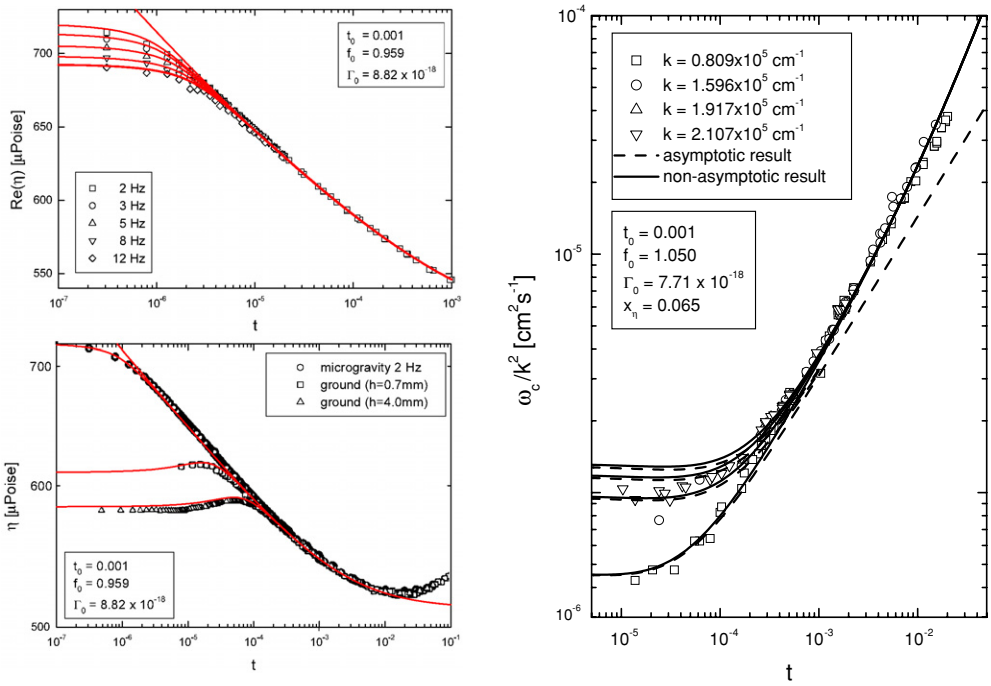

Figure 13. Left: shear viscosity of xenon on earth and in space. Data on earth: [195], data in space: [191]. Top: the shear viscosity as a function of relative temperature distance from the critical point at different frequencies in space. Bottom: the same at a very low frequency in space and on earth in cells with different heights. Solid curves: calculation of RG theory. Right: characteristic width of the light scattering data in xenon at different wave vectors. Data: [196] (from [175]).

(This figure is in colour only in the electronic version)

viscoelastic behaviour. In one-loop order, the frequency-dependent shear viscosity has been calculated [174] which allows to combine frequency and gravitational effects [193, 194]

$$\bar{\eta}(t, \Delta\rho, \omega) = \frac{k_B T}{4\pi} \frac{\xi_0}{\ell f^2(\ell)\Gamma(\ell)} [1 + E_t(f(\ell), v(\ell, t), w(\ell, \omega))] \tag{361}$$

with the functions

$$v(\ell, t) = \frac{\xi^{-2}(t)}{\left(\xi_0^{-1}\ell\right)^2} \qquad w(\ell, \omega) = \frac{\omega}{2\Gamma(\ell)\left(\xi_0^{-1}\ell\right)^4} \tag{362}$$

depending on the flow parameter ℓ, the relative temperature distance t and the frequency ω. The flow parameter ℓ depends via the matching condition (360) on t, ω and the deviation from the critical density $\Delta\rho$. The one-loop contribution E_t is a complicated function given in (5.3) in [174].

The non-asymptotic theory has been used to analyse different experiments: (i) the earthbound experiments of the shear viscosity of xenon in two different cells [195], (ii) the zero gravity experiments and (iii) the characteristic frequency of Xe [196] (see figure 13 (right part) and the following subsection). One has to fix the non-universal parameters entering the theoretical expression. These are the initial conditions of the flow equation for the mode coupling $f(\ell_0)$ and the kinetic coefficient of the OP in the background $\Gamma(\ell_0)$. Since the theoretical expressions were calculated in one-loop order, the exponent x_η was allowed to

differ from its one-loop value and was determined by a fit to the real part of the shear viscosity of the zero gravity experiment. Then, one can calculate the earthbound shear viscosity without any parameter as shown in figure 13. In the earthbound experiments, the asymptotic behaviour is never reached for the cell heights taken in the experiments (see [175] and figure 13 (left part)) due to gravity effects.

Agreement with the experiment can only be reached by introducing a scale factor for the frequency which is thought to take into account higher order terms in the perturbational calculation of the frequency dependence of the shear viscosity (a self-consistent two-loop calculation points in that direction [197]). With such a factor very good agreement of the RG theoretical results [34] is obtained for the real part and less for the imaginary part [175, 198]. On earth one has a combination of frequency effects and gravity effects. Usually, the gravity effects hide the frequency effects apart from very small cell heights (for details of the combined effects see [174]).

A combination of the theoretical results of [199, 200] which describe the crossover of the zero-frequency shear viscosity to the background and the scaling function of the frequency dependent has been used in [191] to analyse the shear viscosity data in space. Using a frequency scale factor in the comparison good agreement is also achieved for the viscoelastic part (this discrepancy to the analysis in [175, 198] can be explained by the asymptotic value of $\lim_{T\to T_c} \mathrm{Im}(\bar{\eta})/\mathrm{Re}(\bar{\eta})$ which is different in the two approaches)

An interesting relation between the complex shear viscosity measured in the critical region at zero shear rate $\dot{\gamma}$, but finite frequency ω_{osc}, and measurements of the real shear viscosity at zero frequency, but at finite shear rate, related to the frequency ω_{osc} has been found [201]:

$$|\bar{\eta}(\omega = \omega_{\mathrm{osc}}, \dot{\gamma} \equiv 0)| = \bar{\eta}(\omega \equiv 0, \dot{\gamma} = \omega_{\mathrm{osc}}/k_{\mathrm{CM}}). \tag{363}$$

Such a type of relation is known in rheology of polymer melts as Cox–Merz rule. It is not understood why such a relation should be valid but attempts have been made to consider shear thinning in the critical region. There are results for shear thinning from mode coupling theory [202] and quite recent results started calculations of a scaling function [203] taking into account a finite frequency and a finite shear rate in order to reach a relation of the Cox–Merz type. For a review of the effects of shear on fluids undergoing a phase transition see [177].

16.2.2. Thermal transport. Another transport coefficient of interest is the thermal conductivity and/or the thermal diffusivity which has been calculated in one-loop order [174]. Using the matching condition (360) for $\omega = 0$ allows to compare in the temperature and density regions around the critical point $(T_c, \rho_c) = (t = 0, \Delta\rho = 0)$ and to relate the transport coefficient to each other. In fact, via the Kawasaki amplitude the asymptotic divergencies of the thermal conductivity and the shear viscosity are related. This also holds in the non-asymptotic region.

16.2.3. Effective Kawasaki amplitude. Further away from the transition point an effective critical amplitude from its experimental counterpart (350) may be defined. From (353) and (354) in one-loop order follows [181]

$$R_K^{(\mathrm{eff})} = \frac{3}{2f^2(\ell)}\left[1 - \frac{f^2(\ell)}{16}\right]\left[1 - \frac{f^2(\ell)}{36}\right]. \tag{364}$$

Inserting the fixed-point value (in the limit $\ell \to 0$) for the mode coupling $f(\ell)$, one obtains the universal asymptotic value. For finite distance from the critical point, the temperature dependence of $R_K^{(\mathrm{eff})}$ is obtained inserting the appropriate matching condition (218). The temperature dependence of $R_K^{(\mathrm{eff})}$ depends on the initial value of the mode coupling f in the

background specific for the fluid system under consideration. However, in general, $f(\ell)$ decreases in the background and $R_K^{(\mathrm{eff})}(t)$ increases further away from T_c. Since the initial value of f can be found from comparing the theoretical expression for another transport coefficient (lets take the shear viscosity) with experimental data, one can predict $R_K^{(\mathrm{eff})}(t)$ without any parameter involved (see, e.g., figure 2 in [205] and figure 1 in [174]).

16.3. Light scattering

Light scattering experiments in fluids measure the dynamical OP correlation function. Due to fluctuations one expects deviation from a pure exponential decay of the critical fluctuations. A first attempt to calculate this deviation has been made in [206] and agreement with light scattering experiments near T_c ($T - T_c = 1.8$ mK) at the consolute point in a binary mixture (belonging to the same universality class as pure fluids) has been found.

Another quantity of interest is the linewidth of the critical scattering function. This is extracted from the scattering data assuming an exponential decay (Lorentzian line shape) as a function of the wave vector k and the relative temperature distance from T_c or correlation length ξ. Considering the whole k_ξ-plane the width crosses over from the asymptotic hydrodynamic region where $k\xi < 1$ and the width is proportional to k^2 to the asymptotic critical region where $k\xi > 1$ and the width is proportional to k^z. This crossover function has been calculated in one-loop order by field theory in [175] and extended to cover also the crossover to the background region.

The width is directly related to the OP vertex function at zero frequency

$$\omega_c(k,\xi) = \Gamma_{\varphi\bar{\varphi}}(k,\xi,\omega=0). \tag{365}$$

The explicit expression is found to be

$$\omega_c(k,x) = \Gamma_{\mathrm{as}} k^{z_\varphi} \left(\frac{1+x^2}{x^2}\right)^{1-x_\lambda/2} c_{\mathrm{na}}(k,x)^{x_\lambda} f(k,x), \tag{366}$$

with the non-asymptotic function

$$c_{\mathrm{na}}(k,x) = \left[1 + \frac{k}{k_0}\sqrt{\frac{1+x^2}{x^2}}\right] \tag{367}$$

and a non-asymptotic scaling function

$$f(k,x) = 1 - \frac{3}{38 c_{\mathrm{na}}(k,x)}[-5 + 6x^{-2}\ln(1+x^2)]. \tag{368}$$

The scaling variable x, the non-asymptotic amplitude of the kinetic coefficient Γ_{as} and a non-asymptotic scale of the wave vector k_0 are defined as

$$x = k\xi(t) \qquad \Gamma_{\mathrm{as}} = \Gamma(\ell_0)\left(\frac{f^2(\ell_0)\ell_0}{(f^\star)^2\xi_0}\right)^{x_\lambda} \qquad k_0^{-1} = \left(\frac{(f^\star)^2}{f^2(\ell_0)} - 1\right)\frac{\xi_0}{\ell_0}. \tag{369}$$

It contains several non-universal parameters: (i) the initial value $f(\ell_0)$ of the dynamic mode coupling at some background value of the flow parameter ℓ_0 and (ii) the initial value of the kinetic coefficient $\Gamma(\ell_0)$. They appear when one solves for the flow equations of these functions. The matching condition

$$\frac{\xi^{-2} + k^2}{\left(\xi_0^{-1}\ell\right)^2} = 1 \tag{370}$$

relates the flow parameter ℓ to the wave vector k and the correlation length ξ. It contains the asymptotic amplitude of the correlation length ξ_0 (see (219)). This expression allows to discuss the specific limiting power laws appearing in the different regions.

Asymptotic region. In the asymptotics, the non-universal value of $f(\ell_0)$ assumes the fixed-point value $f^\star$ and the non-asymptotic function becomes $c_{\rm na} = 1$ and drops out. Then, the characteristic frequency (366) can be written in scaling form ($f(k, x)$ is a function of x alone)

$$\omega_c(k, x) = \Gamma_{\rm as} k^{z_\varphi} \left(\frac{1+x^2}{x^2}\right)^{1-x_\lambda/2} \left(1 - \frac{3}{38}[-5 + 6x^{-2}\ln(1+x^2)]\right). \quad (371)$$

This one-loop result might be compared with other approximations often calculated directly in $d = 3$, see [52, 207, 208]. A field-theoretic calculation at $d = 3$ has been performed in [173]. Due to the fixed dimensional computation, an arbitrariness concerning the exponentiation of certain terms remains. This arbitrariness is avoided in the approach using the RG equation result for the vertex function and an appropriate matching condition [175].

Background region. In the background, the correlation length ξ is small or the wave vector k is large (i.e., the limit $\xi k_0 \to 0$ or $k/k_0 \to \infty$). Thus, $c_{\rm na}$ is dominated by its second term and $f(k, x)$ reduces to 1 and the characteristic frequency (366) is obtained in a form

$$\omega_c(k, x) = \Gamma(\ell_0)\left(1 - \frac{f^2(\ell_0)}{(f^\star)^2}\right)^{x_\lambda} k^4 \left(\frac{1+x^2}{x^2}\right), \quad (372)$$

which recovers the van Hove result when the mode coupling in the background f_0 is set to zero. A non-asymptotic expression has been derived by Olchowy (see [180]) however the function does not allow the limit of large values of the modulus of the wave vector, so formally the limit of the van Hove result cannot be reached.

16.4. Computer simulations

Quite recently, molecular dynamics simulations have been used to predict asymptotic dynamical critical exponents [209], which has been commented in [210, 211]. Whereas this first paper considers mixtures (belonging to the same universality class as pure fluids, see the following section) in [212], simulations have been performed for a Lennard–Jones fluid. Both simulations extract an exponent which is easily related to the exponent of a diffusion coefficient (mass diffusion or thermal diffusion) diverging as

$$D \sim \xi^{-x_D} \qquad \text{with} \quad x_D = 1 + x_\eta \quad (373)$$

where the relation for x_D follows from (285). In the first case, the value found $x_D = 1.26 \pm 0.08$ [209] is much larger than theoretical and experimental values [210], whereas the second value $x_D = 1.023 \pm 0.018$ [212] is closer to these values but with its upper bound lower than the latest accurate prediction $x_D = 1.0679 \pm 0.0007$ [176] (see the discussion of the asymptotics above). However, it seems to be promising that one observes in the simulations the strong effect of fluctuations. In van Hove theory, the diffusion coefficient would diverge as

$$D \sim 1/C_p \sim \xi^{-\gamma/\nu} = \xi^{-(2-\eta)} \quad (374)$$

since the kinetic coefficient is constant (we have used static scaling laws).

The discrepancy between the results of the simulations in a mixture and a pure fluid could be resolved quite recently in [213]. A symmetric binary Lennard–Jones mixture has been studied by a combination of semi-grandcanonical Monte Carlo and molecular dynamics simulations. The results for the critical behaviour of the shear viscosity and the mutual

diffusion coefficient are in agreement with the asymptotics of model H ($x_D = 1.068$) provided finite-size effects and background contributions are taken into account. A value of $R_K = 1.05$ for the Kawaski amplitude has been adopted in the analysis.

17. Model H′ (gas–liquid and liquid–liquid transitions in binary mixtures)

Although the asymptotic universality class of a binary mixture is the same as the one of a pure fluid [1], it has become obvious by experiment that, e.g., the critical behaviour of the transport coefficients near the critical point in a mixture might be quite different. There exist two types of critical points in normal liquid mixtures. The first one is the gas/liquid transition analogous to simple fluids usually denoted as plait point. The second one is a demixing transition into two phases of liquids with different mole fractions, which is called the consolute point. As an example, we mention the behaviour of the thermal conductivity near a consolute point and a plait point. The thermal conductivity measured in a mixture is the thermal conductivity at zero mass flow and it is asymptotically finite (non-divergent) contrary to the thermal conductivity at zero concentration gradient which would diverge asymptotically with the same exponent as the thermal conductivity of a pure fluid. This holds at the consolute point as well as the plait point. In the non-asymptotic region, it turns out that the behaviour in these two different cases might be quite different. Whereas at the consolute point the measurable thermal conductivity is almost constant, it seems to diverge for a plait point [13, 15]. However, this difference could be clarified by taking into account the complete dynamical model in a non-asymptotic field-theoretical calculation of the thermal conductivity. At both critical points, the model equations have the same structure. We have to consider dynamical equations as in model H (see the previous subsection), including a conserved OP ϕ_0 and the transverse momentum current $\vec{j}_t$, which are now extended by a conserved scalar secondary density m_0. The Poisson brackets necessary for the reversible part of the equations have been discussed in (145)–(151). The equations read

$$\frac{\partial \phi_0}{\partial t} = \mathring{\Gamma}\nabla^2 \frac{\delta \mathcal{H}}{\delta \phi_0} + \mathring{L}\nabla^2 \frac{\delta \mathcal{H}}{\delta m_0} - \mathring{g}(\vec{\nabla}\phi_0)\frac{\delta \mathcal{H}}{\delta \vec{j}_t} + \theta_\phi, \tag{375}$$

$$\frac{\partial m_0}{\partial t} = \mathring{L}\nabla^2 \frac{\delta \mathcal{H}}{\delta \phi_0} + \mathring{\mu}\nabla^2 \frac{\delta \mathcal{H}}{\delta m_0} - \mathring{g}(\vec{\nabla}\phi_0)\frac{\delta \mathcal{H}}{\delta \vec{j}_t} + \theta_m, \tag{376}$$

$$\frac{\partial \vec{j}_t}{\partial t} = \mathring{\lambda}_t \nabla^2 \frac{\delta \mathcal{H}}{\delta \vec{j}_t} + \mathring{g} \overleftrightarrow{\mathcal{T}} \left\{ (\vec{\nabla}\phi_0)\frac{\delta \mathcal{H}}{\delta \phi_0} + (\vec{\nabla} m_0)\frac{\delta \mathcal{H}}{\delta m_0} - \sum_k \left[j_k \vec{\nabla}\frac{\delta \mathcal{H}}{\delta j_k} + \nabla_k \vec{j}\frac{\delta \mathcal{H}}{\delta j_k} \right] \right\} + \vec{\theta}_t. \tag{377}$$

Different to the models C′, E′ and F′, the KC L is now the dissipative coupling between the OP and the secondary density. Another difference is that only one mode coupling $\mathring{g}$ is present due to translational invariance (see the discussion in subsection 7.2). Plait point and consolute point differ in the assignment of the OP and the scalar secondary density to thermodynamic densities. At the plait point, ϕ_0 is related to the entropy density per mass σ and m_0 is related to the mass concentration c, while at the consolute point the assignment is reversed.

From the ζ- and β-functions (see the ζ-functions (A.75) and (A.76)) and the corresponding fixed points, one finds the asymptotic behaviour of model H for the shear viscosity diverging with the exponent x_η, the kinetic coefficient of the mass diffusion diverging with x_λ (see table 10).

Table 10. Asymptotic critical behaviour of the transport coefficients in mixtures and pure fluids. Values calculated by RG $x_\eta \sim 0.07$ and $x_\lambda = 3 - \eta - x_\eta$. The thermal conductivity in mixtures is given for zero mass current.

System	Shear viscosity	Thermal conductivity	Thermal diffusion ratio	Mass diffusion
Pure fluid	$\bar{\eta} \sim \xi^{x_\eta}$	$\kappa \sim \xi^{x_\lambda}$	–	–
mixture	$\bar{\eta} \sim \xi^{x_\eta}$	Constant	$k_T \sim \xi^{-(x_\lambda - \gamma/\nu)}$	$D \sim \xi^{x_\lambda - \gamma/\nu}$

17.1. Transport coefficients

Apart from the thermal conductivity κ_T, the dissipation in a binary liquid mixture is also determined by the mass diffusion D and the thermal diffusion ratio k_T as already presented in ^{3}He–^{4}He mixtures at the superfluid transition. Although the plait point and the consolute point belong to the same universality class, the theoretical expressions of the transport coefficient depend on the type of critical point in the mixture [218]. The critical behaviour of the transport coefficients and the sound propagation also including the non-asymptotic region in binary mixtures near a plait point has been presented in [15]. A more comprehensive discussion, where the non-asymptotic critical behaviour of the transport coefficients near the consolute point has also been considered, can be found in [16, 219].

The critical theory predicts that in binary mixtures at the plait point [15] and the consolute point, the thermal conductivity (at zero mass current) shows an enhancement to a finite value at T_c, which is in contrast to pure fluids where κ_T diverges at the critical point. While at the consolute point the finite plateau value at T_c has been also verified experimentally (see, e.g., [220]), the situation at the plait point appeared quite different. Contrary to the theoretical predictions, the experimentally measured thermal conductivity revealed a divergent-like behaviour in the accessible temperature region. This can be seen for instance in ^{3}He–^{4}He mixtures at the plait point in figure 14 where the experimental results of the thermal conductivity at a mole fraction $X = 0.8$ are plotted together with the data of pure ^{3}He and pure ^{4}He (left figure, second plot). The theoretical calculation (solid line) indeed shows that the crossover to a finite value occurs far outside the region where experiments can be performed. This situation should be improved by choosing a mixture of pure liquids with components differing much more than ^{3}He and ^{4}He. For a 50% mixture of methane and ethane indeed the onset of the crossover could be verified [13] and quantitatively corroborated by mode coupling theory [221] (see the solid curve in the right part of figure 14).

There is a relation between the critical behaviour of the thermal diffusion ratio k_T and the mass diffusion D, however this relation depends on the type of phase transition in the mixture.

Consolute point. Near a consolute point, the relation simply reads

$$k_T(t) = \frac{\rho}{R}\frac{\mathring{L}}{D(t)}, \tag{378}$$

where R is the general gas constant and ρ is the mass density. Thus, the product of the two transport coefficients should be a constant over the whole critical region. This has already been observed long ago [222] (see figure 2 therein).

Plait point. A more complicated relation holds near the plait point [16], which is

$$k_T(t) = -\frac{\rho}{R}\frac{1}{D(t)}\left[\mathring{L} + \frac{\mathring{\mu}}{a}\right] - \left(\frac{\partial c}{\partial T}\right)_{\sigma,P}. \tag{379}$$

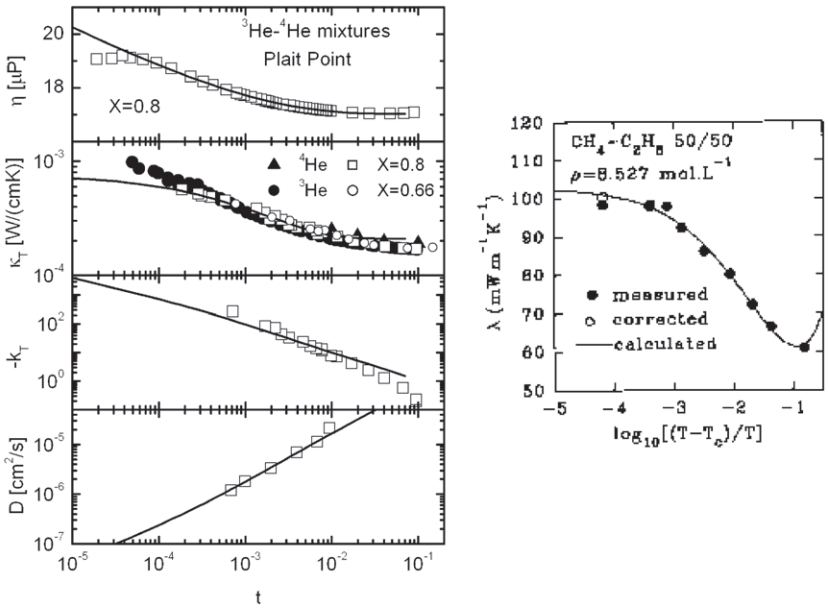

Figure 14. Left: transport coefficients of ^{3}He–^{4}He mixtures at the plait point for the mole fraction $X = 0.8$. The initial values of $w(t_0)$ and $f(t_0)$ are found from a fit of the shear viscosity. Then the thermal conductivity κ_T, the thermal diffusion ratio k_T and the mass diffusion coefficient D are determined (solid curves). Additionally, thermal conductivity data for $X = 0, 0.66, 1$. The data are taken from: $\bar{\eta}$ [214], κ_T [215], k_T [216] and D [217]. Right: 50% mixture of methane and ethane (from [13]).

The product $k_T D$ is now temperature dependent, but the asymptotic power-law behaviour obeys relation (378) (see, e.g., [223]). $a \equiv (\partial c/\partial\sigma)_{\Delta,P}$ is only weakly varying with the temperature.

As already mentioned, the non-asymptotic theory allows one to calculate the different transport coefficients from the flow of the dynamic model parameters using theoretical expressions of the transport coefficients. Analogous to model F′, the flow is determined by the flow equations of types (207)–(214). In the current model, these equations simplify considerably because $w_1 = \Gamma/\lambda_t = 0$ and $w_2 = \Gamma/\mu = 0$ are irrelevant and only one mode coupling parameter $f = g/\sqrt{\Gamma\lambda_t}$ is present. Thus, only a flow equation of type (201) for the mode coupling parameter and a flow equation of type (209) for the cross coefficient $w_3 = L/\sqrt{\Gamma\lambda_t}$ remain. The corresponding ζ-functions ζ_Γ, ζ_{λ_t} and ζ_L of model H′ have to be inserted (see (A.75) and (A.76)). The initial values are determined by the fit of the data of one or more transport coefficients.

As an example of the calculation of transport coefficients at the plait point in figure 14, the shear viscosity $\bar{\eta}$, the thermal conductivity κ_T, the thermal diffusion ratio k_T and the mass diffusion coefficient D in ^{3}He–^{4}He mixtures at a mole fraction $X = 0.8$ are presented. The initial values $w_3(t_0)$ and $f(t_0)$ of the dynamic flow are completely determined by a fit of the shear viscosity data (left figure, first plot). The remaining coefficients can then be calculated (solid lines) without adjustable parameter.

An example for the consolute point, the 2-butoxyethanol–water mixture, is presented in figure 15. Measurements of the shear viscosity [224] (and also of the correlation length $\xi(t)$ showing the crossover to a finite value in the background) and the thermal conductivity [225]

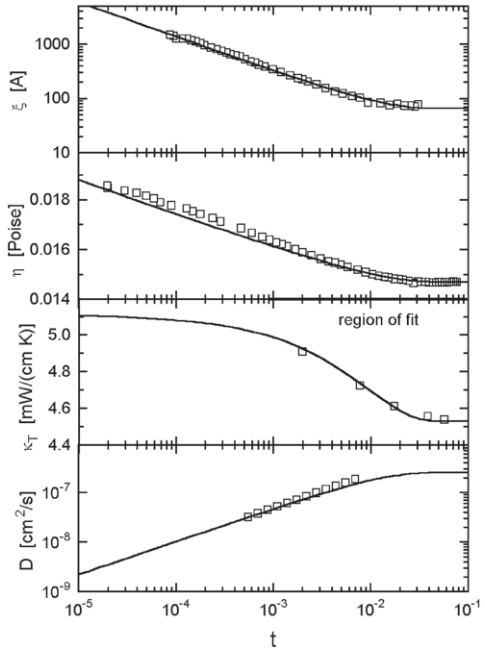

Figure 15. Comparison of theory with 2-butoxyethanol–water data. Shown is the fit of the correlation length ξ [225] used in the matching condition, the fit of the shear viscosity η (with background subtracted) [225] and the thermal conductivity κ_T [224] and our prediction for the mass diffusivity D [225] (from [219]).

have been performed. We have used the temperature dependence of the correlation length [70] and determined the dynamic parameters, f and w_3, from a fit of the viscosity and the thermal conductivity in order to predict the mass diffusion $D(t)$. A reevaluation and overview of the critical exponents of the shear viscosity in several mixtures has been given in [226]. Recently, measurements of the shear viscosity in nitrobenzene–alkane mixtures [227] confirmed the critical exponent x_η in agreement with earlier measurement and in agreement with the value in pure fluids (see table 9).

17.2. Kawasaki amplitude

Analogous to pure fluids, it is possible to introduce a Kawasaki amplitude. The relation to experimental quantities depends on the type of the critical point which is considered.

Consolute point. At the demixing transition, one only has to replace the thermal diffusion in (350) by the mass diffusion coefficient. Thus, one obtains

$$R_{K,\mathrm{cons}}^{(\mathrm{exp})} = \frac{6\pi\bar{\eta}D\xi}{k_B T}. \tag{380}$$

Plait point. At the plait point, the situation is more complex. In [70], it has been shown that an amplitude

$$R_{K,\mathrm{plait}}^{(\mathrm{exp})} = \frac{6\pi\bar{\eta}\xi}{\rho k_B T^2}\left(\frac{\partial T}{\partial \sigma}\right)_{\Delta,P}\left[\kappa_T + \rho T D\left(\frac{\partial \Delta}{\partial c}\right)_{T,P}\left(\frac{k_T}{T} + \left(\frac{\partial c}{\partial T}\right)_{\Delta,P}\right)^2\right] \tag{381}$$

can be introduced, which has the required properties. The above expression reduces in the asymptotic limit to

$$R^{(\mathrm{exp})}_{K,\mathrm{plait}} \overset{t\to 0}{=} \frac{6\pi\bar{\eta}D\xi}{k_B T} \tag{382}$$

equal to the expression at the consolute point.

In the same way as for the gas–liquid point in a pure fluid, an effective Kawasaki amplitude can be calculated at the plait point or at the consolute point in a mixture. It involves on the one hand the non-asymptotic expression of the shear viscosity, which is the same for all types of phase transitions in the mixture, on the other hand the expression for the mass diffusion is different (compare the expressions for D given by the vertex functions (3.35) and (3.26) in [16] respectively). Introducing the theoretical expressions for the quantities in (380) and (381), it has been shown [70] that both expressions lead to the same effective Kawasaki amplitude which reads in one-loop order

$$R^{\mathrm{eff}}_K = \frac{3}{2f^2(\ell)}\left(1-\frac{1}{16}f^2(\ell)\right)\left(1-\frac{1}{36}\frac{f^2(\ell)}{1-w_3^2(\ell)}\right). \tag{383}$$

Inserting for the flow parameter, the matching condition (218) gives the temperature dependence. The Kawasaki amplitude for a series of binary mixtures has been measured and an overview has been given in [228]. In some cases the temperature dependence has also been plotted showing either an increase (figure 6 therein for nitroethane–3-methypentane mixture) or a decrease (figure 8 therein for the triethylamine–water mixture). This behaviour in the background can be understood from the flow of the dynamic parameters involved. The mode coupling f decreases whereas the time scale ratio w_3 increases approaching the background region. Depending on the strength of this decrease and increase both behaviour can be obtained.

The light scattering spectrum in the hydrodynamic region has been considered in [229] using the non-asymptotic expression near a consolute point for the transport coefficients involved [221]. One observes two diffusive modes, whose nature depend on the concentration of the mixture. At low concentration the slowest mode crosses over from a mass-diffusion-like mode to a thermal-diffusion-like mode as one expects. No corresponding field-theoretical calculation is available.

18. Models G and J (magnetic transitions in Heisenberg magnets)

The appropriate tool for investigating the critical properties of magnetic systems (i.e., Heisenberg magnets) is neutron scattering. An important quantity involved in the measurements is the dynamical structure factor. Usually, it is assumed to have the shape of a Lorentzian. Dynamic scaling however shows (see subsection 8.1) that this is not true near the phase transition. The non-Lorentzian shape has to be considered in a quantitative comparison with experiment and these fluctuation effects are visible in (i) constant energy scans and (ii) constant wave vector scans. The shape function of ferromagnets at T_c has been calculated within field theory in [26] and corroborated later by [28]. A RG calculation in the whole q–ξ–ω-space, where the asymptotic crossover between the hydrodynamic and critical region could be studied, was carried out in [29]. For the antiferromagnet, renormalization group theory fails to reproduce the shape function observed in experiments. Whereas, experimentally, a central critical component is observed this is not the case in theory (this also holds for calculations within mode coupling theory).

18.1. Model J (isotropic ferromagnet)

Model J only includes the equation for a conserved real OP $\vec{\phi}_0$ representing the local magnetization (128). The reversible part of the dynamic equation following from the Poisson brackets (129) describes the Larmor precession of the three-dimensional vector [230]:

$$\frac{\partial\vec{\phi}_0}{\partial t} = \mathring{\Gamma}\nabla^2\frac{\delta\mathcal{H}}{\delta\vec{\phi}_0} + \mathring{g}\vec{\phi}_0 \times \frac{\delta\mathcal{H}}{\delta\vec{\phi}_0} + \vec{\theta}_\phi. \tag{384}$$

The static functional $\mathcal{H} = \mathcal{H}_{\mathrm{GLW}}$ is the GLW functional (24). In the paramagnetic phase, the critical mode is the spin diffusion which at T_c has the critical dispersion

$$\omega_c(k) = A_\varphi k^{z_\varphi} \tag{385}$$

and in the hydrodynamic limit ($\xi k < 1$) reads

$$\omega_c(\xi, k) = D(\xi)k^2 \tag{386}$$

with the critical diffusion coefficient

$$D(\xi) \sim \xi^{-(z_\varphi-2)}. \tag{387}$$

The asymptotic dynamical critical exponent is known exactly—in $d = 3$, $z_\varphi = 2.5 - \eta/2 \sim 2.5$ (see (289))—and deviates considerably from the van Hove value $z_\varphi = 4-\eta$ (which is the model B value). The value of the critical exponent has been verified experimentally [231] and by computer simulations (see below).

As already mentioned, in the case of model J the upper critical dimension, where critical fluctuations do not affect the kinetic coefficient, is $d = 6$.

A dynamical amplitude ratio is defined by

$$R_\lambda = \frac{\Gamma\xi^{(d-4)/4}}{g\sqrt{\chi}} = \lim_{k\to 0}\frac{\omega_\phi(k,\xi)}{\omega_-(k,\xi)} \tag{388}$$

where ω_- is a characteristic frequency related to the spin-wave frequency *below* T_c and χ is the static magnetic susceptibility. Another somewhat different dynamical ratio is

$$\bar{R}_\lambda = \frac{\omega_\phi(k,\xi)}{\omega_-(k,\xi\to\infty)}(k\xi)^{1-d/2} = \left(\frac{2}{2\varepsilon}\right)^{1/2}[1+0.07\varepsilon] \tag{389}$$

and has been calculated in two-loop order in [28].

The large upper critical dimension leads to larger fluctuation effects in $d = 3$ and therefore ferromagnets are suitable for measuring deviations of the shape function from the Lorentzian form. The OP correlation function has been calculated in one-loop order at T_c in [26, 28]. These calculations were extended to the whole k–ξ-plane in [29]. According to the scaling form (224), the shape function reads

$$\mathcal{F}(x, y) = 2\,\mathrm{Re}\left(\frac{1}{-\mathrm{i}y + [Z(x)\Pi(x, \mathrm{i}yZ(x)(1+1/x^2)]^{-1}}\right) \tag{390}$$

with $x = k\xi$ and the scaled frequency $y = \omega/\omega_c(\xi, k)$. The characteristic frequency ω_c is defined as the half width at half maximum in constant momentum scans. It also defines a scaling function

$$\omega_c(\xi, k) = \Gamma k^{z_\varphi} Z(x)(1 + 1/x^2). \tag{391}$$

Once the self-energy Π has been calculated in one-loop order, Z is found by the solution of the equation defining the half width (228). Using these two functions in (390), the shape function is calculated. However since this is a cumbersome method, a more suitable analytic

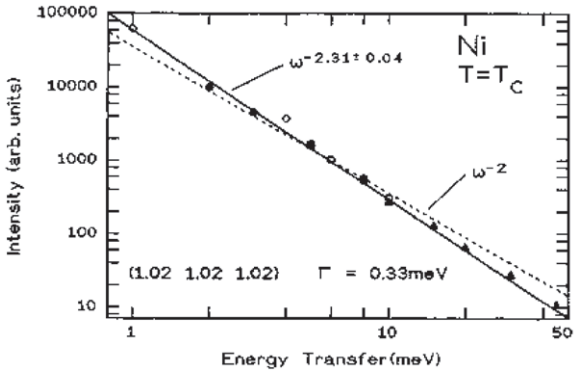

Figure 16. Scattering intensity at large energy transfer shows a power-law behaviour with exponent -2.31 ± 0.04. RG theory predicts -2.6. This demonstrates that the shape function definitively deviates from a Lorentzian. From [234].

expression to find the shape for comparison with experiment has been given [232]. It consists in writing Π and Z as

$$\Pi(x, \mathrm{i}w) = \left[\left(1 + \frac{b}{x^2}\right)^{2-\varepsilon/4} - aiw\right]^{\varepsilon/(8-\varepsilon}, \qquad \text{with} \quad w = \frac{\omega}{\Gamma k^{z_\varphi}}, \tag{392}$$

$$Z(x) = \left[1 - c \arctan\left(a \frac{1 + 1/x^2}{(1 + b/x^2)^2}\right)^{2-\varepsilon/4}\right]^{-1} \left(1 + \frac{b}{x^2}\right)^{-\varepsilon/4}. \tag{393}$$

RG theory leads to the following values of the parameters $a = 46$, $b = 3.16$ and $c = 0.51$. In $d = 3$, one has $\varepsilon = 3$.

The shape function has been measured in neutron scattering experiments at different temperatures both in constant energy scans and constant momentum scans [231, 233]. According to table 2, the asymptotic behaviour of the scattering intensity S at T_c reads

$$S(k, \omega \to \infty) \sim \omega^{-\upsilon_\varphi} \sim \omega^{-(z_\varphi+4)/z_\phi} \sim \omega^{-2.6}. \tag{394}$$

The experiment definitively rules out a Lorentzian shape and finds an exponent of $\upsilon_\varphi = 2.31 \pm 0.04$ over four decades of intensity [234].

Analysing the experimental scattering intensities for Ni [234] with the corresponding RG theoretical result for the width (see figure 16) and shape function (see figure 17), good agreement is obtained if one allows to adjust the parameters introduced in the analytic result (392) and (393). Then one obtains $a = -0$, $b = 3.2$ and $c = 1.5$. With these parameters, one obtains agreement also further away from T_c up to $T = 1.21T_c$ describing the crossover to an almost Lorentzian shape. A complication in the experimental determination of the scaling function for the width is its dependence on the form of the shape. This is demonstrated in figure 17 where the widths for two different shapes are compared.

There may be several reasons for the deviation from the theoretical result. On the theoretical side, one does not know how large the corrections are due to two-loop order since $\varepsilon = 6 - d$ is large in $d = 3$. On the experimental side, the itinerancy of Ni may play an important role. Similar comparisons for EuO [231] and EuS [236] agree with the RG theoretical result. However in these systems one has to be cautious in the interpretation of

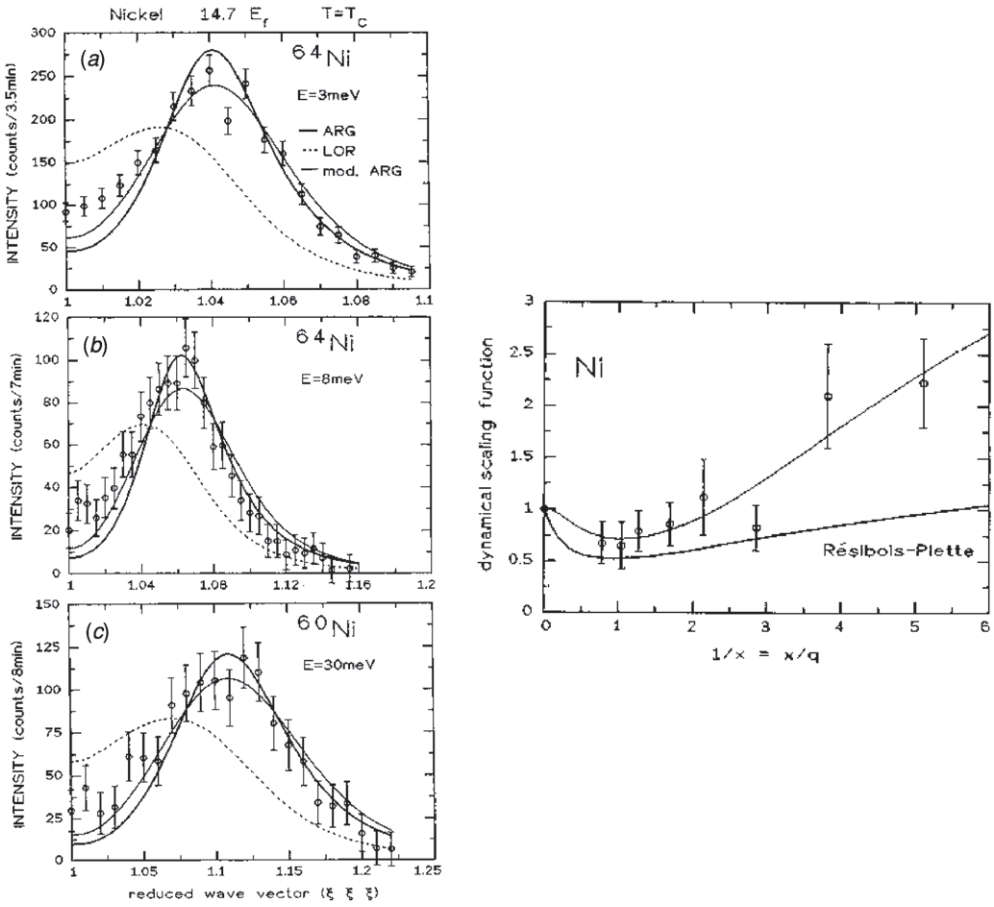

Figure 17. Left: constant energy scans in Ni at T_c compared with the asymptotic result of RG theory [29] (thick solid line), modified version (see the text) of the RG result (thin solid line) and the Lorentzian shape (dashed line) (from [234]). Right: dynamic scaling function for the width of constant wave vector scans. The thin line is based on a non-Lorentzian shape. The thicker line is based on a Lorentzian shape calculated by mode coupling theory by Resibios and Piette [235] (from [234]).

experiments since dipolar forces cause a crossover to another dynamical universality class. This crossover may happen at different values of k, ξ or ω depending on the physical quantity. For example, the crossover in the shape may be at different values as the crossover in the width (for further discussion see the review [41]).

A more stringent test of RG theory is possible by Monte Carlo simulations [237]. Excellent agreement with the RG value for the dynamical critical exponent has been obtained using finite-size scaling (the simulations have been performed for a body-centred cubic magnet with nearest neighbour interaction). The median frequency was used to extract the critical exponent z_φ. This characteristic frequency can be calculated in simulations without making an assumption about the shape of the dynamic correlation function. A numerical test of the existing shape functions is more complicated and has to incorporate finite-size scaling explicitly into the analytic expressions for the shape function. This is a nontrivial task which needs more theoretical effort, better algorithms and much more CPU time.

18.2. Model G (isotropic antiferromagnet)

The order parameter $\vec{\phi}_0$ for isotropic antiferromagnets is the non-conserved staggered magnetization (133), while the magnetization (134) now represents the secondary density $\vec{m}_0$. The Poisson brackets (135)–(137) lead to Larmor precession terms of the staggered magnetization around itself and the magnetization. Since the magnetization is conserved, it belongs to the set of slow variables and has to be taken into account. Thus, we have two sets of equations of motion containing besides the Larmor precession terms also a relaxational term in the equations for the staggered magnetization and a diffusive term in the set of equations for the magnetization [30]. Some terms have been shown in [136] to be irrelevant for the critical dynamics, thus the relevant set of equations read

$$\frac{\partial \vec{\phi}_0}{\partial t} = -\mathring{\Gamma}\frac{\delta \mathcal{H}}{\delta \vec{\phi}_0} + \mathring{g}\vec{\phi}_0 \times \frac{\delta \mathcal{H}}{\delta \vec{m}_0} + \vec{\theta}_\phi, \tag{395}$$

$$\frac{\partial \vec{m}_0}{\partial t} = \mathring{\lambda}\nabla^2 \frac{\delta \mathcal{H}}{\delta \vec{m}_0} + \mathring{g}\vec{m}_0 \times \frac{\delta \mathcal{H}}{\delta \vec{m}_0} + \mathring{g}\vec{\phi}_0 \times \frac{\delta \mathcal{H}}{\delta \vec{\phi}_0} + \vec{\theta}_m. \tag{396}$$

The field-theoretic functions are those of the SSS model for $n = 3$ (see (A.30) A.31)). It turns out that the time scale ratio $w = \Gamma/\lambda$ is the important parameter of this model, similar to the situation in model E. As in the case of the isotropic ferromagnet, the critical exponent $z_\varphi = z_m = 3/2$ for the isotropic antiferromagnet is known exactly, see (281). Experiments on $RbMnF_2$ find a slightly lower value of $z_m = 1.43 \pm 0.04$ [33]. Monte Carlo simulations presented several values for the dynamic exponent $z_m = 1.48 \pm 0.04$ in [238] then $z_m = 1.43 \pm 0.03$ in [239], but quite recently the simulations were improved to the value $z_m = 1.49 \pm 0.03$ [240] in agreement with RG theory. One should remark that the critical exponent z_m has been extracted by considering the median frequency of the magnetization correlation function. This procedure is allowed since at $d = 3$ and $n = 3$ the critical dynamics of the isotropic antiferromagnet is described by the scaling fixed point (see section 15.1 for the SSS model).

In one-loop order, the OP correlation function at T_N has been calculated in [31] for different n (using the SSS model [24] for generalizations to values of $n \neq 3$)

$$S_\phi(q, \omega) = \text{constant}\frac{1}{q^{2-\eta}}\frac{1}{\omega_c(q)}\mathcal{F}(\omega/\omega_c(q)), \tag{397}$$

with

$$\mathcal{F}(y) = \frac{1}{y}\,\mathrm{Im}\left(1 + \frac{h(\mathrm{i}y w_{\mathrm{SC}}, (w_{\mathrm{SC}})^{-1})}{(\mathrm{i}y)^{4/d}}\right) \tag{398}$$

with the one-loop fixed-point value $w_{\mathrm{SC}}^{1l} = 2n - 3$ and the function h given in equation (13) of [31]. For small arguments $|\mathrm{i}y w_{\mathrm{SC}}| \leqslant 1$, the shape reads

$$h(s, w) = s^{\varepsilon/(4-\varepsilon)}\left(1 - \frac{\varepsilon}{4}\left[\ln(1+s) + (1 + w(1+s))\ln\left(1 + \frac{1}{w(1+s)}\right) - 1\right]\right). \tag{399}$$

The field-theoretic calculation at T_N for $n = 3$ confirmed earlier results [30] for the staggered magnetization correlations and also agrees qualitatively with mode coupling theory at T_N [241, 242]. Note, however, that the shape function sensitively depends on w. This value of w is changed in two-loop order and turns out to be quite different from the one-loop fixed-point value (see the discussion in section 15.1). Indeed, the isotropic antiferromagnet is described by the strong-scaling fixed point (at $d = 3$ and $n = 3$, see figure 11) with a two-loop fixed-point value of $w_{\mathrm{SC}}^{2l} = 0.96$ three times smaller than the one-loop value. Effectively this value

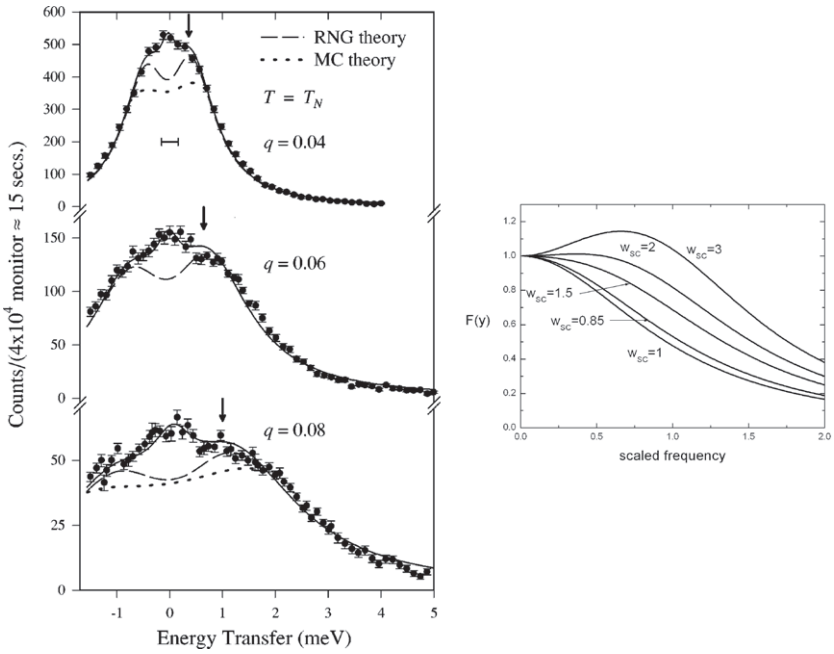

Figure 18. Left: constant wave vector scans of the staggered magnetization correlations in $RbMnF_2$ at T_N compared with the asymptotic result of one-loop RG theory of [30] (dashed line), modified version of the RG result (see [33]) (thin solid line) and Monte Carlo simulations (dotted line) [242] . From [33]. Right: shape function of the SSS model in one-loop order as a function of small values of the scaled frequency according to (398) and (399) at different values of w_{SC}.

corresponds to the one-loop value of w_{SC}^{1l} for $n = 2$ and for this value the shape function has its peak at zero frequency (see figure 1 in [31]). In figure 18, the change of shape with the value of w_{SC} is shown[6]. If the time scales of the staggered magnetization and the magnetization are almost the same, $w_{SC} \sim 1$, no side peak appears, if the time scale is much larger or smaller than one, a side peak appears. Thus, a recalculation of the shape function keeping w as a parameter seems to be indispensable in order to compare the RG result with experiment.

The comparison with experiment [33] (see figure 18) shows the discrepancy with the strict one-loop shape function at T_N. All other features predicted by RG theory are reproduced by experiment and/or computer simulations. Thus, below T_N longitudinal and transverse components of $S(k, \omega)$ with respect to the staggered magnetization are consistent with theory. All the expected features of propagating spin waves and a central peak due to spin diffusion are reproduced.

Computer simulations [239] calculated the dynamic structure factor for the space- and time-dependent spin–spin correlation function, the crossover from hydrodynamics to critical behaviour (in the asymptotic region) and the dynamical critical exponent $z_m = 1.43 \pm 0.03$. Although quite good agreement between simulations and experiment is obtained, the well-known discrepancy to RG and mode coupling calculations (no central peak) at T_N remained (see figure 8 in [239]). Quite recently [240] the simulations results have been improved, much better agreement with the critical exponent was achieved.

[6] In two-loop order both fixed-point values, the value of the dynamical coupling f and of the time scale ratio w are changed. This has not been taken into account in the simple argumentation presented here.

The calculated dynamic magnetization correlation function was considered to be essentially of Lorentzian form [30]. Applying the scaling laws for the dynamical function, one concludes however that the decay of this function goes like $\omega^{-2.3}$ instead of ω^{-2}. Thus, it is not a Lorentzian at T_N.

19. Critical dynamics in superconductors

In the last few years, a discussion is going on about the dynamical universality class of superconductors. Sloppy formulated the debate is on the question whether the relevant dynamical model belongs to the universality class of model A or model F. More precisely, one may expect a new universality class depending on the set of dynamical equations describing the dynamics of a superconductor and the resulting asymptotic dynamic exponents.

It has become clear that the static critical behaviour for type-I materials is driven by the coupling of the OP (the macroscopic complex wavefunction) to the gauge field to a first-order phase transition, while in the type-II materials a new so-called *charged fixed point* governs a continuous phase transition (see, e.g., [243–247]).

In [248], a relaxational dynamics has been suggested. Starting from the static Hamiltonian

$$\mathcal{H} = \int \mathrm{d}^d x \left\{ \frac{1}{2} t_0 |\psi_0|^2 + \frac{1}{2} |(\nabla - \mathrm{i} e_0 \boldsymbol{A}_0)\psi_0|^2 + \frac{u_0}{4!} |\psi_0|^4 + \frac{1}{2} (\nabla \boldsymbol{A}_0)^2 \right\}, \quad (400)$$

where the complex wavefunction for the superconducting condensate ψ_0 is the OP and $\boldsymbol{A}_0$ is the gauge field. The expressions for the β-functions in transverse gauge in two-loop approximation read [244] (where $f = e^2$)

$$\beta_f = -\varepsilon f + \frac{n}{6} f^2 + n f^3, \quad (401)$$

$$\beta_u = -\varepsilon u + \frac{n+8}{6} u^2 - \frac{3n+14}{12} u^3 - 6uf + 18 f^2 + \frac{2n+10}{3} u^2 f + \frac{71n+174}{12} u f^2 - (7n+90) f^3. \quad (402)$$

The use of the ε-expansion in order to find the static fixed points leads for $n = 2$ to complex fixed-point values. Without ε-expansion, a straightforward solution for u and f of the nonlinear two-loop β-functions also does not lead to a real fixed point. Therefore, summation techniques have to be used [247]. Then four fixed points are found: (i) the Gaussian ($u = 0$, $f = 0$), (ii) the uncharged XY fixed point ($u \neq 0$, $f = 0$), (iii) the charged XY fixed point ($u \neq 0$, $f \neq 0$) and (iv) a tricritical fixed point ($u \neq 0$, $f \neq 0$). For initial values u/f large enough, the charged fixed point is the stable one otherwise one obtains runaway solutions indicating a first-order phase transition. At the stable fixed point, the ζ-function of the gauge field assumes the exact result [245]

$$\zeta_A^\star = \varepsilon \quad (403)$$

following from gauge invariance. For a more detailed discussion of the statics see [249].

The simplest equations of motion for the two non-conserved densities ψ_0 and $\boldsymbol{A}_0$ are two relaxational equations as suggested in [248]:

$$\frac{\partial \psi_0}{\partial t} = -\Gamma_\psi \frac{\delta \mathcal{H}(\{\psi_0, \boldsymbol{A}_0\})}{\delta \psi_0^+} + \theta_\psi, \quad (404)$$

$$\frac{\partial A_{0i}}{\partial t} = -\Gamma_A \frac{\delta \mathcal{H}(\{\psi_0, \boldsymbol{A}_0\})}{\delta A_{0i}^+} + \theta_{A_i}. \quad (405)$$

One may retrieve the second equation from Maxwell's equations which shows that the inverse relaxation rate of the gauge field is related to the bare conductivity of the electric current [248]. Assuming that the dynamical critical behaviour is related to a strong-scaling charged fixed point, where the time scale ratio

$$w = \frac{\Gamma_\phi}{\Gamma_A} \tag{406}$$

has a finite non-zero fixed-point value, the OP relaxation rate and the gauge field relaxation rate scale in the same manner. This leads to the prediction that the electric conductivity diverges at T_c like

$$\sigma(k = 0, \omega \to 0) \sim \xi^{z_\varphi + 2 - d} \tag{407}$$

where the value of the dynamic exponent z_φ depends on the value of $w^\star$ and in the one-loop calculation in [248] has been found as (in the Feynman gauge)

$$z_\varphi = 2 + \varepsilon \left(\frac{3}{2w^\star} - 1 \right). \tag{408}$$

In order to get a reliable value of $w^\star$, one has to go at least in statics beyond the one-loop order [250]. The dynamical critical exponent z_φ strongly depends on the fixed-point value of w. The one-loop result of [248] suggests that $z_\varphi > 4$ which is larger than for the diffusive model B. Various values of z_φ have been reported: (i) from experiments $z_\varphi = 1.5$ in [251], $z_\varphi = 2.3$–3.0 in [252], $z_\varphi \sim 2$ in [253]; (ii) from Monte Carlo simulations $z_\varphi \sim 1.5$ [254, 255] and $z_\varphi \sim 2$ in [256]. A calculation of the conductivity shape function has been performed in [257] for a pure relaxational dynamics (model A) for the OP. However, the experimental value of $z_\varphi = 2.65$ observed in the shape function is not compatible with the model A value.

Quite recently, using scaling arguments it has been argued [258] that $z_\varphi = \frac{3}{2}$ exactly and this has been interpreted in favour of the model F universality class however no equations of motion have been defined. The thermal conductivity at this phase transition is predicted to be smooth and non-singular at the phase transition [259].

20. Short remarks on other topics

20.1. Influence of disorder on critical dynamics

So far only homogeneous systems have been considered in this review. However, the critical behaviour of pure systems might be changed by introducing imperfections into a critical system. The changes depend on the type of disorder. It may be introduced: (i) by dilution (random site [260] or (ii) random bond [261] systems) or (iii) as a random field [262] or (iv) random connectivity [263, 264] or (v) as an anisotropy [265]. The defects may be correlated [266, 267] or not.

Whether a change in critical behaviour can be expected is answered by the Harris criterion [268] for systems with short-range-correlated dilution stating that a new diluted critical behaviour might only appear if the specific heat of the pure system is diverging. The disordered critical behaviour then has a non-diverging specific heat. Since the borderline value n_c between a diverging and non-diverging specific heat at space dimension $d = 3$ lies between OP dimensions $n = 1$ (Ising model) and $n = 2$ (XY model) only the Ising case might belong to a new universality class. In consequence, this result led to the conclusion that for the critical dynamics the coupling of conserved quantities to the OP is in any case of no relevance [269, 270]. The argument was the following: for the critical dynamics of a relaxational model, it has been shown (see section 11.1 and [20, 23]) that the coupling to a conserved density is

relevant if the specific heat diverges. Due to disorder, this is never the case and therefore the coupling is of no relevance. Therefore, most of the papers considered only the relaxational dynamics (model A) of Ising systems [104, 271–273].

However, this argumentation is based on the asymptotic properties of the disordered model. Experimental data and computer simulations made clear that in most cases one observes non-asymptotic critical behaviour, described often by non-universal, e.g., dilution dependent, effective exponents (see, e.g., [260, 274]). In the non-asymptotic region the Harris criterion does not hold and therefore one has to consider in dynamics the coupling to the conserved density and its effects on the critical behaviour. In addition, one is not restricted to the Ising case since already in statics the effective critical behaviour for $n > 1$ is different from the pure case [274]. Indeed in many systems (e.g., with site disorder) effective critical behaviour can explain the experimental situation [261, 275].

Therefore, for several systems the effective dynamical critical behaviour has been studied recently: in model A disorder caused by correlated defects [276], for model C site dilution [277] and random anisotropy [278]. Also computer simulations have been performed using the cluster algorithm [279] and Metropolis algorithm [280–282].

20.2. Critical dynamics near Lifshitz points, dipolar systems

Competing interactions may lead at special points in the thermodynamic space to a dispersion in the Hamiltonian where the usual gradient term is zero and higher order derivations have to be taken into account in a Landau–Ginzburg expansion. In general, this may happen in a subspace only, then one has a Hamiltonian

$$\mathcal{H}_{\mathrm{GLW}} = \int \mathrm{d}^d x \left\{ \frac{1}{2} \mathring{r} \vec{\varphi}_0^+ \vec{\varphi}_0 + \frac{1}{2} \sum_{i=1}^{m} \nabla_i^2 \vec{\varphi}_0^+ \nabla_i^2 \vec{\varphi}_0 + \frac{1}{2} \sum_{i=m+1}^{d} \nabla_i \vec{\varphi}_0^+ \nabla_i \vec{\varphi}_0 + \frac{\mathring{u}}{4!} (\vec{\varphi}_0^+ \vec{\varphi}_0)^2 \right\}. \tag{409}$$

Such a functional describes an m-axial Lifshitz point (for a review see [283], for a field-theoretic two-loop calculation of the statics see [284]). Whereas Lifshitz points are realized mainly in solid-state systems (magnetic or ferroelectric) with small spatial anisotropy $m = 1$, in liquid polymer blends isotropic Lifshitz points might be realized [285–287].

Not much work has been done in dynamics for these systems. The asymptotic critical exponents of Heisenberg magnets have been discussed within mode coupling theory in [288] finding break down of strong scaling due to the critical spatial anisotropy. Model A and/or model B like dynamics have been considered in [289, 290].

There are also other systems with spatial anisotropy like uniaxial dipolar systems [291]. So far Larmor precession terms have not been taken into account. Even more complicated systems exist (e.g., the ferroelectric $Sn_2\ P_2\ S_6$ compound) where spatial anisotropies in the dispersion due to Lifshitz terms as well as uniaxial dipolar interactions are present [292].

21. Conclusion and outlook

Considerable progress has been made in the field of critical dynamics since the middle of the 1970s. The comparison with experiment and computer simulations has reached a high quantitative level. Non-asymptotic aspects became of interest and extended the possibility to test RG theory in more details. Calculations to higher loop order became possible and indispensable in order to cope the experimentally reached accuracy.

Problems with the ε-expansion due to logarithmic terms in the fixed-point equations can be avoided by directly solving the specific equations for fixed points or stability exponents.

In this way, the dynamic time scale ratio can be treated in a proper way and non-analyticities can be handled. This lead to solutions of longstanding problems in model C and model SSS.

In comparison with experiment amplitude ratios and shape functions play a fundamental role. Less results are known for crossover functions between different critical points and calculations in the ordered phase are rare (also due to the increased complexity). More results are expected for the critical dynamics under non-equilibrium conditions, in reduced geometry and for finite-size systems [293]. Further work might be expected for other systems such as polymers and their solutions or liquid crystals.

Promising new developments may be expected from the application of the nonperturbative RG approach (for the application in static critical phenomena see the review [294]) theory to dynamics. In several systems the crossover between two critical points may be described by field theoretical models with different upper critical dimensions making it difficult to find a consistent renormalization for both models.

Computer simulations use algorithms which are different from the Metropolis algorithm and define new dynamic critical exponents [295–297]. Its a challenge for dynamic RG theory to calculate these exponents within appropriate formulated dynamic models.

Acknowledgments

This work was supported by the Fonds zur Förderung der wissenschaftlichen Forschung under project nos 15247TPH and P18592-N08. RF would like to thank V Dohm, H Iro, Yu Holovatch, F Schwabl and W Selke for collaboration in the field of critical dynamics and field theory. He also thanks M A Anisimov, J van Senger and H Meyer for their continuous interest in our results. We also like to thank A Gambassi and N Antonov for suggesting useful references and the referee for constructive comments.

Appendix A. Field-theoretic functions in two-loop order for different models

In this appendix, a summary is given over two-loop expressions of the dynamic ζ-functions in the different established models. In order to make the results comparable only expressions are presented, which are calculated with the same renormalization group approach, namely, minimal subtraction scheme. Quite recently, the large-order asymptotics for dynamical systems has been considered and the effect of the instantons discussed. The result demonstrates that the series expansions for the dynamic models related to the static GLW model are asymptotic with zero radius of convergence [298–300]. The instantons lead to a factorial growth of the Nth-order contribution to the expansion.

A.1. Models without a secondary density

Model A/A⋆. Within model A⋆ (complex Γ), the only dynamic ζ-function is

$$\zeta_\Gamma^{(A^\star)}(u,\Gamma) = \frac{n+2}{36}u^2\left(L_A - \frac{1}{2}\right), \tag{A.1}$$

where

$$L_A = L_0 + x_1 L_1 \tag{A.2}$$

has been introduced. In the complex case, the quantities in (A.2) are

$$L_0 = 2\ln\frac{2}{1+\frac{\Gamma^+}{\Gamma}}, \qquad L_1 = \ln\frac{\left(1+\frac{\Gamma^+}{\Gamma}\right)^2}{1+2\frac{\Gamma^+}{\Gamma}} \tag{A.3}$$

and

$$x_1 = 2 + \frac{\Gamma}{\Gamma^+}. \tag{A.4}$$

In model A, Γ is real ($\Gamma = \Gamma^+$) and L_A reduces to

$$L_A = 3 \ln \tfrac{4}{3}. \tag{A.5}$$

The dynamic ζ-function becomes independent of Γ and can be written as [97]

$$\zeta_\Gamma^{(A)}(u) = \frac{n+2}{36} u^2 \left(3 \ln \frac{4}{3} - \frac{1}{2} \right). \tag{A.6}$$

A.2. Models with one secondary density

In this appendix, models including either one scalar density, as described by the static functional (40), or one vector or vector component, as described by the static functional (41), are considered.

*Model C/C**. In the case of a complex OP kinetic coefficient Γ (model C*), a complex time scale ratio

$$w = \frac{\Gamma}{\lambda} \tag{A.7}$$

is introduced. The dynamic ζ-function for the OP kinetic coefficient is [23, 80]

$$\zeta_\Gamma(u, \gamma, \Gamma, w) = \zeta_\Gamma^{(A^\star)}(u, \Gamma) + \frac{w\gamma^2}{1+w} \left[1 - \frac{n+2}{6} u (1 - L_A) + \frac{1}{2} \frac{w\gamma^2}{1+w} \left(\frac{n+2}{2} L_A - \frac{n}{2} + \mathcal{Y}(w) \right) \right] \tag{A.8}$$

where we have defined the complex function

$$\mathcal{Y}(w) = \frac{1}{1+w} \left[w + (1+2w) \ln \frac{(1+w)^2}{1+2w} \right]. \tag{A.9}$$

$\zeta_\Gamma^{(A^\star)}(u, \Gamma)$ has been introduced in (A.1) and L_A is defined in (A.2)–(A.4). In (A.8), relations (50) have been used in order to introduce the GLW parameters r and u instead of τ and $\tilde{u}$. In the case of a real Γ (model C) also w is real and one simply has to insert $L_A = 3 \ln(4/3)$ and to replace $\zeta_\Gamma^{(A^\star)}(u, \Gamma)$ with $\zeta_\Gamma^{(A)}(u)$.

The ζ-function for the kinetic coefficient of the secondary density

$$\zeta_\lambda = 2\zeta_m = \frac{n}{2} \gamma^2 \tag{A.10}$$

is determined by statics because the model includes no mode couplings. All dynamic contributions to this function are proportional to mode couplings.

*Model E/E**. Introducing a complex time scale ratio w as defined in (A.7) and mode coupling parameters

$$F = \frac{g}{\lambda} \qquad \text{and} \qquad f = \frac{F}{\sqrt{w'}} = \frac{g}{\sqrt{\Gamma' \lambda}}, \tag{A.11}$$

the dynamic ζ-function of the OP for a complex Γ (model E*) reads

$$\zeta_\Gamma(u, w, F) = -\frac{F^2}{w(1+w)} \left\{ 1 + \frac{2}{3} u (L_0 + x_- x_1 L_1) - \frac{F^2}{w} \mathcal{M}_E(\Gamma, w) \right\} + \zeta_\Gamma^{(A^\star)}(u, \Gamma) \tag{A.12}$$

with

$$\mathcal{M}_E(\Gamma, w) = \frac{1}{2(1+w)}[2(L_0 + x_- L_1) + L_R + \mathcal{Y}(w)], \tag{A.13}$$

where $\mathcal{Y}(w)$ has been introduced in (A.9), and

$$L_R = \left[x_+ + \frac{\Gamma}{\Gamma^+} + x_+^2\left(x_+^2 + 2\left(\frac{\Gamma}{\Gamma^+}\right)^2\right)\right]\frac{L_1}{x_+} - 3\frac{\Gamma}{\Gamma^+}. \tag{A.14}$$

The parameters L_0, L_1 and x_1 are defined in (A.3) and (A.4), while

$$x_\pm = 1 \pm \frac{\Gamma}{\Gamma^+}, \tag{A.15}$$

$\zeta_\Gamma^{(A^\star)}$ is given in (A.1) for general n. In (A.12) it is taken at $n = 2$.

The dynamic ζ-function corresponding to the kinetic coefficient λ of the secondary density reads

$$\zeta_\lambda(w, f) = -\frac{f^2}{2}(1 + f^2 N_E(w)) \tag{A.16}$$

where $N_E(w)$ is the real function

$$N_E(w) = \frac{\mathcal{N}(w) + \mathcal{N}^+(w)}{2} \tag{A.17}$$

with

$$\mathcal{N}(w) = \frac{1}{2(1+w)}\left[\frac{1}{2} + w(1 - W^{(m)}L^{(m)}) - \ln\frac{1+w}{1+w^+}\right]. \tag{A.18}$$

In the above expression, the quantities

$$W^{(m)} = w + w^+ + ww^+, \qquad L^{(m)} = \ln\left(1 + \frac{1}{W^{(m)}}\right) \tag{A.19}$$

have been defined.

In the case of a real kinetic coefficient Γ ($w'' = 0$ and $w' = w$), (A.12) and (A.16) simplify to [4, 100]

$$\zeta_\Gamma(u, w, f) = -\frac{f^2}{1+w}(1 - f^2 M_E(w)) + \zeta_\Gamma^{(A)}(u) \tag{A.20}$$

$$\zeta_\lambda(w, f) = -\frac{f^2}{2}(1 + f^2 N_E(w)) \tag{A.21}$$

which are the ζ-functions of model E. $\zeta_\Gamma^{(A)}(u)$ can be taken from (A.6) at $n = 2$. The functions (A.13) and (A.17) reduce to

$$M_E(w) = \frac{1}{2(1+w)}\left[\frac{27}{2}\ln\frac{4}{3} - 3 + Y(w)\right] \tag{A.22}$$

where $Y(w)$ has the same form as $\mathcal{Y}(w)$ in (A.9) but is now a real function because w is real, and $\mathcal{N}(w)$ reduces to

$$N_E(w) = \frac{1}{2(1+w)}\left[\frac{1}{2} + w - w^2(2+w)\ln\frac{(1+w)^2}{w(2+w)}\right]. \tag{A.23}$$

Model F. The dynamic model for ^{4}He at the λ-transition always has a complex Γ because it includes a static coupling γ as well as a mode coupling g, which is in contrast to all other models (except model F′ of course) considered in this review where only either γ or g exists.

When both couplings are present, perturbational terms proportional to $\mathrm{i}g\gamma$ contribute to Γ'' and it would be inconsistent to consider a real Γ only. With the time scale ratio w from (A.7) and mode couplings defined in (A.11), the ζ-function of the OP kinetic coefficient Γ reads

$$\zeta_\Gamma(u,\gamma,\Gamma,w,F) = \frac{D^2}{w(1+w)} - \frac{2}{3}\frac{uD}{w(1+w)}\mathcal{A}(\gamma,\Gamma,w,F) - \frac{1}{2}\frac{D^2}{w^2(1+w)^2}\mathcal{B}(\gamma,\Gamma,w,F) + \zeta_\Gamma^{(A^\star)}(u,\Gamma) \tag{A.24}$$

where a coupling $D = w\gamma - \mathrm{i}F$ has been introduced. The model A* function $\zeta_\Gamma^{(A^\star)}$ has already been presented in (A.1) and here has to be taken at $n = 2$. The complex functions $\mathcal{A}$ and $\mathcal{B}$ are defined as

$$\mathcal{A}(\gamma,\Gamma,w,F) = w\gamma(1 - x_1L_1) + \mathrm{i}Fx_-x_1L_1 - DL_0, \tag{A.25}$$

$$\mathcal{B}(\gamma,\Gamma,w,F) = w^2\gamma^2(1-2x_1L_1) - (\mathrm{i}F)^2(2x_-L_1 + L_R) + 2w\gamma\mathrm{i}F(1+2x_-x_1L_1) - D^2[2L_0 + \mathcal{Y}(w)]. \tag{A.26}$$

The logarithmic terms L_0, L_1 and L_R have been defined in (A.3) and (A.14), while the parameters x_1 and $x_\pm$ are given in (A.4) and (A.15). $\mathcal{Y}(w)$ has been defined in (A.9).

The dynamic ζ-function of the kinetic coefficient of the secondary density reads

$$\zeta_\lambda(\gamma,w,F) = \gamma^2 - \frac{f^2}{2}(1 + Q(\gamma,w,F)). \tag{A.27}$$

The function $Q(\gamma,w,F)$ contains all higher loop orders starting with two-loop order. It is a real function and can be written as

$$Q(\gamma,w,F) = \tfrac{1}{2}\,\mathrm{Re}[\mathcal{X}_2(\gamma,w,F)]. \tag{A.28}$$

The complex function $\mathcal{X}_2(\gamma,w,F)$ reads

$$\mathcal{X}_2(\gamma,w,F) = \frac{D}{w'(1+w)}\left[D\left(\frac{1}{2} + \ln\frac{1+w}{1+w^+}\right) + D^+(1+w) - (W^{(m)}\gamma + w\mathrm{i}F)W^{(m)}L^{(m)}\right] \tag{A.29}$$

where we have introduced the definitions for $W^{(m)}$ and $L^{(m)}$ in (A.19).

SSS model. The two-loop expressions for the dynamic ζ-functions are given in [25] and are in agreement with the results presented in [4] (correcting one misprint in (4.10)). This also corrects expressions which have been presented in [99].

We can write

$$\zeta_\Gamma = -\frac{f^2(n-1)}{1+w}(1 - f^2M_{\mathrm{SSS}}(w)) + \zeta_\Gamma^{(A)}(u) \tag{A.30}$$

$$\zeta_\lambda = -\frac{f^2}{2}(1 + f^2N_{\mathrm{SSS}}(w)) \tag{A.31}$$

with functions

$$M_{\mathrm{SSS}}(w) = \frac{1}{2(1+w)^2}\left[\frac{1}{2}(1+w)(27\ln\frac{4}{3} - 6) + (n-1)w + 2(2-n)w(1+w)\ln 2 + (1+nw)\ln(1+w) + (1+(2-n)w)(1+2w)\ln\frac{1+w}{1+2w}\right] \tag{A.32}$$

and

$$N(w)_{\mathrm{SSS}} = \frac{1}{2(1+w)}\left[\frac{1}{2}(3-n) + w - (2-n+w)w(2+w)\ln\frac{(1+w)^2}{(2+w)w}\right]. \tag{A.33}$$

Model DP. The results for this model have been presented in [4]. In our notation, we can write

$$\zeta_\Gamma = -\frac{f^2}{1+w}(1 - f^2 M_{\rm DP}(w)) + \zeta_\Gamma^{(A)}(u), \tag{A.34}$$

$$\zeta_\lambda = -\frac{f^2 n}{4}(1 + f^2 N_{\rm DP}(w)) \tag{A.35}$$

with functions

$$M_{\rm DP}(w) = \frac{1}{8(1+w)^2}\left[9(4+n)(1+w)\ln\frac{4}{3} - (4+2n)w + 2(2-n)w(1+w)\ln 2 \right.$$
$$\left. + (1+nw)\ln(1+w) - (8+2n) + 4(1+2w)\ln\frac{(1+w)^2}{1+2w}\right] \tag{A.36}$$

and

$$N_{\rm DP}(w) = \frac{1}{2(1+w)}\left[\frac{1}{2} + w - (2+w)w^2\ln\frac{(1+w)^2}{(2+w)w}\right]. \tag{A.37}$$

Model H. The ζ-functions in the minimal subtraction scheme have been given in [34] in one-loop order. Subsequently, a two-loop calculation of these functions has been presented in [172] (see equation (46) therein). The ζ-functions read

$$\zeta_\Gamma = -\frac{3f^2}{4} + \frac{Bf^4}{32} + \zeta_\phi(u), \tag{A.38}$$

$$\zeta_{\lambda_t} = -\frac{f^2}{24}\left(1 + \frac{5f^4}{16}\right) \tag{A.39}$$

with $B = -0.0623$. The two-loop expression for $\zeta_\phi(u)$ is presented in (179) and has to be taken for $n = 1$.

A.3. Models with two secondary densities

When more than one secondary density is present in a dynamic model, the kinetic coefficients of them build a matrix $\mathbf{\Lambda}$ (see (325) for instance). For two secondary densities, this matrix is

$$\mathbf{\Lambda} = \begin{pmatrix} \lambda & L \\ L & \mu \end{pmatrix}. \tag{A.40}$$

In models with two secondary densities of different tensor character $L = 0$. Because the dynamic perturbation expansion gets extremely extensive when a nondiagonal kinetic coefficient L is present, it is absolutely necessary to diagonalize the matrix (A.40). The eigenvalues of this matrix are

$$\lambda_1 = \tfrac{1}{2}(\lambda + \mu + K), \qquad \lambda_2 = \tfrac{1}{2}(\lambda + \mu - K) \tag{A.41}$$

with

$$K = \sqrt{(\lambda-\mu)^2 + 4L^2}. \tag{A.42}$$

The diagonal dynamic coefficient matrix is then obtained by

$$\bar{\mathbf{\Lambda}} \equiv \begin{pmatrix} \lambda_1 & 0 \\ 0 & \lambda_2 \end{pmatrix} = \boldsymbol{R}^T \cdot \mathbf{\Lambda} \cdot \boldsymbol{R}. \tag{A.43}$$

The superscript T denotes the transposed matrix. The transformation matrix $\boldsymbol{R}$ is obtained from the eigenvectors corresponding to (A.41). It is an orthogonal matrix ($\boldsymbol{R}^{-1} = \boldsymbol{R}^{T}$) and has the structure

$$\boldsymbol{R} = \begin{pmatrix} R_{11} & -R_{21} \\ R_{21} & R_{11} \end{pmatrix} \tag{A.44}$$

with

$$R_{11} = \sqrt{\frac{\lambda - \mu + K}{2K}}, \qquad R_{21} = \sqrt{\frac{\mu - \lambda + K}{2K}}. \tag{A.45}$$

Dynamic models with two scalar secondary densities are transformed to models with a diagonal matrix (A.43) for the corresponding kinetic coefficients. Thus, all static and dynamic parameters have to be transformed too. The results for the dynamic ζ-functions are then explicitly presented in the parameters of the dynamic diagonal model. Analogous to the dynamic parameters (203)–(205) the parameters for dynamic diagonal model

$$\bar{w}_1 = \frac{\Gamma}{\lambda_1}, \qquad \bar{w}_2 = \frac{\Gamma}{\lambda_2} \tag{A.46}$$

$$\bar{F}_1 = \frac{\bar{g}_1}{\lambda_1}, \qquad \bar{F}_2 = \frac{\bar{g}_2}{\lambda_2} \tag{A.47}$$

are introduced. The relation between the two sets of parameters is determined by the transformation matrix (A.45). Using the definition (203) of the time scale ratios, the coefficients of the transformation matrix (A.45) can be rewritten as

$$R_{11} = \sqrt{\frac{w_2 - w_1 + K_w}{2K_w}}, \qquad R_{21} = \sqrt{\frac{w_1 - w_2 + K_w}{2K_w}} \tag{A.48}$$

with

$$K_w = \sqrt{(w_2 - w_1)^2 + 4w_1 w_2 w_3^2}. \tag{A.49}$$

Inserting the eigenvalues (A.41) into (A.46) and using the definition of the time scale ratios (203), one obtains

$$\bar{w}_1 = \frac{2w_1 w_2}{w_1 + w_2 + K_w}, \qquad \bar{w}_2 = \frac{2w_1 w_2}{w_1 + w_2 - K_w}. \tag{A.50}$$

Applying the same procedure to the mode coupling parameters (A.47), the relations between the mode coupling parameters in the diagonal and nondiagonal model read

$$\bar{F}_1 = \frac{2(w_2 R_{11} F_1 + w_1 R_{21} F_2)}{w_1 + w_2 + K_w}, \qquad \bar{F}_2 = \frac{2(-w_2 R_{21} F_1 + w_1 R_{11} F_2)}{w_1 + w_2 - K_w}. \tag{A.51}$$

The dynamic diagonalization procedure described above generates a second static coupling γ, thus in the dynamic diagonal model two couplings $\bar{\gamma}_1$ and $\bar{\gamma}_2$ exist. Both static couplings are related to the single coupling γ in the original model by the relations

$$\bar{\gamma}_1 = R_{21}\gamma, \qquad \bar{\gamma}_2 = R_{11}\gamma. \tag{A.52}$$

Model C′/C′⋆. The ζ-function of the OP kinetic coefficient reads [71]

$$\zeta_\Gamma(u, \{\bar{\gamma}\}, \Gamma, \{\bar{w}\}) = \zeta_\Gamma^{(A^\star)}(u, \Gamma) + \sum_i \frac{\bar{w}_i \bar{\gamma}_i^2}{1 + \bar{w}_i} \left\{ 1 - \frac{n+2}{6} u(1 - L_A) \right.$$
$$\left. + \frac{1}{2} \sum_j \frac{\bar{w}_j \bar{\gamma}_j^2}{1 + \bar{w}_j} \left[\frac{n+2}{2} L_A - \frac{n}{2} + \mathcal{Y}_{ij}(\{\bar{w}\}) \right] \right\} \tag{A.53}$$

where the brackets $\{\cdot\}$ denote the set of parameters embraced. In (A.53), we have introduced the complex function

$$\mathcal{Y}_{ij}(\{\bar{w}\}) = \frac{1}{1+\bar{w}_i}\left(\bar{w}_i + \bar{w}_j^2 l_{ij}^{(a)} - \bar{w}_i^2 l_{ji}^{(a)} + (1+\bar{w}_i-\bar{w}_j)(1+\bar{w}_i+\bar{w}_j) l_{ij}^{(s)}\right). \tag{A.54}$$

Note that the above expression is valid not only for two secondary densities but also for an arbitrary number. The indices run in this case over all secondary densities. $\zeta_\Gamma^{(A^\star)}(u,\Gamma)$ has been introduced in (A.1). The logarithmic terms are defined as

$$l_{ij}^{(s)} = \ln\frac{(1+\bar{w}_i)(1+\bar{w}_j)}{1+\bar{w}_i+\bar{w}_j}, \qquad l_{ij}^{(a)} = \ln\frac{1+\bar{w}_i}{1+\frac{\bar{w}_i}{\bar{w}_j}}. \tag{A.55}$$

Setting $i=j$ and removing the summation leads to the corresponding expression (A.8) for model C/C*. L_A has been defined in (A.2) for complex Γ and reduces to $L_A = 3\ln(4/3)$ for real Γ.

According to (A.9), the dynamic ζ-functions for the secondary densities are

$$\zeta_\lambda = 0, \qquad \zeta_L = \zeta_m = \frac{n}{4}\gamma^2, \qquad \zeta_\mu = 2\zeta_m = \frac{n}{2}\gamma^2. \tag{A.56}$$

Model $E'/E'^\star$. For complex Γ (model E$'^\star$), the ζ-function of the OP kinetic coefficient reads

$$\zeta_\Gamma(u,\Gamma,\{\bar{w}\},\{\bar{F}\}) = -\sum_i \frac{\bar{F}_i^2}{\bar{w}_i(1+\bar{w}_i)}\left\{1+\frac{2}{3}u(L_0+x_-x_1L_1) - \sum_j \frac{\bar{F}_j^2}{\bar{w}_j}\mathcal{M}_{ij}(\Gamma,\{\bar{w}\})\right\} + \zeta_\Gamma^{(A^\star)}(u,\Gamma) \tag{A.57}$$

with

$$\mathcal{M}_{ij}(\Gamma,\{\bar{w}\}) = \frac{1}{2(1+\bar{w}_j)}[2(L_0+x_-L_1)+L_R+\mathcal{Y}_{ij}(\{\bar{w}\})]. \tag{A.58}$$

The complex function $\mathcal{Y}_{ij}(\{\bar{w}\})$ is defined in (A.54). The parameters x_i and L_i have been introduced in (A.3), (A.14), (A.4) and (A.15). $\zeta_\Gamma^{(A^\star)}$ is (A.1) taken at $n=2$.

From the structure of the loop expansion follows that the ζ-functions for the KCs of the secondary densities are

$$\zeta_\lambda = -\frac{f_1^2}{2}(1+Q(u,\{\bar{w}\},\{\bar{f}\})), \tag{A.59}$$

$$\zeta_\mu = -\frac{f_2^2}{2}(1+Q(u,\{\bar{w}\},\{\bar{f}\})), \tag{A.60}$$

$$\zeta_L = -\frac{f_1 f_2}{2w_3}(1+Q(u,\{\bar{w}\},\{\bar{f}\})). \tag{A.61}$$

The function Q contains all higher order contributions of loop expansion beginning with two loop. Note that the parameters w_i, f_i outside the brackets are defined in the dynamically nondiagonal model (see (203)–(205)), while Q is considered as a function of the parameters $\bar{w}_i$ and $\bar{f}_i$ in the dynamically diagonal model (see (A.46) and (A.46)). In order to obtain Q as a function of w_i, f_i, one has to insert the transformation rules (A.50) and (A.51). In two-loop order, the function Q reads

$$Q(u,\{\bar{w}\},\{\bar{f}\}) = \sum_j \bar{f}_j^2 N_E(\bar{w}_j). \tag{A.62}$$

The function $N_E(w)$ is given in (A.17) and (A.18).

In the case of a real kinetic coefficient Γ (model E′), the ζ-function (A.57) reduces to [17]

$$\zeta_\Gamma(u,\{\bar w\},\{\bar f\}) = -\sum_i \frac{\bar f_i^2}{1+\bar w_i}\left\{1-\sum_j \bar f_j^2 M_{ij}(\{\bar w\})\right\} + \zeta_\Gamma^{(A)}(u) \tag{A.63}$$

where $\bar w = \bar w'$ is now a real quantity. Inserting $w'' = 0$, $w' = w$ into (A.58), one obtains immediately

$$M_{ij}(\{\bar w\}) = \frac{1}{2(1+\bar w_j)}\left[\frac{27}{2}\ln\frac{4}{3} - 3 + Y_{ij}(\{\bar w\})\right] \tag{A.64}$$

where $Y_{ij}(\{\bar w\})$ is identical to (A.54) but with real $\bar w$. The ζ-functions ζ_λ, ζ_L and ζ_μ are in this case also given by (A.59)–(A.62) but with the function $N_E(w)$ from (A.23).

Model F′. The ζ-function of the OP kinetic coefficient reads [72, 139, 157]

$$\begin{aligned}\zeta_\Gamma(u,\bar\gamma,\{\bar w\},\{\bar F\}) = {}& \sum_i \frac{\bar D_i^2}{\bar w_i(1+\bar w_i)} - \frac{2}{3}\sum_i \frac{u\bar D_i}{\bar w_i(1+\bar w_i)}\mathcal{A}_i(\gamma,\Gamma,\{\bar w\},\{\bar F\}) \\ & - \frac{1}{2}\sum_{i,j}\frac{\bar D_i\bar D_j}{\bar w_i(1+\bar w_i)\bar w_j(1+\bar w_j)}\mathcal{B}_{ij}(\gamma,\Gamma,\{\bar w\},\{\bar F\}) + \zeta_\Gamma^{(A^\star)}(u,\Gamma)\end{aligned} \tag{A.65}$$

where we have introduced the coupling

$$\bar D_i = \bar w_i\bar\gamma_i - \mathrm{i}\bar F_i. \tag{A.66}$$

$\zeta_\Gamma^{(A^\star)}(u,\Gamma)$ can again be taken from (A.1) at $n=2$. The functions $\mathcal{A}_i$ and $\mathcal{B}_{ij}$ are defined as

$$\mathcal{A}_i(\gamma,\Gamma,\{\bar w\},\{\bar F\}) = \bar w_i\bar\gamma_i(1-x_1L_1) + \mathrm{i}\bar F_i x_- x_1 L_1 - \bar D_i L_0 \tag{A.67}$$

$$\begin{aligned}\mathcal{B}_{ij}(\gamma,\Gamma,\{\bar w\},\{\bar F\}) = {}& \bar w_i\bar\gamma_i\bar w_j\bar\gamma_j(1-2x_1L_1) - \mathrm{i}\bar F_i\mathrm{i}\bar F_j(2x_-L_1+L_R) \\ & + (\bar w_i\bar\gamma_i\mathrm{i}\bar F_j + \bar w_j\bar\gamma_j\mathrm{i}\bar F_i)(1+2x_-x_1L_1) - \bar D_i\bar D_j[2L_0+\mathcal{Y}_{ij}(\{\bar w\})]\end{aligned} \tag{A.68}$$

with the complex function $\mathcal{Y}_{ij}(\{\bar w\})$ from (A.54). All parameters L_i and x_i have already been defined in the previous subsections.

The structure of the loop expansion implies that the ζ-functions for the KCs of the secondary densities are of the form

$$\zeta_\lambda = -\frac{f_1^2}{2}(1+Q(u,\{\bar\gamma\},\{\bar w\},\{\bar f\})), \tag{A.69}$$

$$\zeta_\mu = \gamma^2 B_{\psi^2}(u) - \frac{f_2^2}{2}(1+Q(u,\{\bar\gamma\},\{\bar w\},\{\bar f\})), \tag{A.70}$$

$$\zeta_L = \frac{1}{2}\gamma^2 B_{\psi^2}(u) - \frac{f_1 f_2}{2w_3}(1+Q(u,\{\bar\gamma\},\{\bar w\},\{\bar f\})). \tag{A.71}$$

The above ζ-functions are valid in all orders of loop expansion. Quite analogous to model E′⋆ (see the previous item), the function Q contains all higher order dynamic contributions of loop expansion beginning with two loop. The function $B_{\psi^2}(u)$ is determined by the renormalization of the specific heat within the GLW model. In two-loop order at $n=2$ we have $B_{\psi^2}(u)=1$. The parameters w_i, f_i outside the brackets are defined in the dynamically nondiagonal model (see (203)–(205)), while Q is considered as a function of the parameters $\bar w_i$, $\bar f_i$ in the dynamically diagonal model (see (A.46) and (A.46)). In order to obtain Q as

a function of w_i and f_i one has to insert the transformation rules (A.50) and (A.51). The function Q has the structure

$$Q = \tfrac{1}{2}\,\mathrm{Re}[\mathcal{X}_2] \tag{A.72}$$

from which immediately follows that it is a real quantity. $\mathcal{X}_2$ reads

$$\mathcal{X}_2 = \sum_k \frac{\bar{D}_k}{\bar{w}_k'(1+\bar{w}_k)}\left[\bar{D}_k\left(\frac{1}{2}+\ln\frac{1+\bar{w}_k}{1+\bar{w}_k^+}\right)+\bar{D}_k^+(1+\bar{w}_k)-\left(W_k^{(m)}\bar{\gamma}_k+\bar{w}_k\mathrm{i}\bar{F}_k\right)W_k^{(m)}L_k^{(m)}\right]. \tag{A.73}$$

According to (A.19), we have introduced the definitions

$$W_k^{(m)} = \bar{w}_k + \bar{w}_k^+ + \bar{w}_k\bar{w}_k^+, \qquad L_k^{(m)} = \ln\left(1+\frac{1}{W_k^{(m)}}\right). \tag{A.74}$$

The functions ζ_Γ and Q are invariant under transformation (A.44). Therefore, they are functions of the parameters w_i and F_i of the dynamically nondiagonal model by inserting the transformation relations (A.50)–(A.52) for the time scale ratios and couplings. This would lead to very extensive expressions, thus it is more useful to present them as functions of $\bar{w}_i$ and $\bar{F}_i$ in the following.

Model H′. So far the field-theoretic functions for model H′ have only been calculated in one-loop order [16]. The ζ-functions which are also present in model H (compare (A.38) and (A.39)) read

$$\zeta_\Gamma = -\frac{3}{4}f^2, \qquad \zeta_{\lambda_t} = -\frac{1}{24}\frac{f^2}{1-w_3^2} \tag{A.75}$$

with $w_3^2 = L^2/(\Gamma\mu)$ and $f^2 = g^2/(\Gamma\lambda_t)$. The additional ζ-functions appearing in model H′ are related to static ζ-functions. They can be written as

$$\zeta_L = \tfrac{1}{2}\zeta_\phi + \zeta_m, \qquad \zeta_\mu = 2\zeta_m. \tag{A.76}$$

In one-loop order, we have $\zeta_\phi = 0$ and $\zeta_m = (n/4)\gamma^2$. Although the model contains two secondary densities, the ζ-functions simplify considerably because $w_1 = 0$ and $w_2 = 0$ and only one mode coupling f is present.

Appendix B. Notations

Table B1. Notations and their meaning.

Notation	Quantity I_a
a_i	General set of densities
A_d	Geometric factor (99)
β_{index}	β-function (175); its zeros give fixed points
f	Mode coupling parameter; $f = g/(\Gamma\lambda)^{1/2}$
F	Mode coupling parameter; g/λ
$\mathcal{F}_{\mathrm{index}}$	Shape function
g	Coefficient in the Poisson bracket relation
Γ	Relaxation rate of a non-conserved OP
$\Gamma^{(s)}_{a_i a_j}$	Genuine static vertex function
$\Gamma^{(d)}_{a_i \tilde{a}_j}$	Genuine dynamic vertex function

Table B1. (Continued.)

Notation	Quantity I_a
γ	Static coupling in asymmetric models (models C, F, F′)
GLW	Ginzburg–Landau–Wilson
$\mathcal{H}_{\text{index}}$	Static functional for specific densities
k	Wave vector
κ	Wave number scale
κ_T	Thermal conductivity (at zero mass current in mixtures)
KC	Kinetic coefficient
L	Kinetic coefficient; cross term
λ	Kinetic coefficient of a conserved density
ℓ	Flow parameter
μ	kinetic coefficient, mass transport
m, $\mathbf{m}$	Conserved secondary densities
n	Number of components
OP	Order parameter
$\vec{\phi}$	n-component real OP
$\vec{\varphi}$	$n/2$-component complex OP
ψ	Scalar complex OP
r	Mass coefficient in the GLW static functional
$R^{\text{index}}_{\text{index}}$	Experimental, universal and/or effective amplitude
RC	Renormalization constant
RG	Renormalization group
SVP	Saturated vapour pressure
τ	Mass coefficient in the extended static functional (50)
Θ_{index}	Noise
t	Reduced temperature $((T - T_c)/T_c)$ or time
u	Static fourth-order coupling
w	Time ratio; in most cases $w = \Gamma/\lambda$
ω	Frequency
ω_c	Characteristic frequency
Ω_d	Surface of d-dimensional unit sphere
ξ	Correlation length (37)
x	$k\xi$
y	ω/ω_c
Z_{index}	Renormalization
z_{index}	Dynamic critical exponent
ζ_{index}	ζ-function (162); its fixed-point value gives exponents

References

[1] Hohenberg P C and Halperin B I 1977 *Rev. Mod. Phys.* **49** 435
[2] Martin P C, Siggia E D and Rose H A 1973 *Phys. Rev.* A **8** 423
[3] Bausch R, Janssen H-K and Wagner H 1976 *Z. Phys.* B **24** 113
[4] De Dominicis C and Peliti L 1978 *Phys. Rev.* B **18** 353
[5] Janssen H K 1979 *Lecture Notes in Physics* vol 104, ed C P Enz p 25
[6] Ahlers G 1971 *Proc. 12th Int. Conf. on Low Temperature Physics* ed E Kanda (Tokio: Keigaku)
[7] Tam W Y and Ahlers G 1985 *Phys. Rev.* B **32** 5932
[8] Lipa J A, Nissen J A, Stricker D A, Swanson D R and Chui T C P 2003 *Phys. Rev.* B **68** 174518
[9] Dohm V and Ferrell R A 1978 *Phys. Lett.* A **67** 387
[10] Folk R and Dohm V 1981 *Phys. Rev. Lett.* **46** 349
[11] Dohm V and Folk R 1980 *Z. Phys.* B **40** 79
[12] Dohm V and Folk R 1981 *Z. Phys.* B **41** 251
[13] Sakonidou E P, van den Berg H R, ten Seldam C A and Sengers J V 1997 *Phys. Rev.* E **56** R4943

Sakonidou E P, van den Berg H R, ten Seldam C A and Sengers J V 1998 *J. Chem. Phys.* **109** 717
[14] Cohen L H, Dingus M L and Meyer H 1983 *Phys. Rev. Lett.* **50** 1058
Cohen L H, Dingus M L and Meyer H 1985 *J. Low Temp. Phys.* **61** 79
[15] Folk R and Moser G 1993 *Europhys. Lett.* **24** 533
[16] Folk R and Moser G 1998 *Phys. Rev.* E **58** 6246
[17] Dohm V and Folk R 1983 *Phys. Rev.* B **28** 1332
[18] Ahlers G 1980 *Rev. Mod. Phys.* **52** 489
[19] Privman V, Hohenberg P C and Aharony A 1991 *Phase Transitions and Critical Phenomena* ed C Domb and J L Lebowitz (London: Academic)
[20] Halperin B I, Hohenberg P C and Ma S-k 1974 *Phys. Rev.* B **10** 139
[21] Brezin E and De Dominicis C 1975 *Phys. Rev.* B **12** 4954
[22] Dohm V 1991 *Phys. Rev.* B **44** 2697
Dohm V 2006 *Phys. Rev.* B **73** 09990 (erratum)
[23] Folk R and Moser G 2003 *Phys. Rev. Lett.* **91** 030601
[24] Sasvári L, Schwabl F and Szepfalusy P 1975 *Physica* A **81** 108
[25] Dohm V 1978 *Z. Phys.* B **31** 327
[26] Dohm V 1976 *Solid State Commun.* **20** 657
[27] Nolan M J and Mazenko G F 1977 *Phys. Rev.* B **15** 4471
[28] Bhattacharjee J and Ferrell R A 1981 *Phys. Rev.* B **24** 8449
[29] Iro H 1987 *Z. Phys.* B **68** 485
[30] Freedman R and Mazenko F 1976 *Phys. Rev.* B **13** 4967
[31] Janssen H-K 1977 *Z. Phys.* B **26** 187
[32] Tucciarone A, Lau H Y, Corliss L M, Delapalme A and Hastings J M 1971 *Phys. Rev.* B **4** 3206
[33] Coldea R, Cowley R A, Perring T G, McMorrow D F and Roessli B 1998 *Phys. Rev.* B **57** 5281
[34] Folk R and Moser G 1998 *Phys. Rev.* E **57** 683, 705
[35] Pankert J and Dohm V 1989 *Phys. Rev.* B **40** 10842
[36] Dohm V 1983 *Multicritical Phenomena* ed R Pynn and Skjeltorp (New York: Plenum)
[37] Calabrese P and Gambassi A 2005 *J. Phys. A: Math. Gen.* **38** R133
[38] Janssen H K and Täuber U C 2005 *Ann. Phys., NY* **315** 147
[39] Gambassi A and Dietrich S 2005 *Preprint* cond-mat/0509770 (2006 *J. Stat. Phys.* submitted)
[40] Diehl H W, Krech M and Karl H 2002 *Phys. Rev.* B **66** 024408
[41] Frey E and Schwabl F 1994 *Adv. Phys.* **43** 577
[42] Täuber U C 2005 *J. Phys. A: Math. Gen.* **38** R79–131
[43] Antonov H V 2006 *J. Phys. A: Math. Gen.* **39** R1
[44] Vasil'ev A N 2004 *The Field-Theoretic Renormalization Group in Critical Behaviour Theory and Stochastic Dynamics* (London: Chapman and Hall/CRC Press)
[45] Anisimov M A 1991 *Critical Phenomena in Liquids and Liquid Crystals* (London: Gordon and Breach)
[46] Onuki A 2002 *Phase Transition Dynamics* (Cambridge: Cambridge University Press)
[47] Partial textbook on the webpage http://www.phys.vt.edu/tauber/utaeuber.html announced for Cambridge University Press
[48] Cardy J 1996 *Scaling and Renormalization in Statistical Physics* (Cambridge: Cambridge University Press)
[49] Fisher M E 1974 *Rev. Mod. Phys.* **46** 597
[50] Halperin B I, Hohenberg P C and Ma S-k 1972 *Phys. Rev. Lett.* **29** 1548
[51] Bray A J 1994 *Adv. Phys.* **43** 357
[52] Halperin B I, Hohenberg P C and Siggia E D 1976 *Phys. Rev.* B **13** 1299
Halperin B I, Hohenberg P C and Siggia E D 1980 *Phys. Rev.* B **21** 2044 (erratum)
[53] Siggia E D and Nelson D R 1977 *Phys. Rev.* B **15** 1427
[54] Ma S-k and Mazenko G F 1975 *Phys. Rev.* B **11** 4077
[55] Green M S 1952 *J. Chem. Phys.* **20** 1281
[56] Zwanzig R 1960 *J. Chem. Phys.* **33** 1338
[57] Dzyaloshinskii I E and Volovick G E 1980 *Ann. Phys., NY* **125** 67
[58] Akkineni V K and Täuber U 2004 *Phys. Rev.* E **69** 036113
[59] Amit D J 1984 *Field Theory, the Renormalization Group and Critical Phenomena* 2nd edn (Singapore: World Scientific)
[60] Kleinert H and Schulte-Frohlinde V 2001 *Critical Properties of ϕ^4-Theories* (Singapore: World Scientific)
[61] Zinn-Justin J 1996 *Quantum Field Theory and Critical Phenomena* 3rd edn (Oxford: Clarendon)
[62] Brezin E, Le Guillou J C and Zinn-Justin J 1974 *Phys. Rev.* B **19** 892
[63] Symanzik K 1973 *Lett. Nuovo Cimento* **8** 771

[64] Parisi G 1980 *J. Stat. Phys.* **23** 49
[65] Bagnuls C and Bervellier C 1985 *Phys. Rev.* B **32** 6995
[66] Schloms R and Dohm V 1989 *Nucl. Phys.* B **328** 639
[67] Zhong F and Barmatz M 2004 *Phys. Rev.* E **70** 066105
[68] Onuki A 1983 *J. Low Temp. Phys.* **53** 189
[69] Moser G and Folk G 1992 *J. Low Temp. Phys.* **86** 57
[70] Folk R and Moser G 1995 *J. Low Temp. Phys.* **99** 11
[71] Folk R and Moser G 2005 *Phys. Rev.* E **71** 026118
[72] Folk R and Moser G 2002 *Phys. Rev. Lett.* **89** 125301 (and [141])
[73] Kadanoff L P and Martin P C 1963 *Ann. Phys., NY* **24** 419
[74] Moser G 1991 Unpublished
[75] Brezin E, Le Guillou J C and Zinn-Justin J 1976 *Phase Transitions and Critical Phenomena* vol 6, ed C Domb and M S Green (New York: Academic)
[76] Lawrie I D 1976 *J. Phys. A: Math. Gen.* **9** 961
[77] Eisenriegler E and Schaub B 1980 *Z. Phys.* B **39** 65
[78] Dohm V 1985 *Z. Phys.* B **60** 61
[79] Larin S A, Mönnigmann M, Strösser M and Dohm V 1998 *Phys. Rev.* B **58** 3394
[80] Folk R and Moser G 2004 *Phys. Rev.* E **69** 036101
[81] Dohm V 1984 *Phys. Rev. Lett.* **53** 1379
[82] Folk R and Moser G 1987 *Phys. Lett.* A **120** 39
[83] Krause H J, Schloms R and Dohm V 1990 *Z. Phys.* B **79** 287
[84] Halfkann F J and Dohm V 1992 *Z. Phys.* B **89** 79
[85] Strösser M and Dohm V 2003 *Phys. Rev.* E **67** 056115
Strösser M and Dohm V 2004 *Phys. Rev.* E **70** 069902
[86] Hardy G H 1948 *Divergent Series* (Oxford: Oxford University Press)
[87] Brezin E and Parisi G 1978 *J. Stat. Phys.* **19** 269
[88] Zinn-Justin J 1981 *Phase Transitions, Cargese Summer Institute 1980* ed M Levy, J C Le Guillou and J Zinn-Justin (New York: Plenum)
[89] Baker G A Jr, Nickel B G, Green M S and Meiron D L 1976 *Phys. Rev. Lett.* **36** 1351
[90] Le Guillou J C and Zinn-Justin J 1977 *Phys. Rev. Lett.* **39** 95
[91] Baker G A Jr, Nickel B G and Meiron D L 1978 *Phys. Rev.* B **17** 1365
[92] Le Guillou J C and Zinn-Justin J 1985 *J. Phys. Lett. (Paris)* **46** L-137
Le Guillou J C and Zinn-Justin J 1987 *J. Phys. (Paris)* **48** 19
Le Guillou J C and Zinn-Justin J 1989 *J. Phys. (Paris)* **50** 1365
[93] Vladimirov A A, Kazakov D I and Tarasov O V 1979 *Sov. Phys.—JETP* **50** 521
Vladimirov A A, Kazakov D I and Tarasov O V 1979 *Zh. Eksp. Teor. Fiz.* **77** 1035 (Engl. Transl.)
[94] Chetyrkin K G, Gorishny S G, S A and Tkachov F V 1983 *Phys. Lett.* B **132** 351
Gorishny S G, Larin S A and Tkachov F V 1984 *Phys. Lett.* A **101** 120
[95] Schloms R and Dohm V 1990 *Phys. Rev.* B **42** 6142
[96] Halperin B I and Hohenberg P C 1969 *Phys. Rev.* **177** 952
[97] De Dominicis C, Brezin E and Zinn-Justin J 1975 *Phys. Rev.* B **12** 4945
[98] Antonov N V and Vasil'ev A N 1984 *Theor. Math. Phys.* **60** 671
[99] De Dominicis C and Peliti L 1977 *Phys. Rev. Lett.* **38** 505
[100] Dohm V 1979 *Z. Phys.* B **33** 79
[101] Siggia E D, Halperin B I and Hohenberg P C 1976 *Phys. Rev.* B **13** 2110
[102] Janssen H-K 1976 *Z. Phys.* B **23** 377
[103] Pelissetto A and Vicari E 2002 *Phys. Rep.* **368** 549
[104] Prudnikov V V and Vakilov A N 1992 *Sov. Phys.—JETP* **74** 990
[105] Prudnikov V V, Ivanov A V and Fedorenko A A 1997 *JETP Lett.* **66** 835
[106] Bausch R, Dohm V, Janssen H K and Zia R K P 1981 *Phys. Rev. Lett.* **47** 1837
[107] Wansleben S and Landau D P 1991 *Phys. Rev.* B **43** 6006
[108] Grassberger P 1995 *Physica* A **214** 547
Grassberger P 1995 **217** 227 (erratum)
[109] Calabrese P, Matin-Mayor V, Pelissetto A and Vicari E 2003 *Phys. Rev.* E **68** 016110
[110] Ossola G and Sokal A D 2004 *Preprint* hep-latt/0402019
[111] Kalle C 1984 *J. Phys. A: Math. Gen.* **17** L801
[112] Pearson R B, Richardson J L and Touissaint 1985 *Phys. Rev.* B **31** 4472
[113] Ito N, Hukushima K, Ogawa K and Ozeki Y 2000 *J. Phys. Soc. Japan* **69** 1931

[114] Blavats'ka V, Dudka M, Folk R and Holovatch Yu 2005 *Phys. Rev.* B **72** 064417
[115] Grinstein G, Jayaprakash C and He Y 1985 *Phys. Rev. Lett.* **44** 2527
[116] Bassler K E and Schmittmann B 1994 *Phys. Rev. Lett.* **73** 3343
[117] Täuber U C and Schwabl F 1992 *Phys. Rev.* B **46** 3337
[118] Sen P 1999 *J. Phys. A: Math. Gen.* **32** 1623
[119] Sen P and Bhattacharjee S M 2002 *J. Phys. A: Math. Gen.* **35** L141
[120] Halperin B I, Hohenberg P C and Ma S-k 1976 *Phys. Rev.* B **13** 4119
[121] Brezin E and De Dominicis C 1975 *Phys. Rev.* B **12** 4954 (There are calculational errors in the field-theoretic function η_{Γ})
[122] Murata K K 1976 *Phys. Rev.* B **13** 2028
[123] Sen P, Dasgupta S and Stauffer D 1998 *Eur. Phys. J.* B **1** 107
[124] Stauffer D 1998 *Int. J. Mod. Phys.* C **8** 1263
[125] Dohm V and Folk R 1980 *Z. Phys.* B **39** 94
[126] Dohm V and Folk R 1979 *Z. Phys.* B **35** 277
[127] Ahlers G 1976 *The Physics of Liquid and Solid Helium: part I (Monographs and Texts in Physics and Astronomy)* vol XXIX ed K H Bennemann and J B Ketterson (New York: Wiley)
[128] Ahlers G 1979 *Phys. Rev. Lett.* **43** 1417
[129] Crooks M J and Robinson B J 1981 *Physica* B **107** 339
[130] Mehrotra R and Ahlers G 1983 *Phys. Rev. Lett.* **51** 2116
[131] Crooks M J and Robinson B J 1983 *Phys. Rev.* B **27** 5433
[132] Mehrotra R and Ahlers G 1984 *Phys. Rev.* B **30** 5116
[133] Dohm V and Folk R 1981 *Z. Phys.* B **45** 129
[134] Tarvin J A, Vidal F and Greytak 1977 *Phys. Rev.* B **15** 4193
[135] Ferrell R A and Bhattacharjee J K 1979 *Phys. Rev.* B **20** 3690
[136] Halperin B I, Hohenberg P C and Siggia E D 1974 *Phys. Rev. Lett.* **32** 1289
[137] Singsaas A and Ahlers G 1984 *Phys. Rev.* B **29** 4951
[138] Kleinert H 1999 *Phys. Rev.* D **60** 085001
Kleinert H and Yukalov V I 2005 *Phys. Rev.* E **71** 026131
[139] Folk R and Moser G 2004 *Phys. Rev. Lett.* **93** 229902 (erratum) (Note the misprint in the notion: x_0 should read x_-)
[140] Dohm V 1985 *Z. Phys.* B **61** 193
[141] Li Q 1991 *PhD Thesis Stanford University*
Lipa J A and Li Q 1996 *Czech. J. Phys.* **46** 185
[142] Folk R and Moser G 2004 *J. Low Temp. Phys.* **136** 159
[143] Dohm V 2006 *Phys. Rev.* B **73** 092503
[144] Dohm V 1984 *Phys. Rev.* B **29** 1497
[145] Frank D and Dohm V 1989 *Phys. Rev. Lett.* **62** 1864
[146] Frank D and Dohm V 1991 *Z. Phys.* B **84** 443
[147] Dohm V 1993 *Phys. Scr.* T **93** 46
[148] Kuehn K, Mehta S, Fu H, Genio E, Murphy D, Liu F, Liu Y and Ahlers G 2002 *Phys. Rev. Lett.* **88** 095702
[149] Töpler and Dohm V 2003 *Physica* B **329–333** 200
[150] Ahlers G 1999 *J. Low Temp. Phys.* **115** 143
[151] Murphy D, Genio E, Ahlers G, Liu F and Liu Y 2003 *Phys. Rev. Lett.* **90** 025301
[152] Hausmann R and Dohm V 1991 *Phys. Rev. Lett.* **67** 3404
[153] Hausmann R and Dohm V 1992 *Z. Phys.* B **87** 229
[154] Hausmann R and Dohm V 1994 *Phys. Rev. Lett.* **72** 3060
[155] Dohm V and Hausmann R 1994 *Physica* B **197** 215
[156] Hausmann R 1999 *Phys. Rev.* B **60** 12349
[157] Folk R and Moser G 2006 *Phys. Rev.* E **73** 016141
[158] Peliti L 1979 *Lecture Notes in Physics* **104** 190 ed Ch Enz
[159] Folk R and Iro H 1985 *Phys. Lett.* A **109** 53
[160] Moser G and Folk R 1992 *J. Low Temp. Phys.* **86** 99
[161] Moser G and Folk R 1991 *Phys. Rev.* B **44** 819
[162] Gestrich D, Walsworth R and Meyer H 1984 *J. Low Temp. Phys.* **54** 37
[163] Dingus M, Zhong F, Tuttle J and Meyer H 1986 *J. Low Temp. Phys.* **65** 213
[164] Zhong F, Gestrich D, Dingus M and Meyer H 1987 *J. Low Temp. Phys.* **68** 55
[165] Zhong F, Tuttle J and Meyer H 1990 *J. Low Temp. Phys.* **79** 9
Zhong F, Tuttle J and Meyer H 1991 *J. Low Temp. Phys.* **83** 283

[166] Ahlers G 1972 *Phys. Rev. Lett.* **24** 1333
[167] Krech M and Landau D P 1999 *Phys. Rev.* B **60** 3375
[168] Sasvári L and Szépfalusy P 1977 *Physica* A **87** 1
[169] Dohm V and Ferrell R a *Phys. Lett.* A **67** 387
[170] Dohm V 1979 *Report of the KFA Jülich Jül-1578*
[171] Dengler R and Schwabl F 1987 *Europhys. Lett.* **4** 1233
Dengler R and Schwabl F 1987 *Z. Phys.* B **69** 327
Adzhemyan L Ts, Vasi'lev A N and Serdukov A V 1998 *Int. J. Mod. Phys.* **12** 1255
Adzhemyan L Ts Vasi'lev A N and Serdukov A V 1998 *J. Exp. Theor. Phys.* **87** 934
Adzhemyan L Ts and Vasi'lev A N 1999 *Theor. Math. Phys.* **119** 1
[172] Adzhemyan L Ts, Vasi'lev A N, Kabrits Yu S and Kompaniets M V 1999 *Theor. Math. Phys.* **119** 454
[173] Paladin G and Peliti L 1982 *J. Phys. Lett. (Paris)* **43** 15
Paladin G and Peliti L 1984 *J. Phys. Lett. (Paris)* **45** 289 (erratum)
[174] Flossmann G, Folk R and Moser G 1999 *Phys. Rev.* E **60** 779
[175] Flossmann G and Folk R 2000 *Phys. Rev.* E **62** 2460
[176] Hao H, Ferrell R A and Bhattacharjee J K 2005 *Phys. Rev.* E **71** 021201
[177] Onuki A 1997 *Phys. Rev.* E **55** 403
[178] Adzhemyan L Ts and Vasi'lev A N 1998 *Theor. Math. Phys.* **117** 1223
[179] Kawasaki K 1970 *Ann. Phys.* **61** 1
[180] Luettmer-Strathmann J, Sengers J V and Olchowy G A 1995 *J. Chem. Phys.* **103** 7482
[181] Folk R and Moser G 1995 *Phys. Rev. Lett.* **75** 2706
[182] Moldover M R, Sengers J V, Gammon R W and Hocken R J 1979 *Rev. Mod. Phys.* **51** 79
[183] Huang C-C and Ho J T 1973 *Phys. Rev.* A **7** 1304
[184] Sengers J V and Levelt Sengers M H 1987 *Progress in Liquid Physics* ed C A Croxton (New York: Wiley)
[185] Agosta C C, Wang S, Cohen L H and Meyer H 1987 *J. Low Temp. Phys.* **67** 237
[186] Strumpf H J, Collings A F and Pings C J 1974 *J. Chem. Phys.* **60** 3109
[187] Roe D B and Meyer H 1978 *J. Low Temp. Phys.* **30** 91
[188] Roe D B, Wallace B A and Meyer H 1974 *J. Low Temp. Phys.* **16** 51
[189] Sarid D and Cannell D S 1977 *Phys. Rev.* A **15** 735
[190] Folk R and Moser G 1998 *Phys. Rev.* E **60** 779
[191] Berg R F, Moldover M R and Zimmerli G A 1999 *Phys. Rev. Lett.* **82** 920
Berg R F, Moldover M R and Zimmerli G A 1999 *Phys. Rev.* E **60** 4079
[192] Das R and Bhattacharjee J K 2003 *Phys. Rev.* E **67** 036103
[193] Hohenberg P C and Barmatz M 1972 *Phys. Rev.* A **6** 289
[194] Sengers J V and Van Leeuwen J M J 1982 *Physica* A **116** 345 (and [188, chapter 4])
[195] Berg R F and Moldover M R 1990 *J. Chem. Phys.* **93** 1926
[196] Swinney H L and Henry D L 1973 *Phys. Rev.* A **8** 2586
[197] Das R and Bhattacharjee J K 2001 *Phys. Rev.* E **63** 020202
[198] Flossmann G, Folk R and Moser G 2001 *Int. J. Thermophys.* **22** 89
[199] Bhattacharjee J, Ferrell R A, Basu R S and Sengers J V 1981 *Phys. Rev.* A **24** 1469
[200] Bhattacharjee J and Ferrell R A 1983 *Phys. Rev.* A **27** 1544
[201] Berg R F 2004 *J. Rheol.* **48** 1365
[202] Oxtoby D W 1975 *J. Chem. Phys.* **62** 1463
[203] Das R and Bhattacharjee J K 2005 *Phys. Rev.* E **71** 036145
[204] Onuki A 1997 *J. Phys.: Condens. Matter* **9** 6119
[205] Folk R and Moser G 1996 *Condens. Matter Phys.* **7** 27
[206] Bhattacharjee J and Ferrell R A 1981 *Phys. Rev.* A **23** 1511
[207] Kawasaki K and Lo S-M 1972 *Phys. Rev. Lett.* **29** 48
[208] Burstyn H C, Sengers J V, Bhattajarjee J K and Ferrell R A 1983 *Phys. Rev.* A **28** 1567
[209] Jagannathan K and Yethiraj A 2004 *Phys. Rev. Lett.* **93** 015701
[210] Sengers J V and Moldover M R 2005 *Phys. Rev. Lett.* **95** 069601
[211] Jagannathan K and Yethiraj A 2005 *Phys. Rev. Lett.* **94** 069602
[212] Chen A, Chimowitz E H and Shapir Y 2005 *Phys. Rev. Lett.* **95** 255701
[213] Das S K, Horbach J, Binder K, Fisher M E and Sengers J V 2006 *Preprint* cond-mat/0603587
Das S K, Fisher M E, Sengers J V, Horbach J and Binder K 2006 *Preprint* cond-mat/0604102
[214] Wang S and Meyer H 1987 *J. Low Temp. Phys.* **69** 377
[215] Cohen L H, Dingus M L and Meyer H 1982 *J. Low Temp. Phys.* **49** 545 (mixtures)
Pittman E, Cohen L H and Meyer H 1982 *J. Low Temp. Phys.* **46** 115 (^{3}He)

Acton A and Kellner K 1977 *Physica* B **90** 192 (^{4}He)
[216] Cohen L H, Dingus M L and Meyer H 1982 *Phys. Rev. Lett.* **50** 1058
Cohen L H, Dingus M L and Meyer H 1985 *J. Low Temp. Phys.* **61** 79
[217] Miura Y, Meyer H and Ikushima A 1984 *J. Low Temp. Phys.* **55** 247
[218] Folk R and Moser G 1995 *Int. J. Thermophys.* **16** 1363
[219] Folk R and Moser G 1998 *Int. J. Thermophys.* **19** 1003
[220] Filippov L P 1968 *Int. J. Heat Mass Transfer* **11** 331
[221] Luettmer-Strathmann J and Sengers J V 1996 *J. Chem. Phys.* **104** 3026
[222] Giglio M and Vendramini A 1975 *Phys. Rev. Lett.* **34** 561
[223] Cohen L H, Dingus M L and Meyer H 1983 *Phys. Rev. Lett.* **50** 1058
[224] Mensah-Brown H and Wakeham W A 1995 *Int. J. Thermophys.* **16** 237
[225] Zielesny A, Schmitz J, Limbergh S, Aizpiri A G, Fusenig S and Woerman D 1994 *Int. J. Thermophys.* **15** 67
[226] Niewoudt J C and Sengers J V 1989 *J. Chem. Phys.* **90** 457
[227] Souto-Caride M, Troncoso J, Peleteiro J, Carballo E and Romaní L 2005 *Phys. Rev.* E **71** 041503
[228] Beysens D, Bourgou A and Palidin G 1984 *Phys. Rev.* A **30** 2686
[229] Anisimov M A, Agayan V A, Povodyrev A A, Sengers J V and Gorodetskii E E 1998 *Phys. Rev.* E **57** 1946
[230] Ma S-K and Mazenko F 1975 *Phys. Rev.* B **11** 4077
[231] Böni P, Chen M E and Shirane G 1987 *Phys. Rev.* B **35** 8449
[232] Iro H 1988 *J. Magn. Magn. Mater.* **73** 175
[233] Shirane G, Böni P and Martinez J L 1987 *Phys. Rev.* B **36** 881
[234] Böni P, Mook H A, Martinez and Shirane G 1993 *Phys. Rev.* B **47** 3171
[235] Résibois P and Piette C 1970 *Phys. Rev. Lett.* **24** 514
[236] Böni P, Shirane G, Bohn H G and Zinn W 1988 *J. Appl. Phys.* B **63** 3089
[237] Chen K and Landau D P 1994 *Phys. Rev.* B **49** 3266
[238] Bunker A, Chen K and Landau D P 2000 *Phys. Rev.* B **54** 925
[239] Tsai S-H, Bunker A and Landau D P 2000 *Phys. Rev.* B **61** 333
[240] Tsai S-H and Landau D P 2003 *Phys. Rev.* B **67** 104411
[241] Wegner F 1969 *Z. Phys.* **218** 260
[242] Cuccoli A, Lovesey W and Tognetti V 1994 *J. Phys.: Condens. Matter* **6** 7553
[243] Dasgupta C and Halperin B I 1981 *Phys. Rev. Lett.* **47** 1556
[244] Kolnberger S and Folk R 1990 *Phys. Rev.* B **41** 4083
[245] Herbut I F and Tesanovic 1996 *Phys. Rev. Lett.* **76** 4588
[246] Berghoff B, Freire F, Litim D F, Lola S and Wetterich C 1996 *Phys. Rev.* B **53** 5734
[247] Folk R and Holovatch Yu 1996 *J. Phys. A: Math. Gen.* **29** 3409
[248] Lannert C, Vishveshwara S and Fisher M P A 2004 *Phys. Rev. Lett.* **92** 097004
[249] Folk R and Holovatch Yu 1999 *Correlations, Coherence, and Order* ed D V Shopova and D I Uzunov (Dordrecht: Kluwer)
[250] Field-theoretic calculations of this model are in progress; Dudka M, Folk R and Moser G in preparation
[251] Jin-Tae Kim, Goldenfeld N, Giapintzakis and Ginsberg D M 1997 *Phys. Rev.* B **56** 118
[252] Booth J C *et al* 1996 *Phys. Rev. Lett.* **77** 4438
[253] Han S H, Eltsev Yu and Rapp Ö 1999 *J. Low Temp. Phys.* **11** 1259
[254] Weber H and Jensen H J 1997 *Phys. Rev. Lett.* **78** 2620
[255] Lidmar J, Wallin M, Wengel C, Girvin S M and Young A P 1998 *Phys. Rev.* B **58** 2827
[256] Aji V and Goldenfeld N 2001 *Phys. Rev. Lett.* **87** 197003
[257] Wickham R A and Dorsey A T 2000 *Phys. Rev.* B **61** 6945
[258] Nogueira F S and Manske D 2005 *Phys. Rev.* B **72** 014541
[259] Vishveshwara S and Fisher M P A 2001 *Phys. Rev.* B **64** 134507
[260] For the recent reviews on criticality of diluted magnets see e.g. Pelissetto A and Vicari E 2002 *Phys. Rep.* **368** 549
Folk R, Holovatch Yu and Yavors'kii T 2003 *Phys.—Usp.* **46** 169
Folk R, Holovatch Yu and Yavors'kii T 2003 *Usp. Fiz. Nauk* **173** 175 (Engl. Transl.)
[261] Berche P E, Chatelain C, Berche B and Janke W 2004 *Eur. Phys. J.* B **39** 463
Berche B, Berche P E, Chatelain C and Janke W 2005 *Condens. Mater. Phys.* **8** 47
[262] Belanger D P and Young A P 1991 *J. Magn. Magn. Mater.* **100** 272
[263] Luck J M 1993 *Europhys. Lett.* **24** 359
[264] Janke W and Weigel M 2004 *Phys. Rev.* B **69** 144208
[265] A review of early work on random anisotropy magnets may be found in Cochrane R W, Harris R and Zuckermann M J 1978 *Phys. Rep.* **48** 1

Recent experimental, numerical and theoretical studies are reviewed in reference Dudka M, Folk R and Holovatch Yu 2005 *J. Magn. Magn. Mater.* **294** 305
[266] Boyanovsky D and Cardy J L 1982 *Phys. Rev.* B **26** 154
Boyanovsky D and Cardy J L 1983 *Phys. Rev.* B **27** 6971
[267] Weinrib A and Halperin B I 1983 *Phys. Rev.* B **27** 413
[268] Harris A B 1974 *J. Phys. C: Solid State Phys.* **7** 1671
[269] Krey U 1976 *Phys. Lett.* A **57** 215
[270] Lawrie I D and Prudnikov V V 1984 *J. Phys. C: Solid State Phys.* **17** 1655
[271] Grinstein G, Ma S-k and Mazenko G F 1977 *Phys. Rev.* B **15** 258
[272] Oerding K and Janssen H K 1995 *J. Phys. A: Math. Gen.* **28** 4271
[273] Janssen H K, Oerding K and Sengenspeick E 1995 *J. Phys. A: Math. Gen.* **28** 6073
[274] Perumal A, Srinivas V, Rao V V and Dunlap R A 2003 *Phys. Rev. Lett.* **91** 137202
Folk R, Holovatch Yu and Yavors'kii T 2000 *Phys. Rev.* B **61** 15114
Calabrese P, Parruccini P, Pelissetto A and Vicari E 2004 *Phys. Rev.* E **69** 036120
[275] Dudka M, Folk R, Holovatch Yu and and Ivaneiko D 2003 *J. Magn. Magn. Mater.* **53** 243
[276] Blavats'ka V, Dudka M, Folk R and Holovatch Yu 2005 *Phys. Rev.* B **72** 064417
[277] Dudka M, Folk R, Holovatch Yu and Moser G 2005 *Phys. Rev.* E **72** 036107
[278] Dudka M, Folk R, Holovatch Yu and Moser G 2005 *Condens. Matter Phys.* **8** 737
[279] Ivaneyko D, Ilnytsyi J, Berche B and Holovatch Yu 2006 *Physica* A submitted (*Preprint* cond-mat/0603521)
[280] Heuer H-O 1993 *J. Phys. A: Math. Gen.* **26** L341
[281] Parisi G, Ricci-Tersenghi F and Ruiz-Lorenzo J J 1999 *Phys. Rev.* E **60** 5198
[282] Schehr G and Paul R 2005 *Phys. Rev.* E **72** 016105
[283] Selke W 1992 *Phase Transitions and Critical Phenomena* ed C Domb and J L Lebowitz (London: Academic)
[284] Diehl H W 2002 *Acta Phys. Slovaca* **52** 271
[285] Schwahn D, Mortensen K, Frielinghaus h, Almdal K and Kielhorn L 2000 *J. Chem. Phys.* **112** 5454
[286] Pipich V, Schwahn D and Willner L 2005 *Phys. Rev. Lett.* **94** 117801
[287] Pipich V, Schwahn D and Willner L 2005 *J. Chem. Phys.* **123** 124904
[288] Huber D L 1976 *Phys. Lett.* A **55** 359
Huber D L 1976 *Phys. Lett.* A **70** 500 (erratum)
[289] Folk R and Selke W 1978 *Phys. Lett.* A **69** 255
[290] Basu A and Bhattacharjee J K 2004 *J. Phys. A: Math. Gen.* **37** 1111
[291] Folk R, Iro H and Schwabl F 1977 *Z. Phys.* B **27** 169
[292] Hlinka J, Currat R, Boissieu de, Livet F and Vysochanskii Yu M 2005 *Phys. Rev.* B **71** 052102
[293] Koch W, Dohm V and Stauffer D 1996 *Phys. Rev. Lett.* **77** 1789
Koch W and Dohm V 1998 *Phys. Rev.* B **58** R1179
[294] Berges J, Tetradis N and Wetterich Ch 2002 *Phys. Rep.* **363** 223
[295] Li X-J and Sokal A D 1989 *Phys. Rev. Lett.* **63** 827
[296] Coddington P D and Baillie C F 1992 *Phys. Rev. Lett.* **68** 962
[297] Ossola G and Sokal A D 2004 *Nucl. Phys.* B **691** 259
[298] Nalimov M, Andreanov J, Honkonen J and Komarova M 2006 *J. Phys. A: Math. Gen.* **39** submitted
[299] Honkonen J, Komarova M and Nalimov M 2005 *Nucl. Phys.* B **707** [FS] 493
[300] Honkonen J, Komarova M and Nalimov M 2005 *Nucl. Phys.* B **714** [FS] 292